Electronic Supplementary Material (ESI) for Journal of Materials Chemistry A.

Rationalising the Multivariate Modulation of MUV-10 for the Defect-Introduction of Multiple Functionalised Modulators

Table of contents

S.1. General Experimental Remarks

Powder X-Ray Diffraction (PXRD):PXRD patterns were collected in a PANalyticalX'Pert PRO diffractometer using copper radiation (Cu Kα = 1.5418 Å) with an X'Celerator detector, operating at 40 mA and 45 kV. Profiles were collected in the 3° < 2θ < 40° range with a step size of 0.017°. (University of Valencia)

Thermogravimetric Analysis (TGA): were carried out with a Mettler Toledo TGA/SDTA 851 apparatus between 25 and 800 °C under ambient conditions (10 °C·min^{-1}scan rate and an air flow of 9 mL·min−1). (University of Valencia)

Nuclear Magnetic Resonance Spectroscopy (NMR): NMR spectra were recorded on either a Bruker AVIII 300 MHz spectrometer and referenced to residual solvent peaks. (University of Valencia)

Gas Uptake: N2 adsorption isotherms were carried out at 77 K on a with a Micromeritics 3Flex gas sorption analyser. Samples were degassed under vacuum at 120 °C for 24 h in a Multisorb station prior to analysis. BET surface areas, micropore surface areas and external surface areas were calculated from the isotherms using the MicroActive operating software. The pore size distributions were calculated using NLDFT oxide surface pore model within the MicroActive software, with no regularisation, whereas the pillared clay model was used for the tri, tetra and penta-modulated MOFs, as the oxide surface pore model as providing higher errors due to the lost of the type I isotherm (University of Valencia)

Scanning Electron Microscopy (SEM) and single point energy-dispersive X-Ray analysis (EDX): particle morphologies, dimensions and point energy-dispersive X-Ray analysis were studied with a Hitachi S-4800 scanning electron microscope at an accelerating voltage of 20 kV. (University of Valencia)

Energy-dispersive X-Ray analysis (EDX) mapping: the mapping of different elements (Ti, Ca, C, O, N, F) was studied using a SCIOS 2 field emission scanning electron microscope with focused ion beam at an accelerating voltage of 20 kV. (University of Valencia)

Fourier Transform Infrared Spectroscopy: IR spectra of solids were collected using a Shimadzu Fourier Transform Infrared Spectrometer, FTIR-8400S, fitted with a Diamond ATR unit. (Universityof Valencia)

S.2. Materials and Synthesis

All reagents unless otherwise stated were obtained from commercial sources and were used without further purification.

General remarks

For all modulated syntheses a mixture of solvents (2.2 mL of AcOH per 9.6 mL of DMF) was prepared in function of the number of reactions to perform (11.8 mL per reaction). This pre-made solvent mixture was used to separately dissolve the different synthetic components as further explained during this section.

In all syntheses the jars were placed in an oven at room temperature and heated to 120℃ with 2℃/min ramp. The temperature was maintained during 24 hours and cooled down to room temperature with 0.4℃/min ramp. The resultant powder was collected by centrifugation (5000 rpm, 5 min) and washed with DMF (X2) and MeOH (x3) through dispersion-centrifugation cycles. The samples were dried under vacuum overnight and further activated by sohxlet with boiling MeOH during approximately 24 hours. The samples were further dried under vacuum for 24 hours prior to characterization.

Procedure MUV-10-Iso-x%: In 25 mL pyrex jars, $CaCl_2$ (1 equivalent) was dissolved in 2 mL of solvent mixture. In a separate vial 1.5 equivalents of btc compared to Ti and Ca were dissolved in 9.8 mL of solvent mixture together with the modulators (1 equivalent compared to the linker of each modulator). Both solutions were mixed in in 25 mL pyrex jars followed by slow Ti(IV) isopropoxide addition (1 equivalent) and gentle stirring.

Table S1: Tabulated synthetic conditions.

$CaCl_2$	btc	Ti(IV) isopropoxide
0.6 mmol	0.9 mmol	0.6 mmol
66.5mg	189.3mg	177.5μL

S.3. Characterisation of MUV-10-Iso-X

S.3.1 Powder X-Ray Diffraction (PXRD)

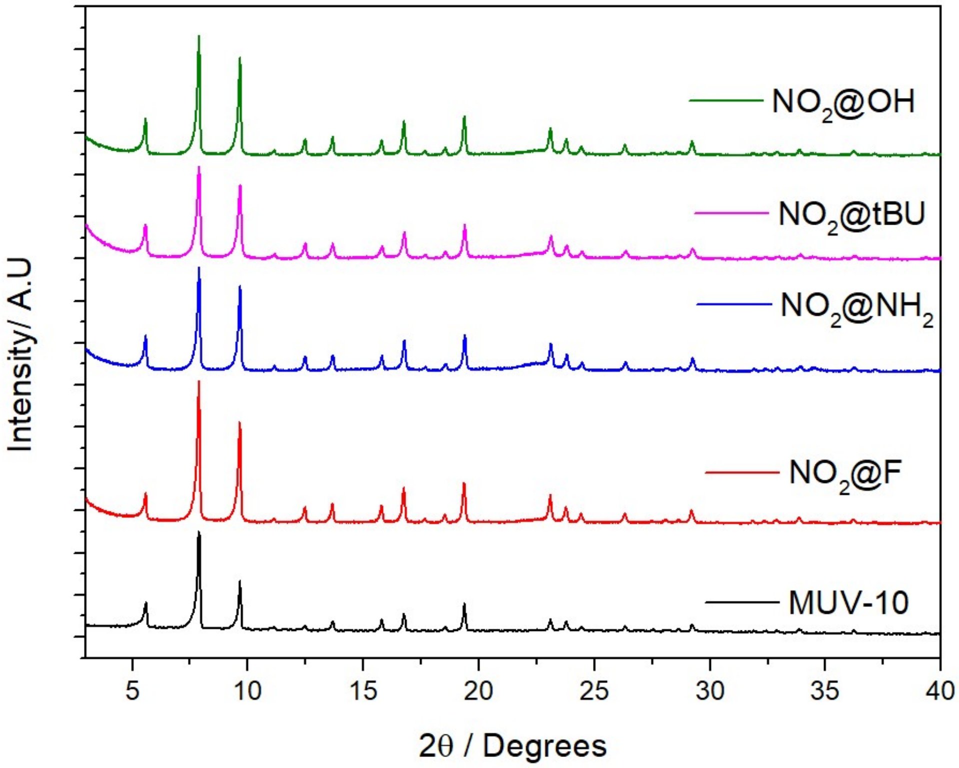

Figure S1: PXRD patterns of NO_2@MOD compared to unmodulated MUV-10.

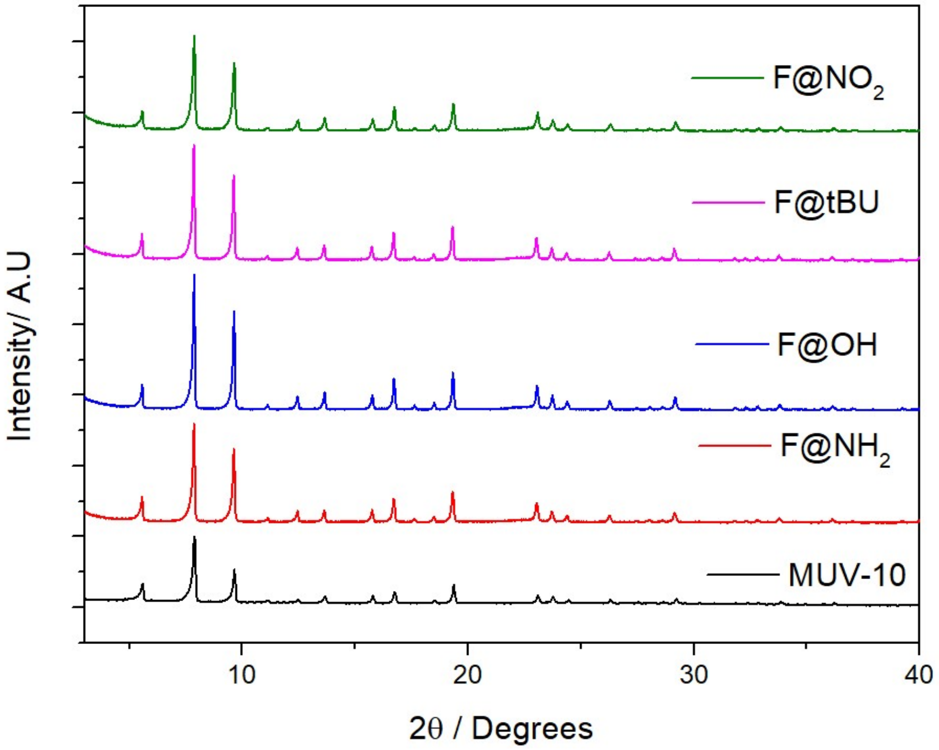

Figure S2: PXRD patterns of F@MOD compared to unmodulated MUV-10.

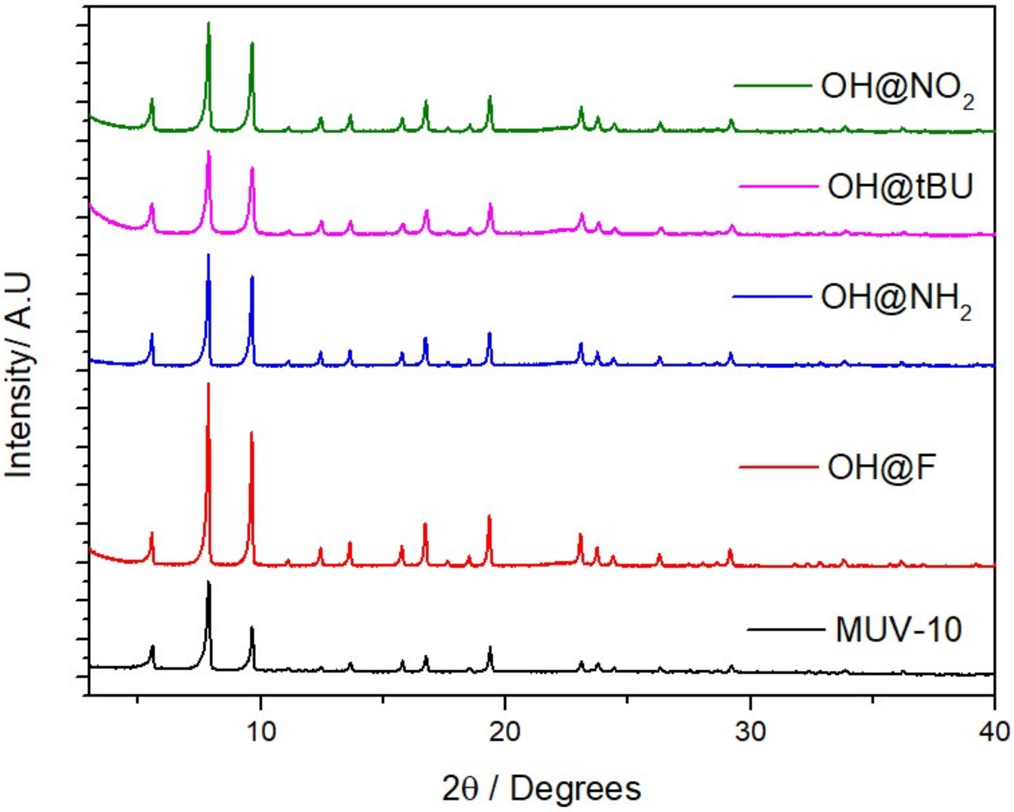

Figure S3: PXRD patterns of OH@MOD compared to unmodulated MUV-10.

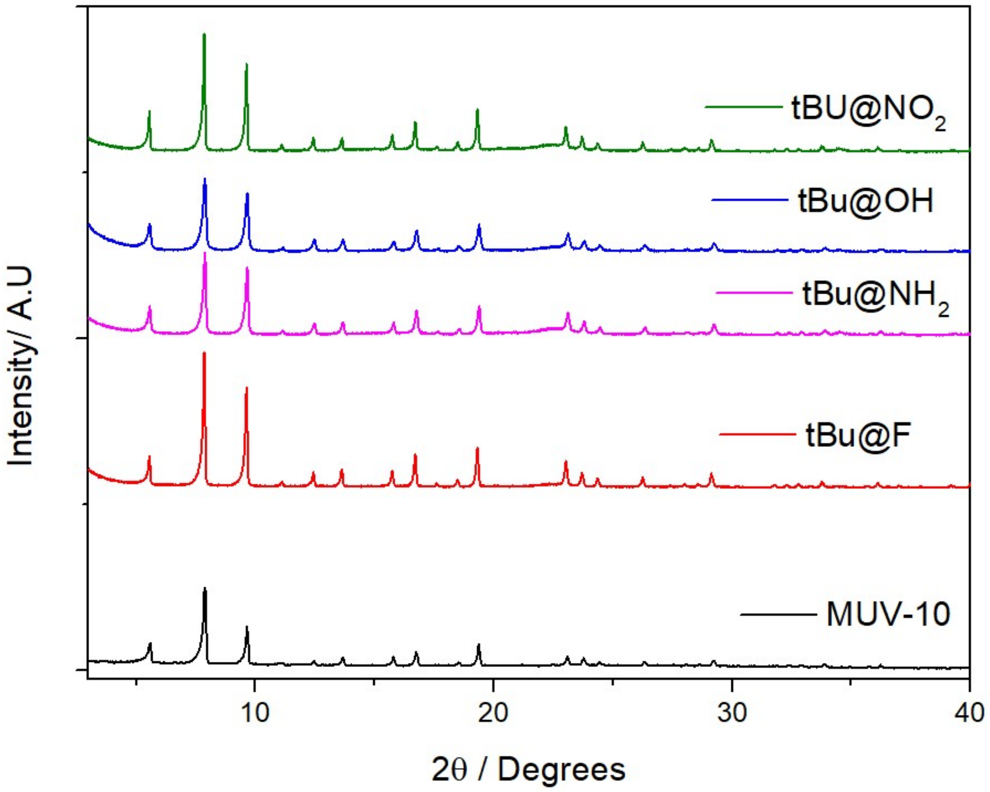

Figure S4: PXRD patterns of tBu@MOD compared to unmodulated MUV-10.

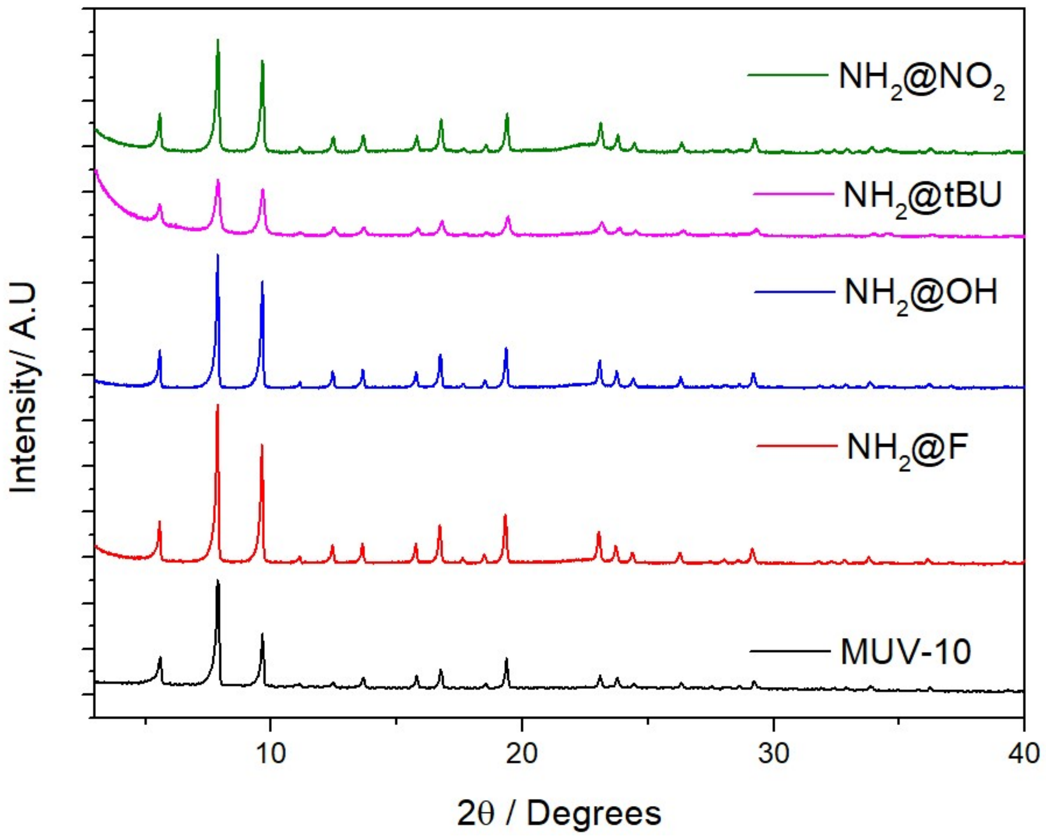

Figure S5: PXRD patterns of NH_2@MOD compared to simulated MUV-10.

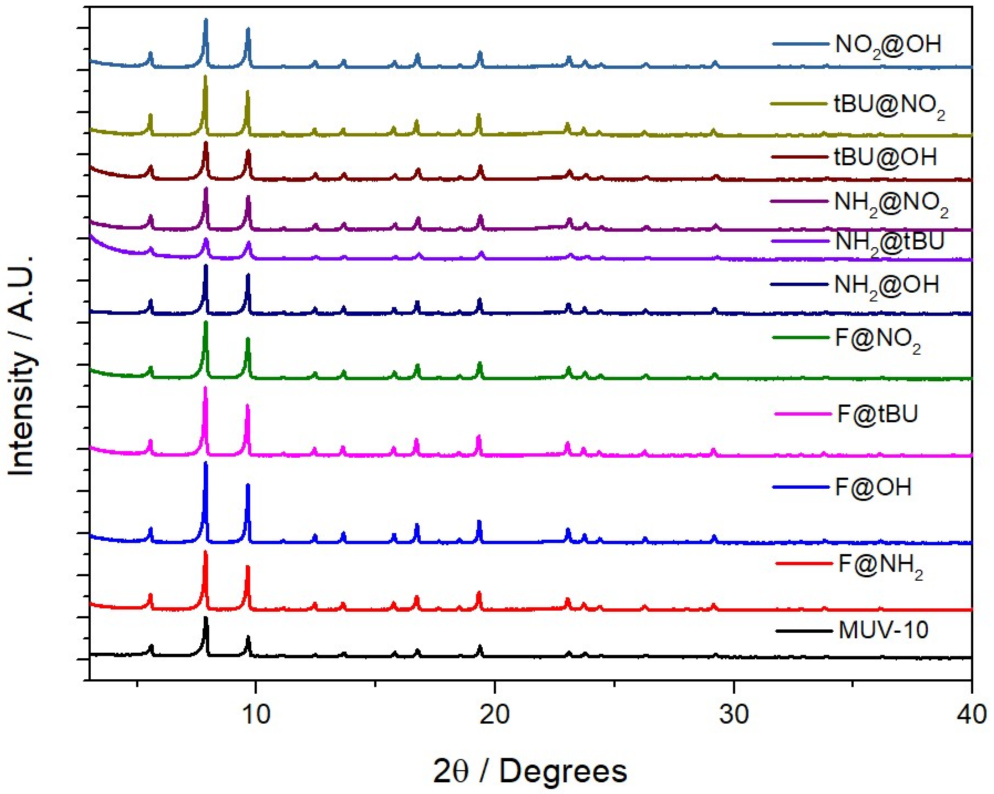

Figure S6: PXRD patterns of di-modulated MOFs compared to unmodulated MUV-10.

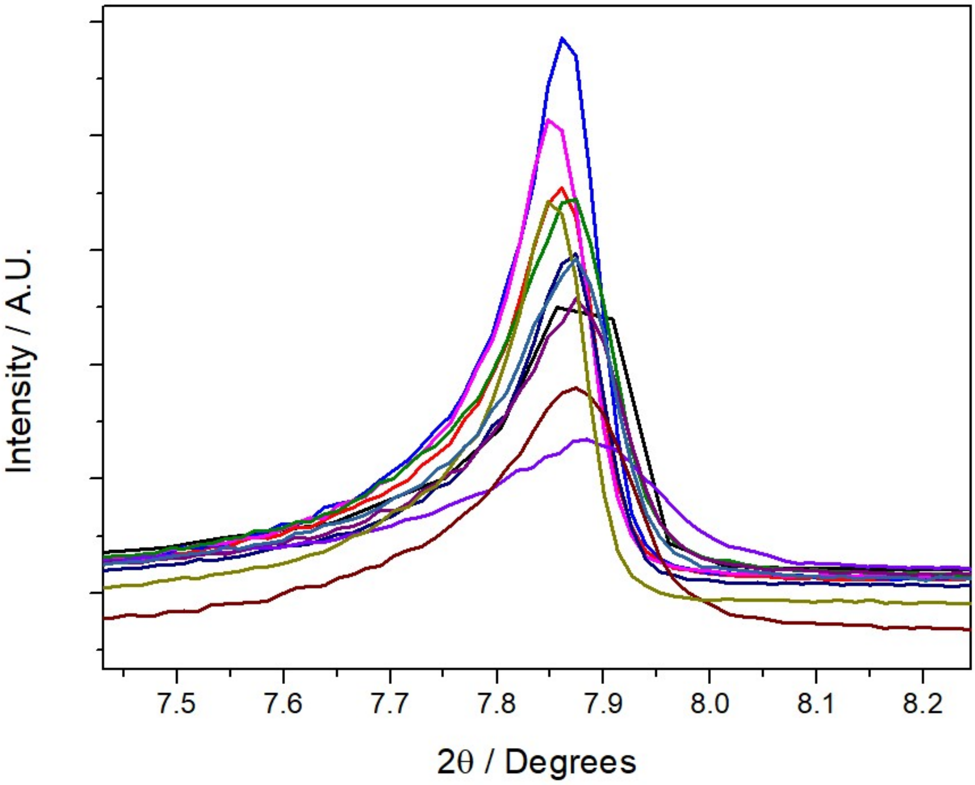

Figure S7: Amplified PXRD patterns of di-modulated MOFs compared to unmodulated MUV-10. The legend from figure S6 applies to this figure.

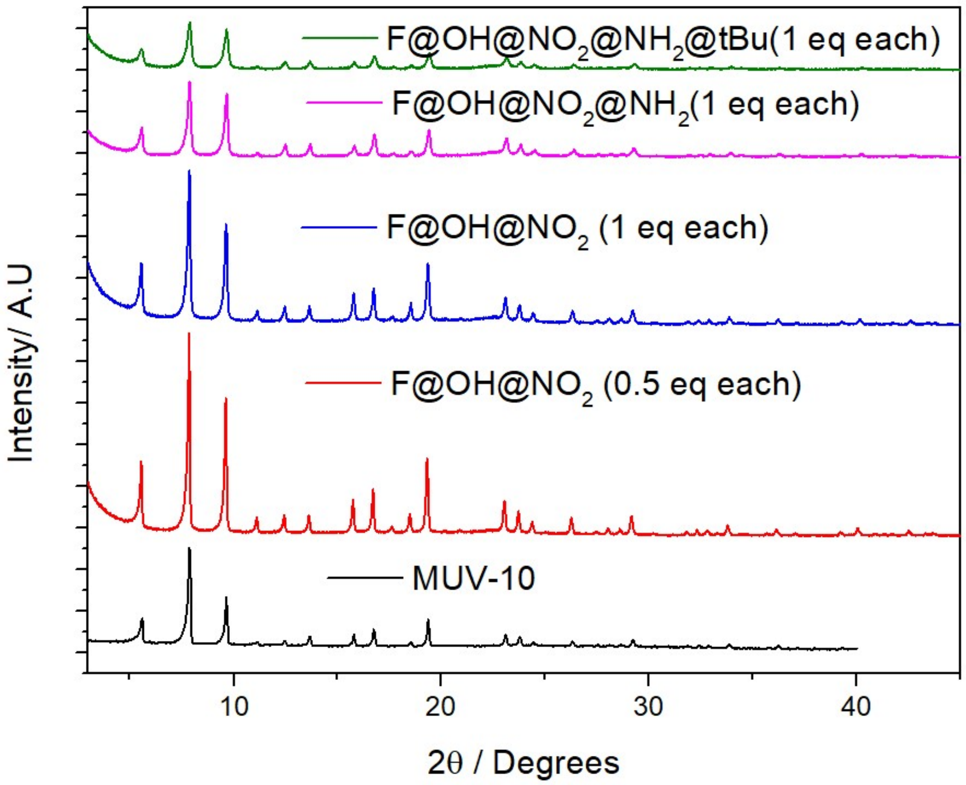

Figure S8: PXRD patterns of multi-modulated MOFs compared to unmodulated MUV-10.

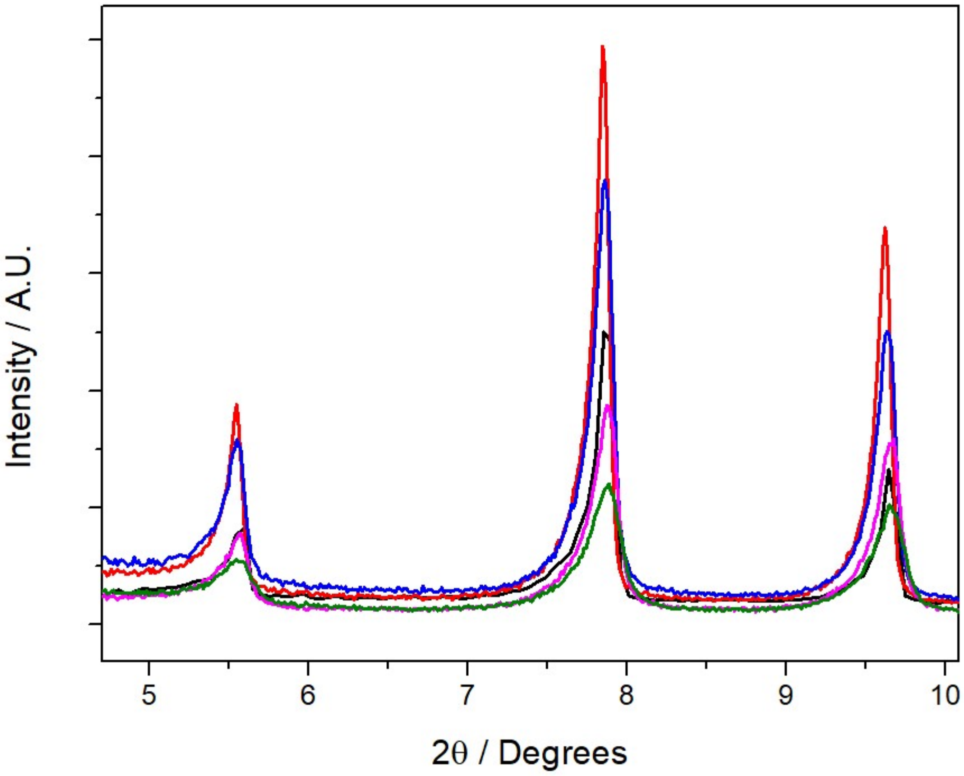

Figure S9: Amplification of PXRD patterns of multi-modulated MOFs compared to unmodulated MUV-10.

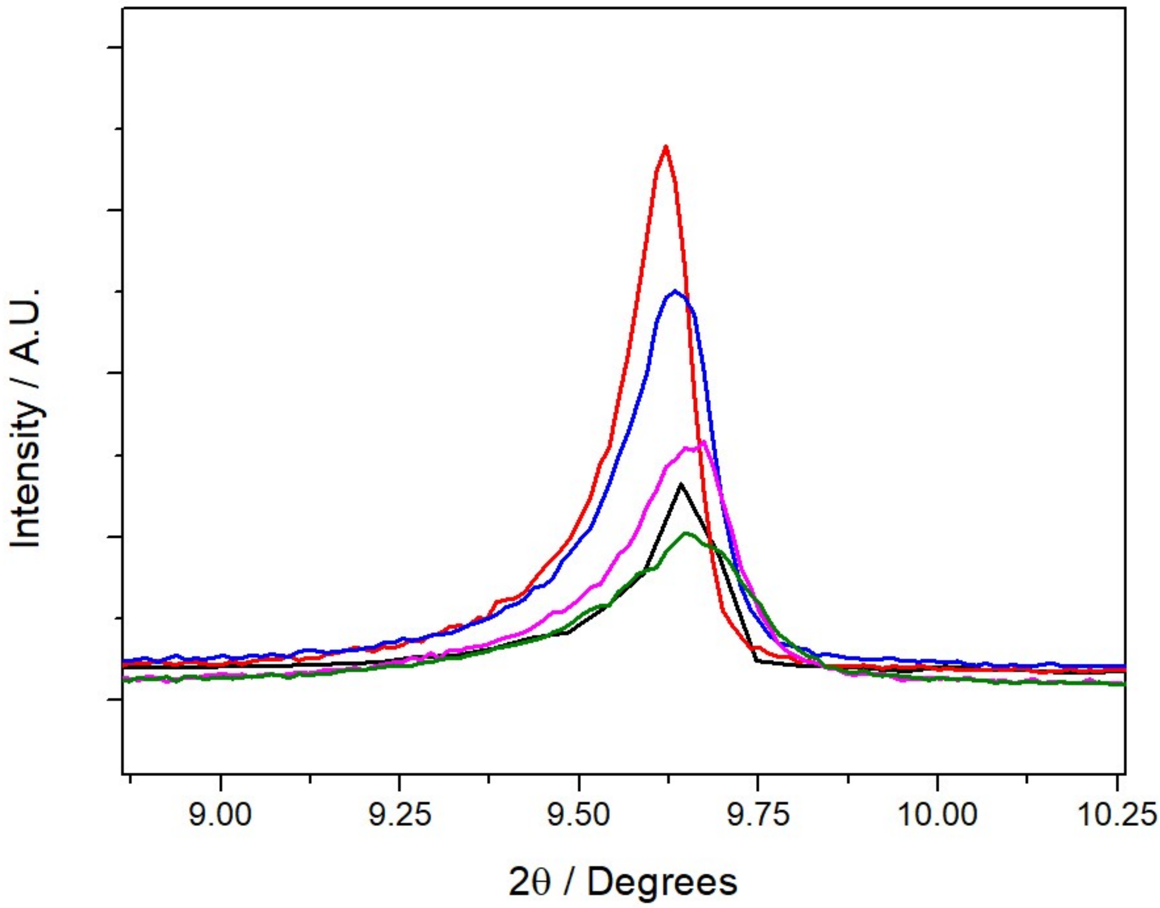

Figure S10: Amplification of PXRD patterns of multi-modulated MOFs compared to unmodulated MUV-10.

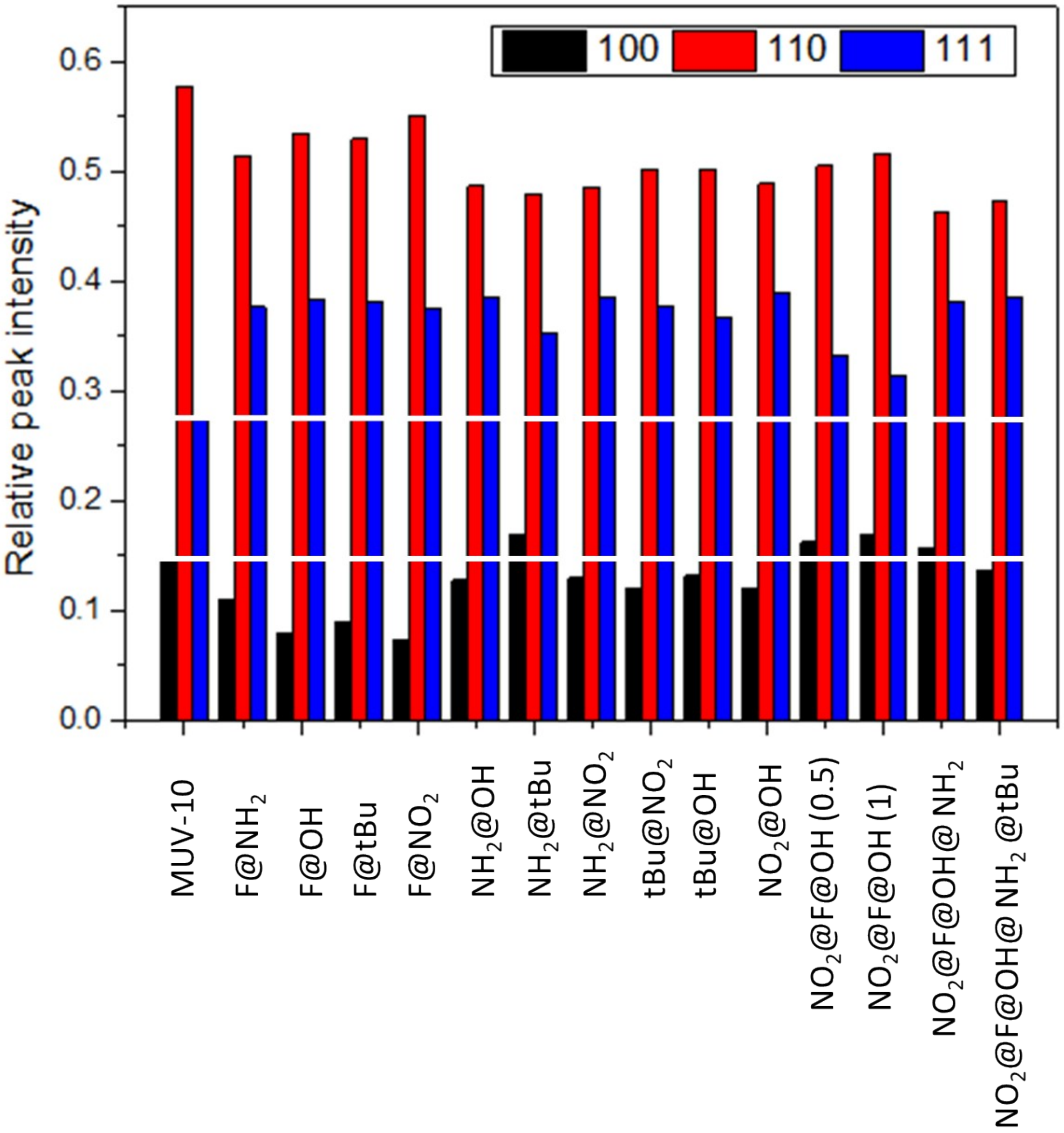

Figure S11: Relative peak intensity of the MTVM MOFs compared to the unmodulated MOF, analysed as the intensity of the peak divided by the intensity of all the peas.

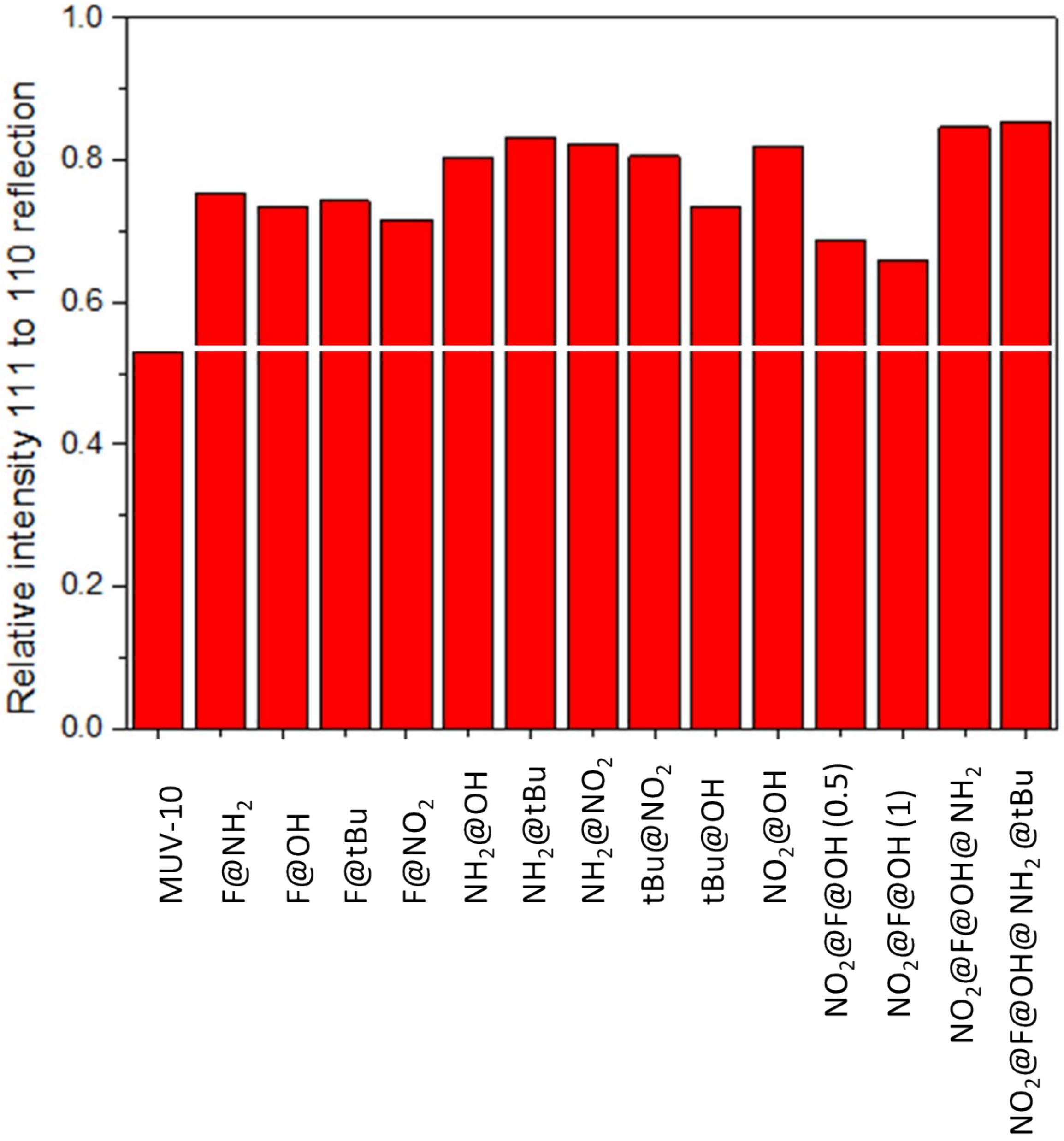

Figure S12: Relative peak intensity of the MTVM MOFs compared to the unmodulated MOF, analysed as the intensity of the <111> reflectin band divided by the intensity of the <111> relection band.

S.3.2 Proton Nuclear Magnetic Resonance (^{1}HNMR)

Iso-X was present in the ^{1}HNMR profiles alongside with formic acid coming from the decomposition of DMF during synthesis. Incorporation of modulator and formic acid is expressed as the **molar ratio** (R_{mod},) between modulator and btc, $Rmod = \frac{Mod}{btc}$ and as the **molar percent** of modulator (mol%) compared to btc, mol% $= \frac{Mod}{Mod + btc} * 100$, while the **total modulator percent** (total mod%) is calculated taking into account modulator, formic acid and btc, $total\, mod\% = \frac{Mod1 + mod2 + mod3\ldots}{Mod1 + mod2, mod3\ldots + btc} * 100$

The benzene tricarboxylate linker appears as a singlet at *ca.* 8.67 ppm (3H). The singlet that corresponds to 1 H at *ca.* 7.9 ppm is attributed to DMF (*grey in figures), while the singlet at *ca*. 8.2 ppm is attributed to formic acid (1H) comping from the decomposition of DMF during synthesis,[1] which in most cases is insignificant during this study.

For the Iso-F modulator, the triplet at *ca*. 8.32 ppm corresponds to 1H, while the doublets of doublets at ca. 7.93 ppm correspond to 2H.

For the Iso-NO_2 modulator, the triplet at *ca*. 8.77 ppm corresponds to 1H, while the doublet at *ca.* 8.80 corresponds to 2H.

For the Iso-OH modulator, the triplet at *ca.* 7.97 correspond to 1H, while the doublet at *ca.* 7.58 corresponds to 2H

For the Iso-tBu modulator, the triplet at *ca.* 8.34 ppm corresponds to 1H, while the doublet at *ca.* 8.19 ppm corresponds to 2 H.

For the Iso-NH_2 modulator, the use of deuterated acid results in the amino group protonation leading to the appearance of two identical species. Thus, the triplets at *ca.* 8.51 and 8.17 ppm correspond to 1H, while the doublets at *ca.* 8.46 and 8.21 ppm correspond to 2 H.

Please note that minor shifting of these signals can be observed due to the use of deuterated sulphuric acid to digest the MOFs for ^{1}HNMR analysis.

S.3.2.A Proton Nuclear Magnetic Resonance (^{1}HNMR) of NO_2@MOD

Table S2: Tabulated data extracted from acid digested ^{1}HNMR of NO_2@MOD MOFs in mol%, showing modulator and total modulator content increasing with the addition of modulator, whereas fa incorporation seems to be constant.

NO_2@MOD	MOL F	MOL NO_2	MOL NH_2	MOL tBu	MOL OH	MOL Total
F	12.993	22.820	0.000	0.000	0.000	30.796
tBu	0.000	19.084	0.000	8.817	0.000	24.956
OH	0.000	18.809	0.000	0.000	2.264	20.308
NH_2	0.000	15.432	2.491	0.000	0.000	17.221

Table S3: Tabulated data extracted from acid digested ^{1}HNMR of NO_2@MOD MOFs in molar ratio, showing modulator and total modulator content increasing with the addition of modulator, whereas fa incorporation seems to be constant.

NO_2@MOD	R F	R NO_2	R NH_2	R tBu	ROH	R Total
F	0.149	0.296	0.000	0.000	0.000	0.445
tBu	0.000	0.236	0.000	0.097	0.000	0.333
OH	0.000	0.232	0.000	0.000	0.023	0.255
NH_2	0.000	0.182	0.026	0.000	0.000	0.208

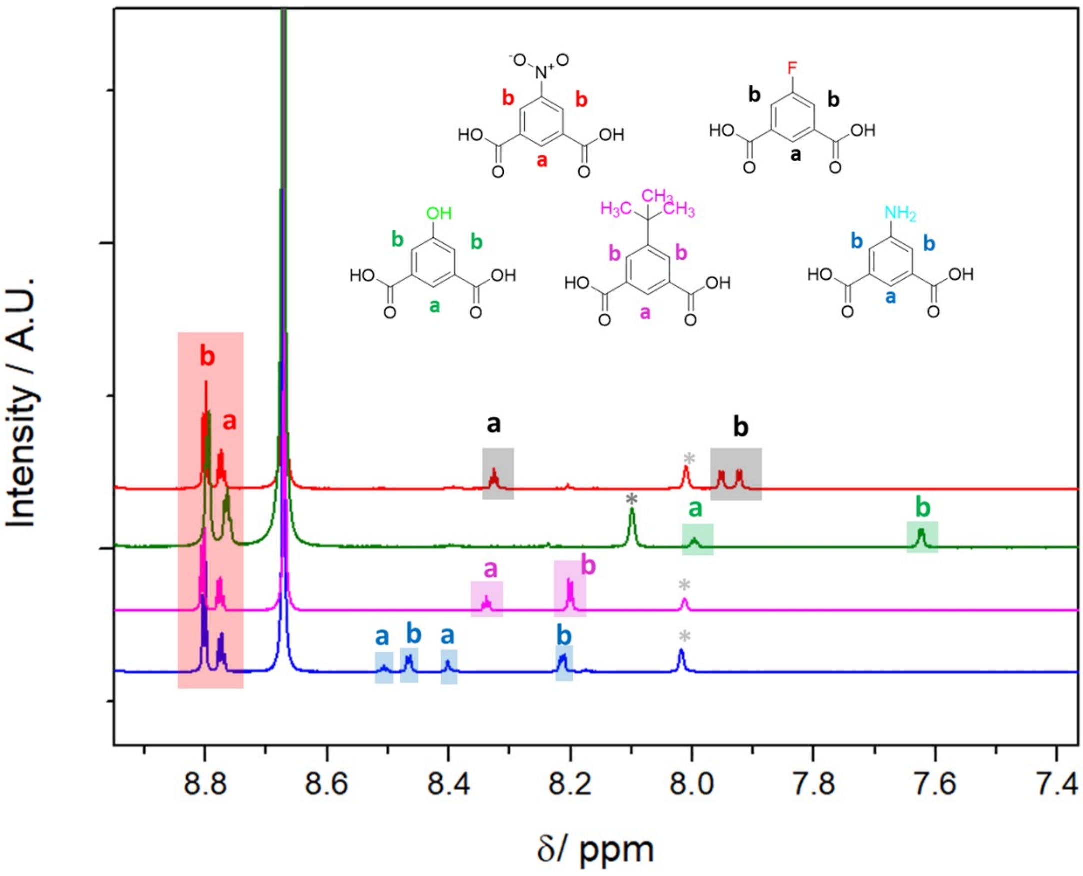

Figure S13: Representation of the acid-digested ^{1}HNMR profiles of the NO_2@MOD MOFs.

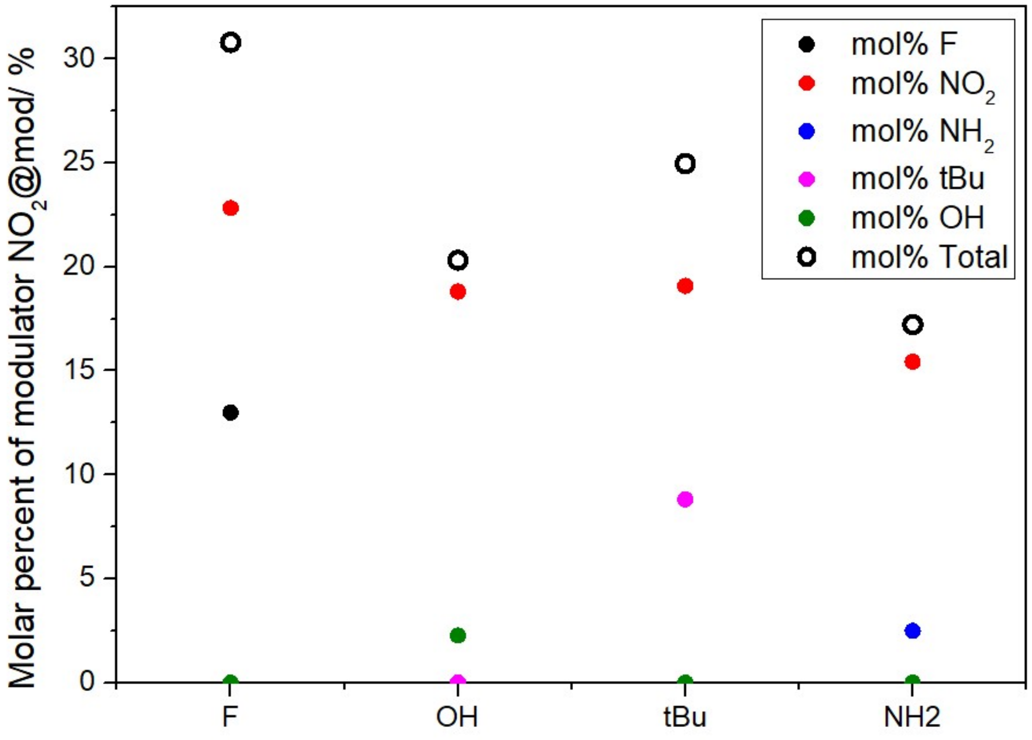

Figure S14: Modulator incorporation in molar percent for the NO_2@MOD MOFs.

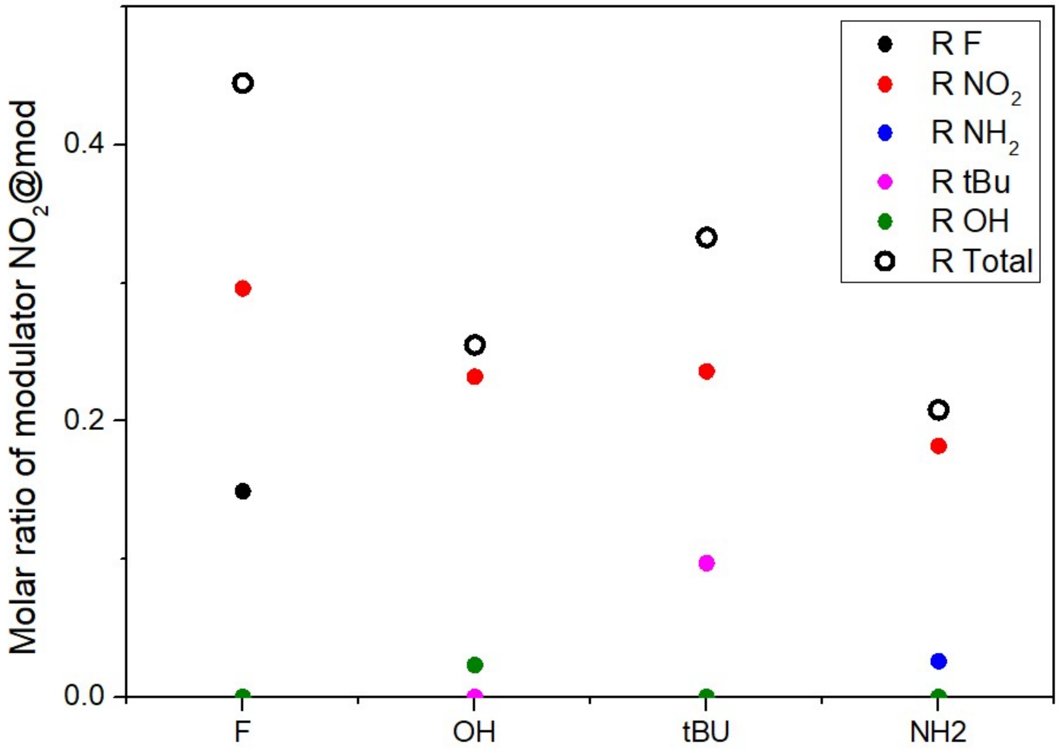

Figure S15: Modulator incorporation in molar ratio for the NO_2@MOD MOFs.

S.3.2.B Proton Nuclear Magnetic Resonance (^{1}HNMR) of F@MOD

Table S4: Tabulated data extracted from acid digested ^{1}HNMR of F@MOD MOFs in mol%, showing modulator and total modulator content increasing with the addition of modulator, whereas fa incorporation seems to be constant.

F@MOD	MOL F	MOL NO_2	MOL NH_2	MOL tBu	MOL OH	MOL Total
NO_2	12.993	22.820	0.000	0.000	0.000	30.796
tBu	11.304	0.000	0.000	8.458	0.000	18.022
OH	10.428	0.000	0.000	0.000	6.833	15.949
NH_2	10.334	0.000	5.449	0.000	0.000	14.740

Table S5: Tabulated data extracted from acid digested ^{1}HNMR of F@MOD MOFs in molar ratio, showing modulator and total modulator content increasing with the addition of modulator, whereas fa incorporation seems to be constant.

F@MOD	R F	R NO_2	R NH_2	R tBu	ROH	R Total
NO_2	0.149	0.296	0.000	0.000	0.000	0.445
tBu	0.127	0.000	0.000	0.092	0.000	0.220
OH	0.116	0.000	0.000	0.000	0.073	0.190
NH_2	0.115	0.000	0.058	0.000	0.000	0.173

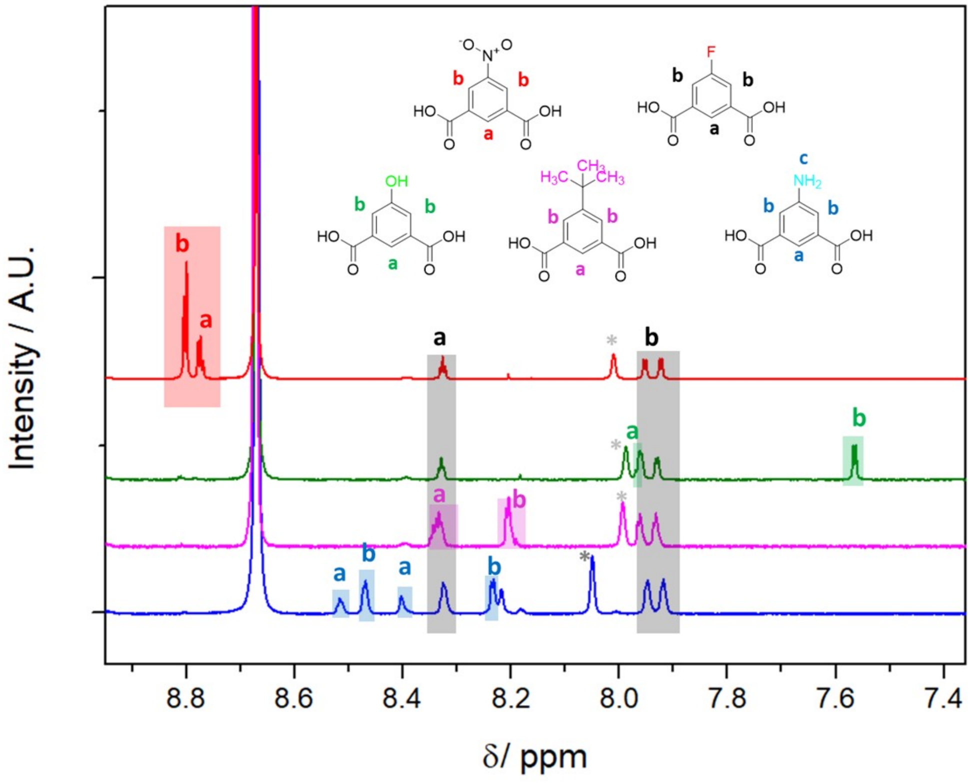

Figure S16: Representation of the acid-digested ^{1}HNMR profiles of the F@MOD MOFs.

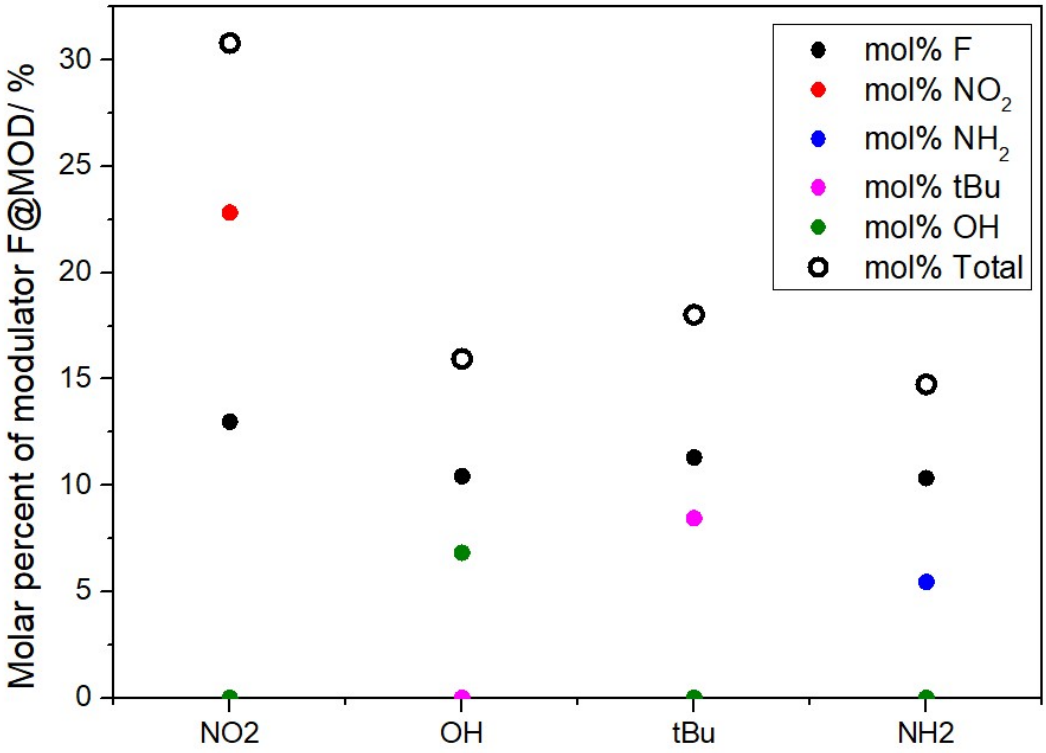

Figure S17: Modulator incorporation in molar percent for the F@MOD MOFs.

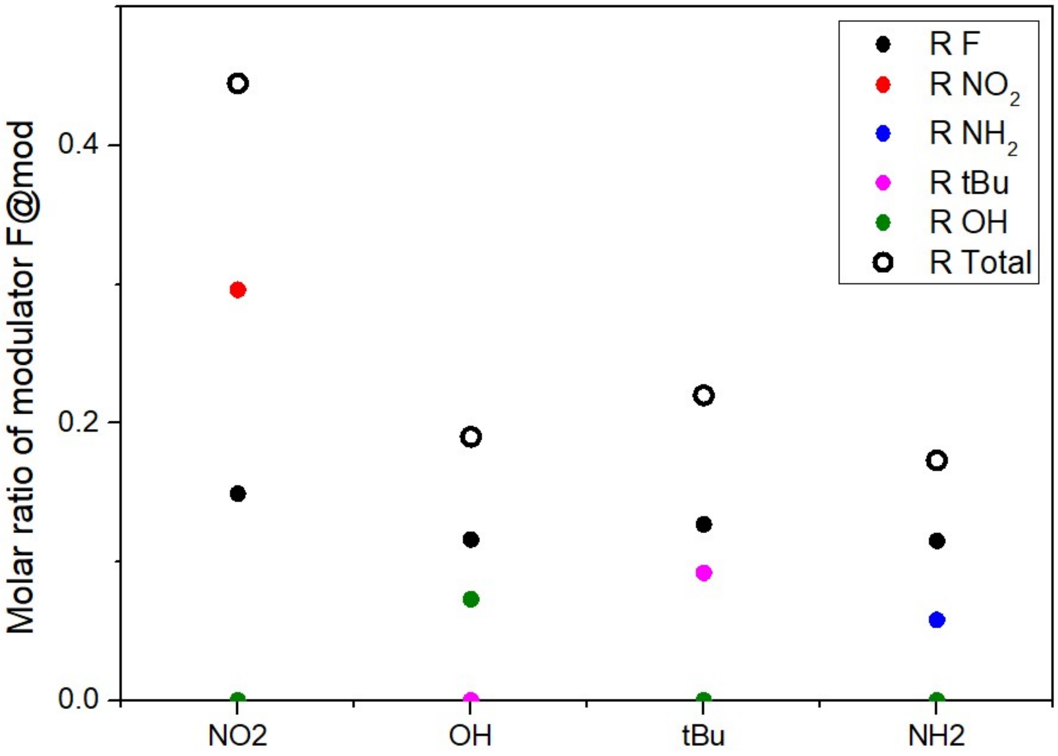

Figure S18: Modulator incorporation in molar ratio for the F@MOD MOFs.

S.3.2.C Proton Nuclear Magnetic Resonance (^{1}HNMR) of OH@MOD

Table S6: Tabulated data extracted from acid digested ^{1}HNMR of OH@MOD MOFs in mol%, showing modulator and total modulator content increasing with the addition of modulator, whereas fa incorporation seems to be constant.

OH@MOD	MOL F	MOL NO_2	MOL NH_2	MOL tBu	MOL OH	MOL Total
NO_2	0.000	18.809	0.000	0.000	2.264	20.308
F	10.428	0.000	0.000	0.000	6.833	15.949
tBu	0.000	0.000	0.000	3.378	4.343	7.439
NH_2	0.000	0.000	4.288	0.000	7.532	11.210

Table S7: Tabulated data extracted from acid digested ^{1}HNMR of OH@MOD MOFs in molar ratio, showing modulator and total modulator content increasing with the addition of modulator, whereas fa incorporation seems to be constant.

OH@MOD	R F	R NO_2	R NH_2	R tBu	ROH	R Total
NO_2	0.000	0.232	0.000	0.000	0.023	0.255
F	0.116	0.000	0.000	0.000	0.073	0.190
tBu	0.000	0.000	0.000	0.035	0.045	0.080
NH_2	0.000	0.000	0.045	0.000	0.081	0.126

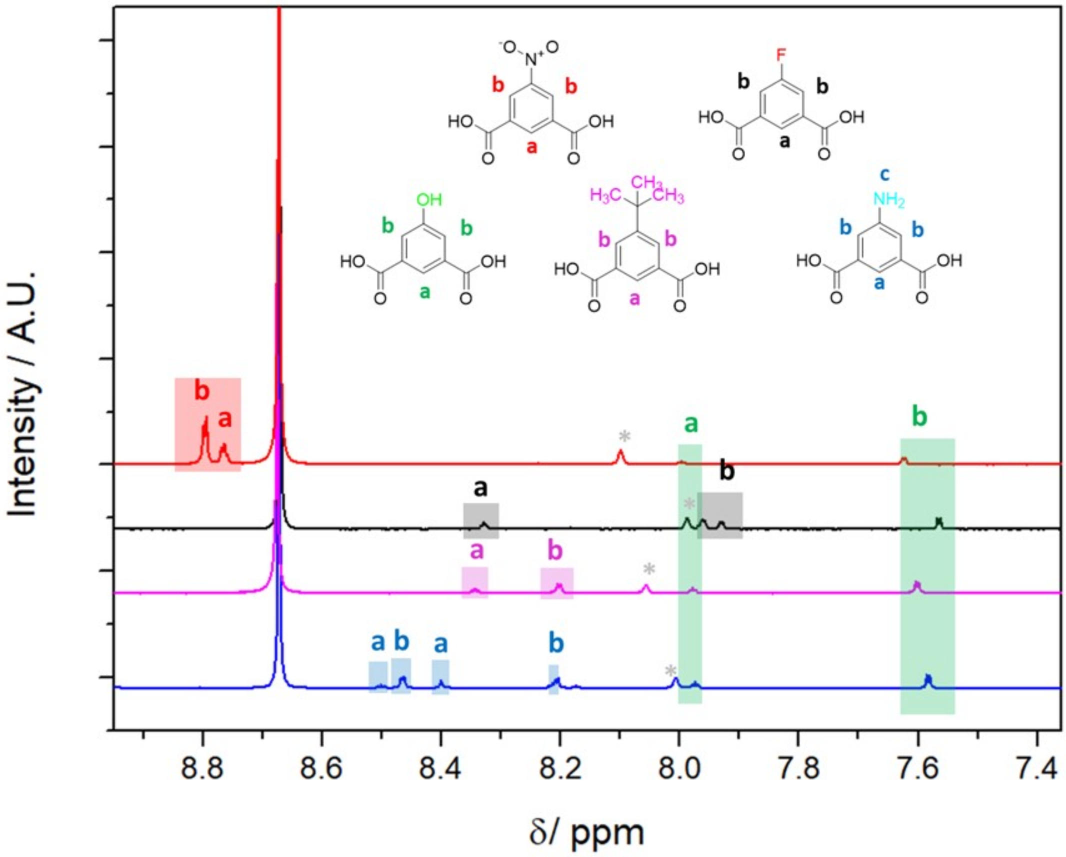

Figure S19: Representation of the acid-digested ^{1}HNMR profiles of the OH@MOD MOFs.

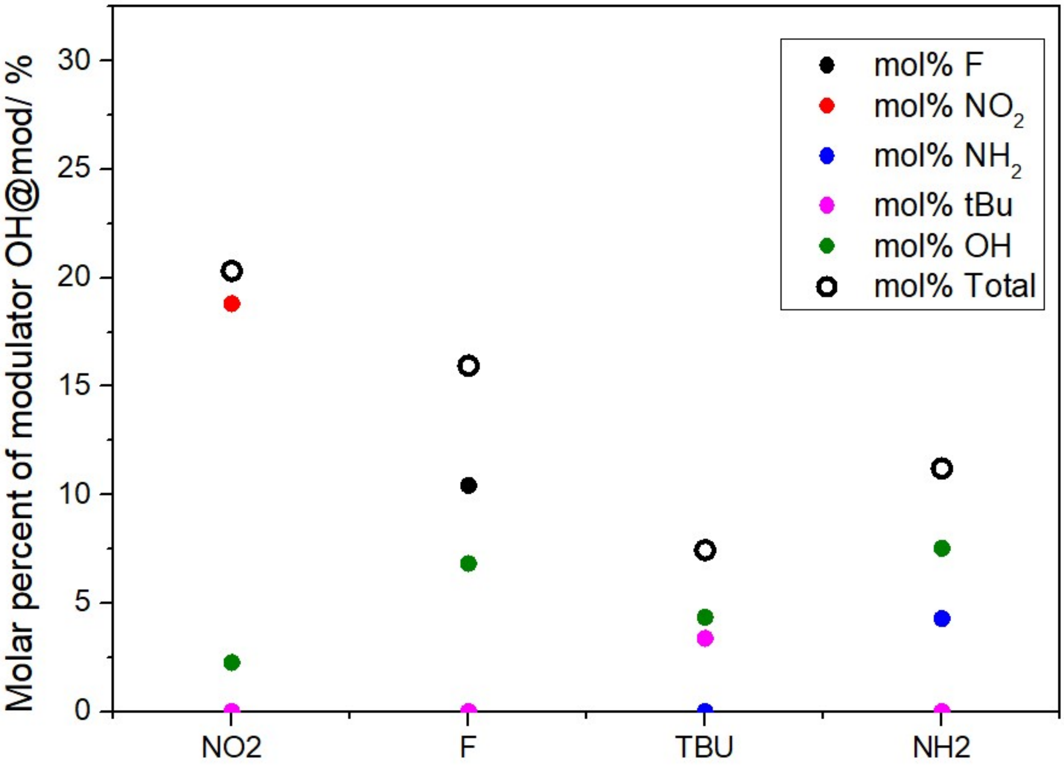

Figure S20: Modulator incorporation in molar percent for the OH@MOD MOFs.

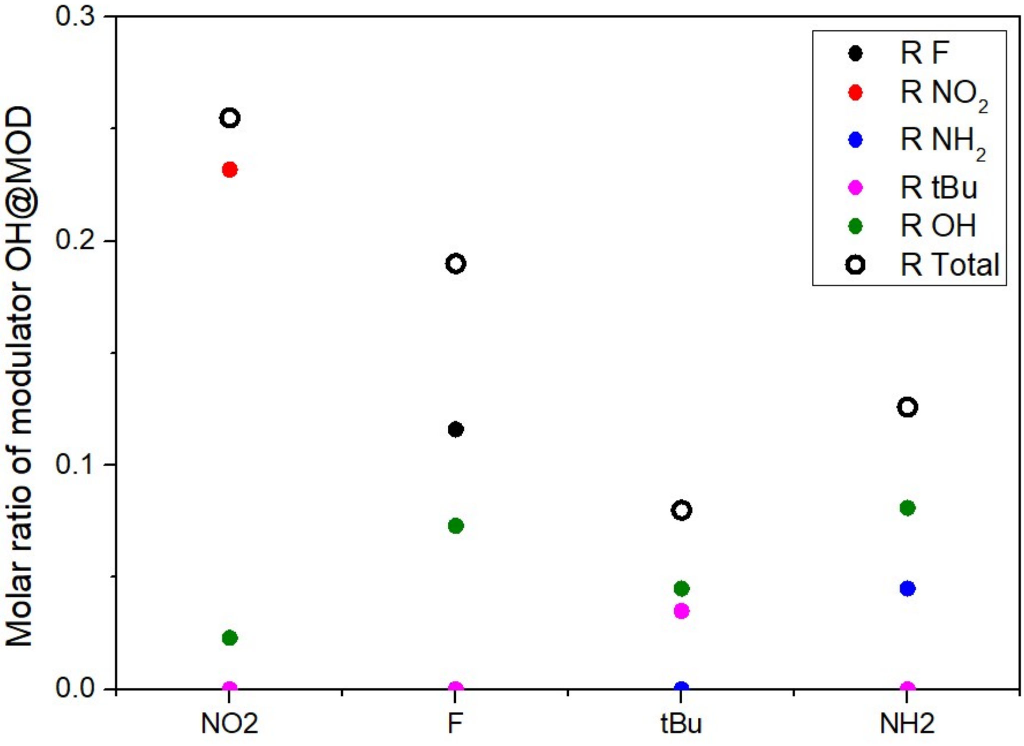

Figure S21: Modulator incorporation in molar ratio for the OH@MOD MOFs.

S.3.2.D Proton Nuclear Magnetic Resonance (^{1}HNMR) of tBu@MOD

Table S8: Tabulated data extracted from acid digested ^{1}HNMR of tBu@MOD MOFs in mol%, showing modulator and total modulator content increasing with the addition of modulator, whereas fa incorporation seems to be constant.

tBu@MOD	MOL F	MOL NO_2	MOL NH_2	MOL tBu	MOL OH	MOL Total
NO_2	0.000	19.084	0.000	8.817	0.000	24.956
F	11.304	0.000	0.000	8.458	0.000	18.022
OH	0.000	0.000	0.000	3.378	4.343	7.439
NH_2	0.000	0.000	4.242	7.212	0.000	10.875

Table S9: Tabulated data extracted from acid digested ^{1}HNMR of tBu@MOD MOFs in molar percent, showing modulator and total modulator content increasing with the addition of modulator, whereas fa incorporation seems to be constant.

tBu@MOD	R F	R NO_2	R NH_2	R tBu	ROH	R Total
NO_2	0.000	0.236	0.000	0.097	0.000	0.333
F	0.127	0.000	0.000	0.092	0.000	0.220
OH	0.000	0.000	0.000	0.035	0.045	0.080
NH_2	0.000	0.000	0.044	0.078	0.000	0.122

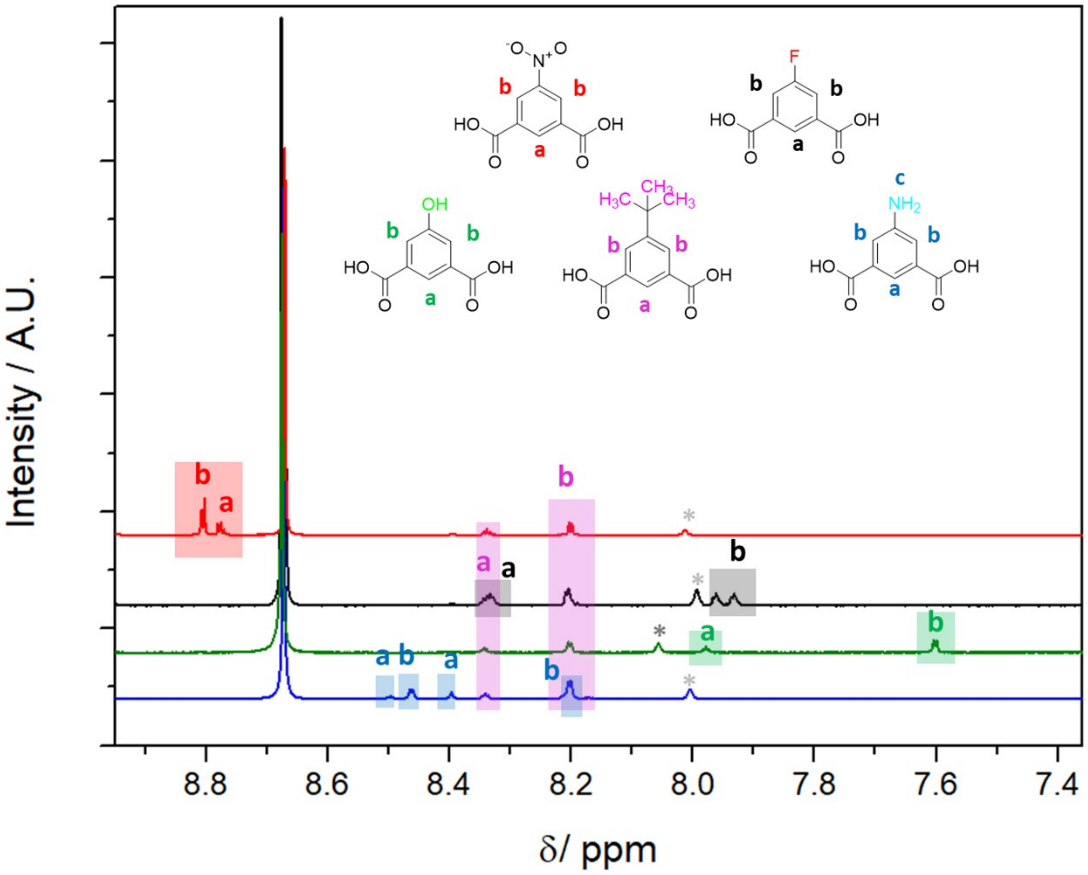

Figure S22: Representation of the acid-digested ^{1}HNMR profiles of the tBu@MOD MOFs.

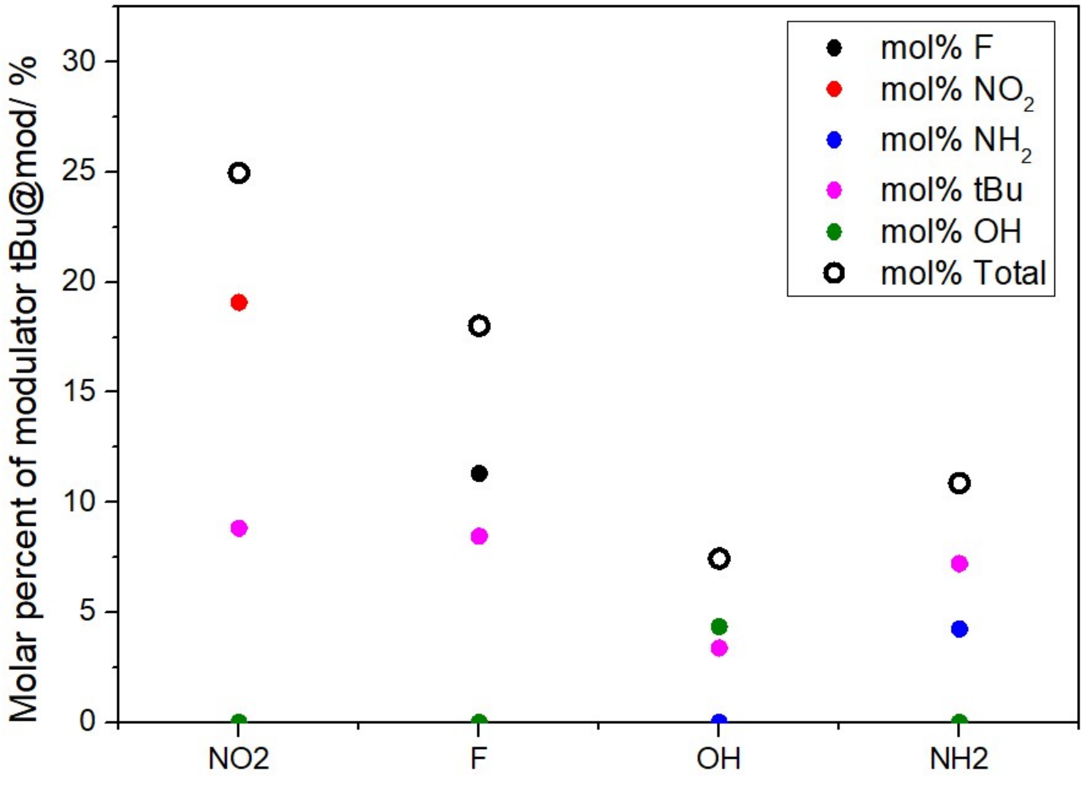

Figure S23: Modulator incorporation in molar percent for the tBu@MOD MOFs.

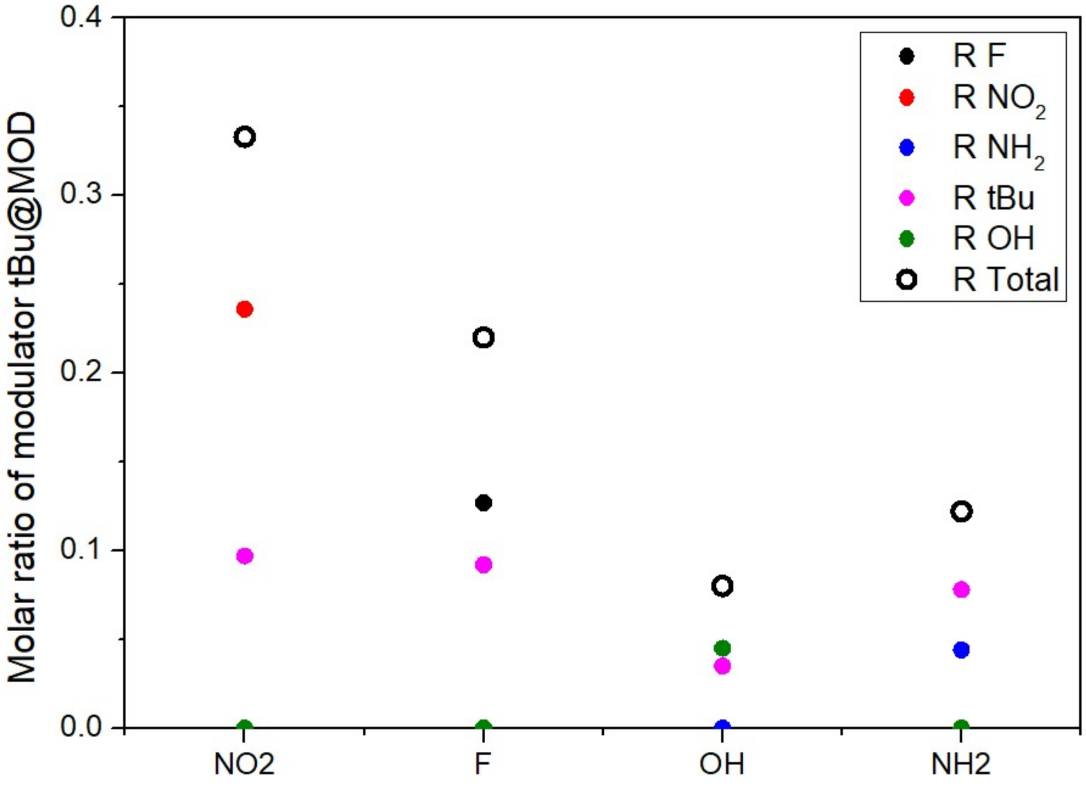

Figure S24: Modulator incorporation in molar ratio for the tBu@MOD MOFs.

S.3.2.e Proton Nuclear Magnetic Resonance (^{1}HNMR) of NH$_2$@MOD

Table S10: Tabulated data extracted from acid digested ^{1}HNMR of NH$_2$@MOD MOFs in mol%, showing modulator and total modulator content increasing with the addition of modulator, whereas fa incorporation seems to be constant.

NH$_2$@MOD	**MOL F**	**MOL NO$_2$**	**MOL NH$_2$**	**MOL tBu**	**MOL OH**	**MOL Total**
NO$_2$	0.000	15.432	2.491	0.000	0.000	17.221
F	10.334	0.000	5.449	0.000	0.000	14.740
tBu	0.000	0.000	4.288	0.000	7.532	11.210
OH	0.000	0.000	4.242	7.212	0.000	10.875

Table S11: Tabulated data extracted from acid digested ^{1}HNMR of NH$_2$@MOD MOFs in molar ratio, showing modulator and total modulator content increasing with the addition of modulator, whereas fa incorporation seems to be constant.

NH$_2$@MOD	**R F**	**R NO$_2$**	**R NH$_2$**	**R tBu**	**ROH**	**R Total**
NO$_2$	0.000	0.182	0.026	0.000	0.000	0.208

F	0.115	0.000	0.058	0.000	0.000	0.173
tBu	0.000	0.000	0.044	0.078	0.000	0.122
OH	0.000	0.000	0.045	0.000	0.081	0.126

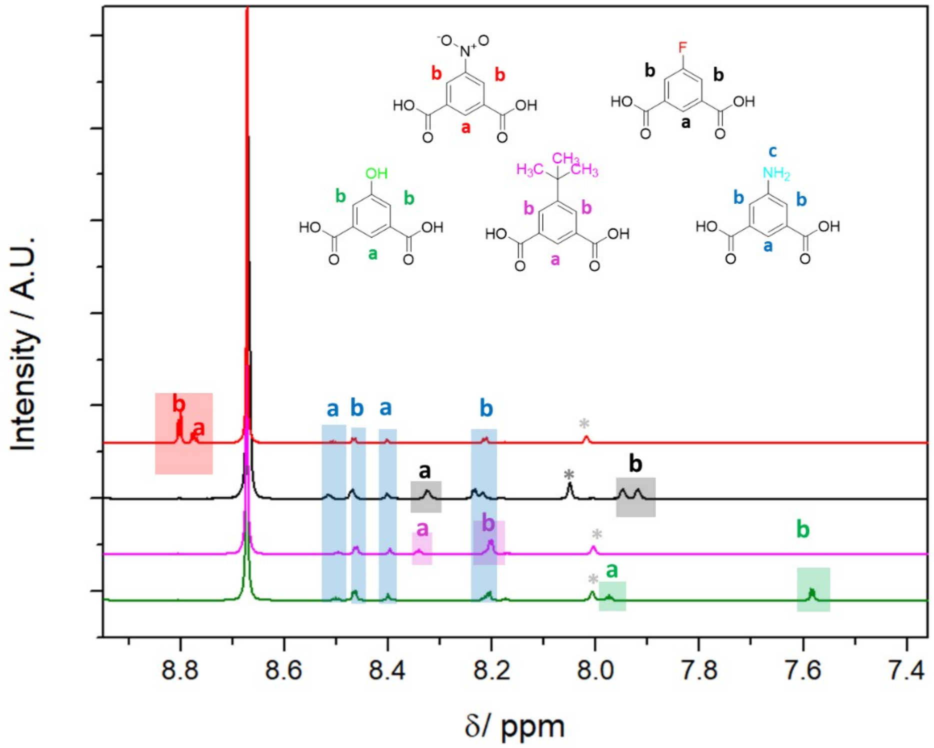

Figure S25: Representation of the acid-digested ^{1}HNMR profiles of the NH_2@MOD MOFs.

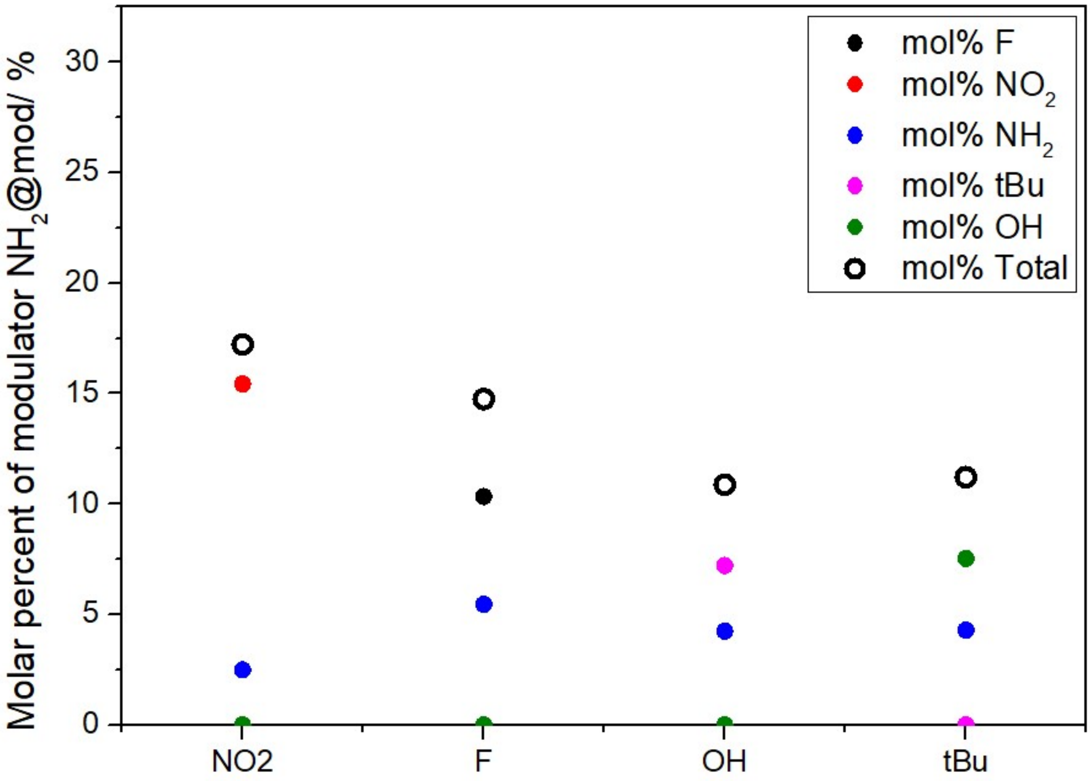

Figure S26: Modulator incorporation in molar percent for the NH_2@MOD MOFs.

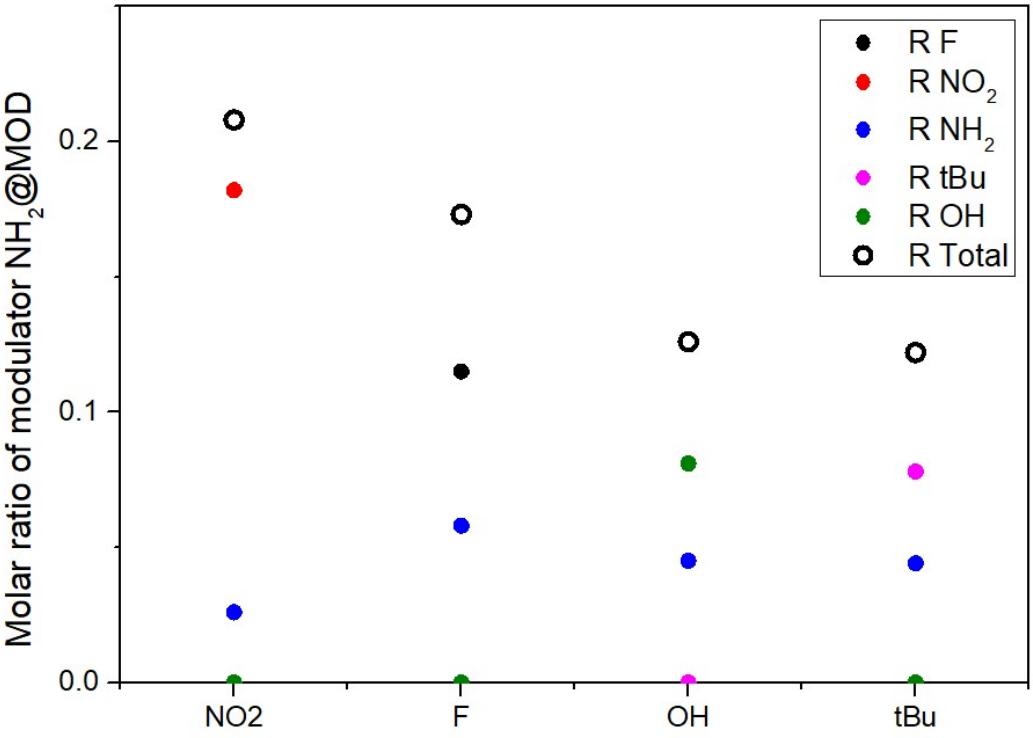

Figure S27: Modulator incorporation in molar ratio for the NH_2@MOD MOFs.

S.3.2.f Proton Nuclear Magnetic Resonance (^{1}HNMR) of tri-, tetra- and penta-modulated MOFs

Table S12: Tabulated data extracted from acid digested ^{1}HNMR of MTVM MOFs in mol%, showing modulator and total modulator content increasing with the addition of modulator, whereas fa incorporation seems to be constant.

mod@MOD	MOL F	MOL NO_2	MOL NH_2	R tBu	MOL OH	MOL Total
F@NO_2@OH (0.5)	5.466	11.058	0	0	1.817	16.712
F@NO_2@OH (1)	10.438	20.037	0	0	1.606	27.717
F@NO_2@OH@NH_2	7.773	16.713	1.774	0.000	1.967	24.419
F@NO_2@OH@NH_2@tBu	8.205	15.699	3.417	4.956	2.541	28.016

Table S13: Tabulated data extracted from acid digested ^{1}HNMR of MTVM MOFs MOFs in molar ratio, showing modulator and total modulator content increasing with the addition of modulator, whereas fa incorporation seems to be constant.

mod@MOD	R F	R NO_2	R NH_2	R tBu	R OH	R Total
F@NO_2@OH (0.5)	0.058	0.124	0	0	0.019	0.201
F@NO_2@OH (1)	0.117	0.251	0	0	0.016	0.383
F@NO_2@OH@NH_2	0.084	0.201	0.018	0.000	0.020	0.323
F@NO_2@OH@NH_2@tBu	0.089	0.186	0.035	0.052	0.026	0.389

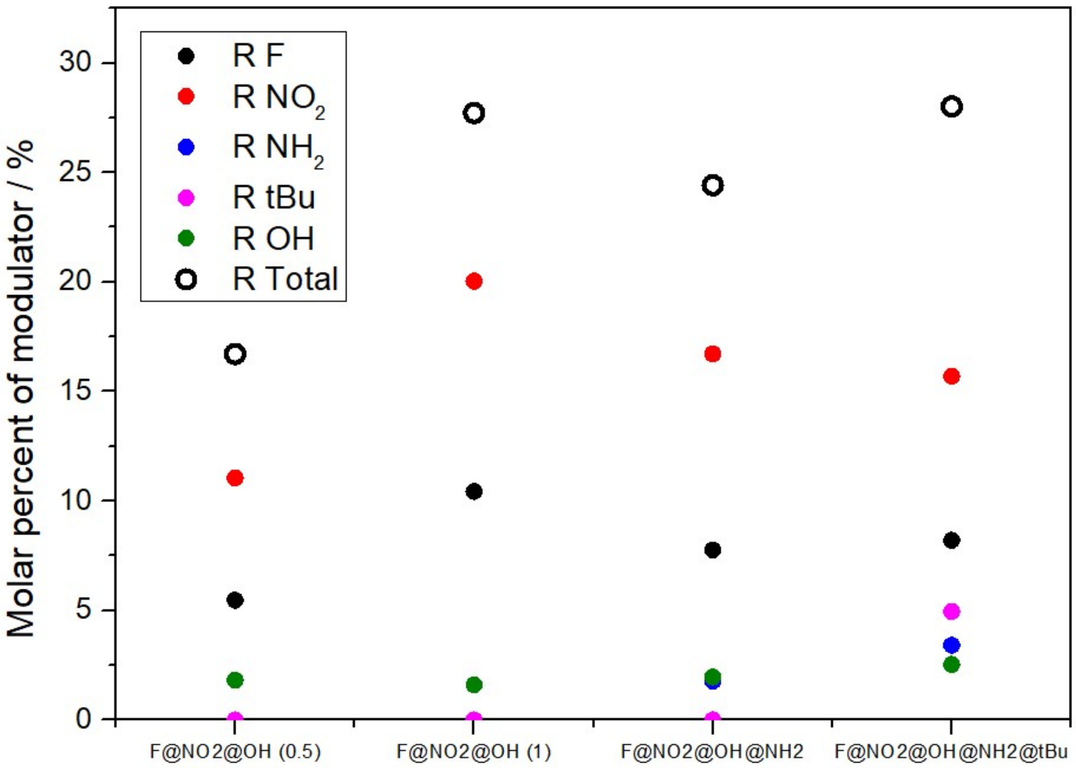

Figure S28: Modulator incorporation in molar percent for the multi-modulated MOFs.

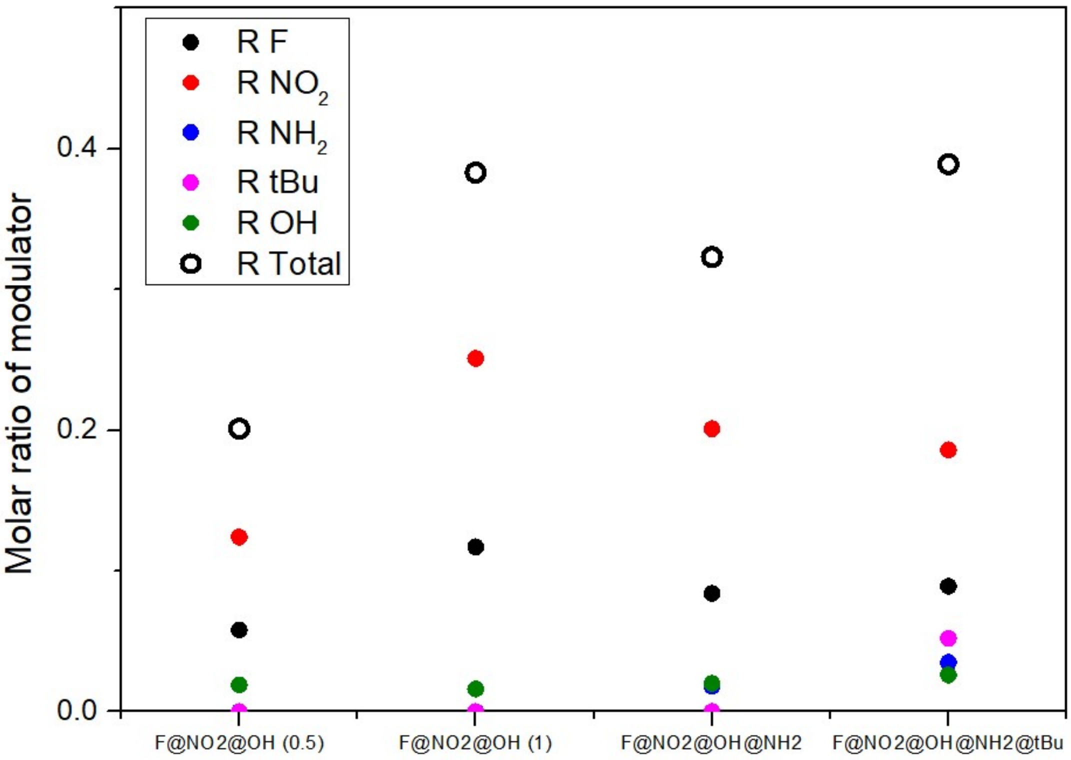

Figure S29: Modulator incorporation in molar ratio for the multi-modulated MOFs.

S.3.3 Fourier transformed Infra-Red (FT-IR)

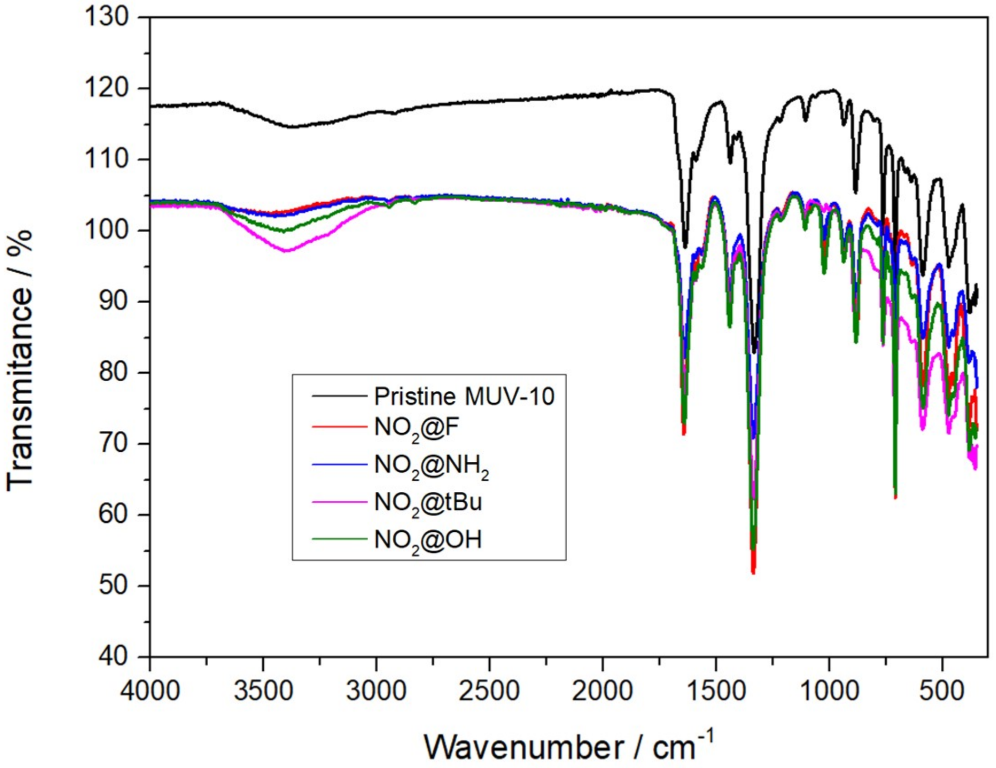

Figure S30: Raw FT-IR profiles of NO$_2$@MOD MUV-10 compared to pristine MUV-10.

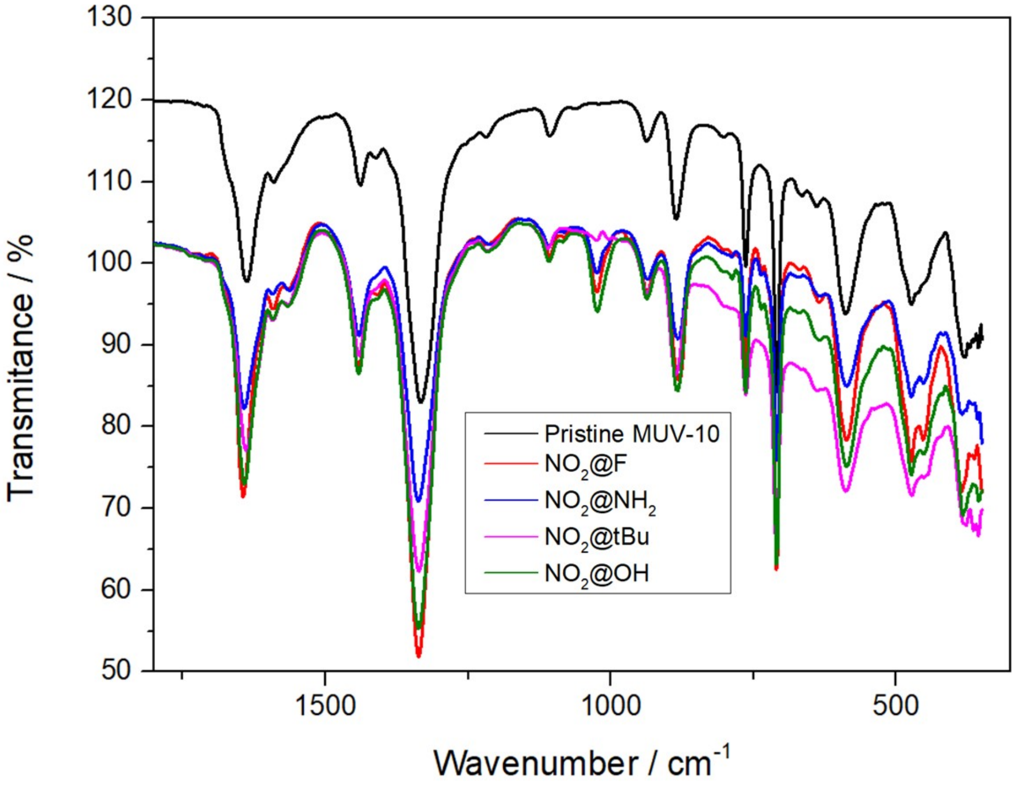

Figure S31: Amplification of the raw FT-IR profiles of NO$_2$@MOD MUV-10 compared to pristine MUV-10.

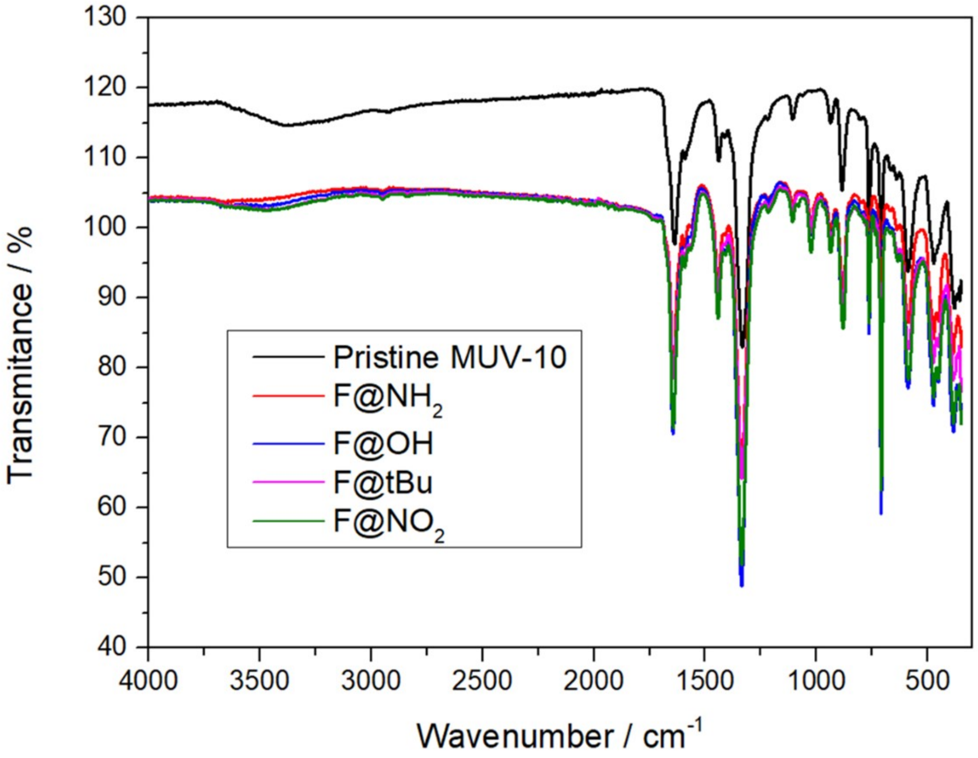

Figure S32: Raw FT-IR profiles of F@MOD MUV-10 compared to pristine MUV-10.

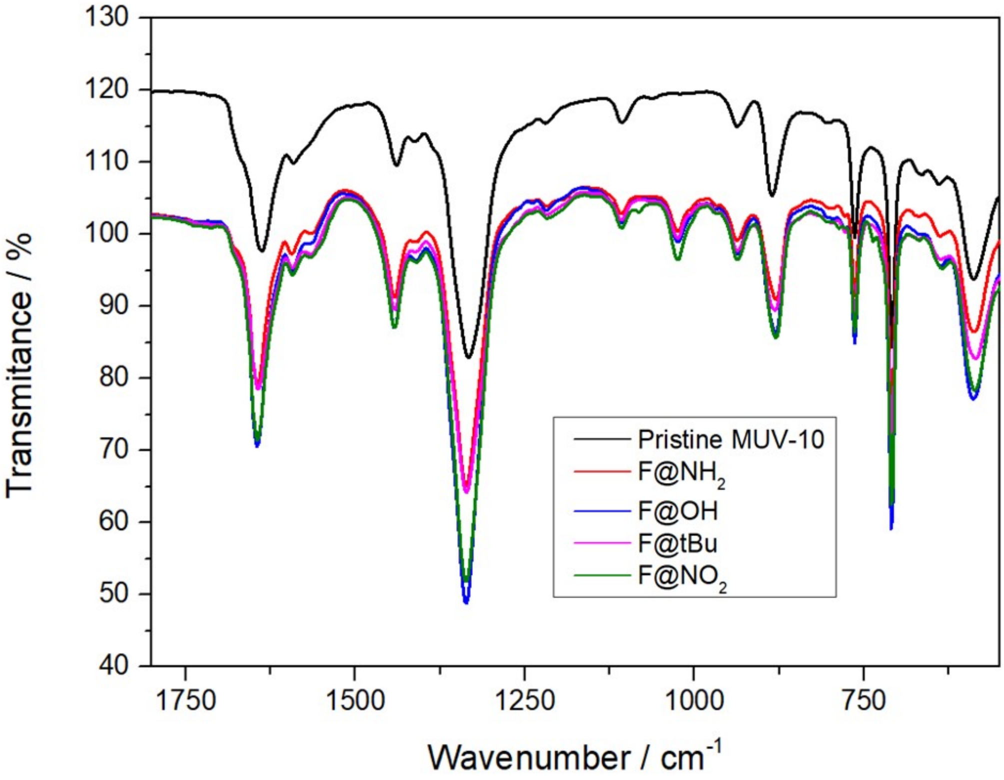

Figure S33: Amplification of the raw FT-IR profiles of F@MOD MUV-10 compared to pristine MUV-10.

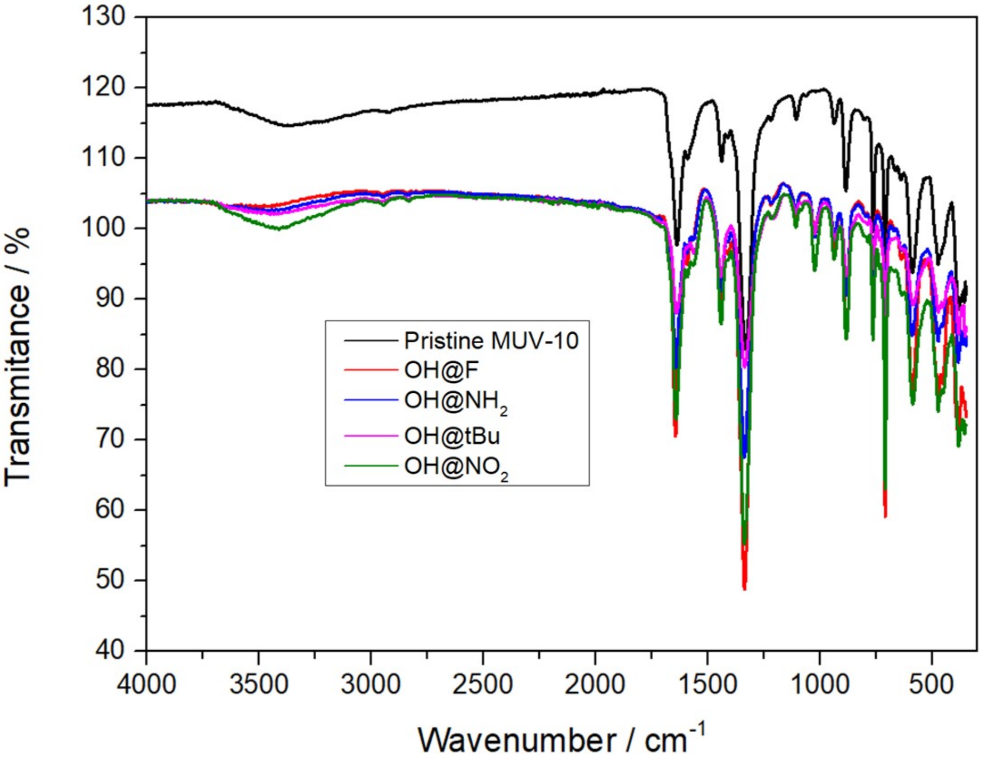

Figure S34: Raw FT-IR profiles of OH@MOD MUV-10 compared to pristine MUV-10.

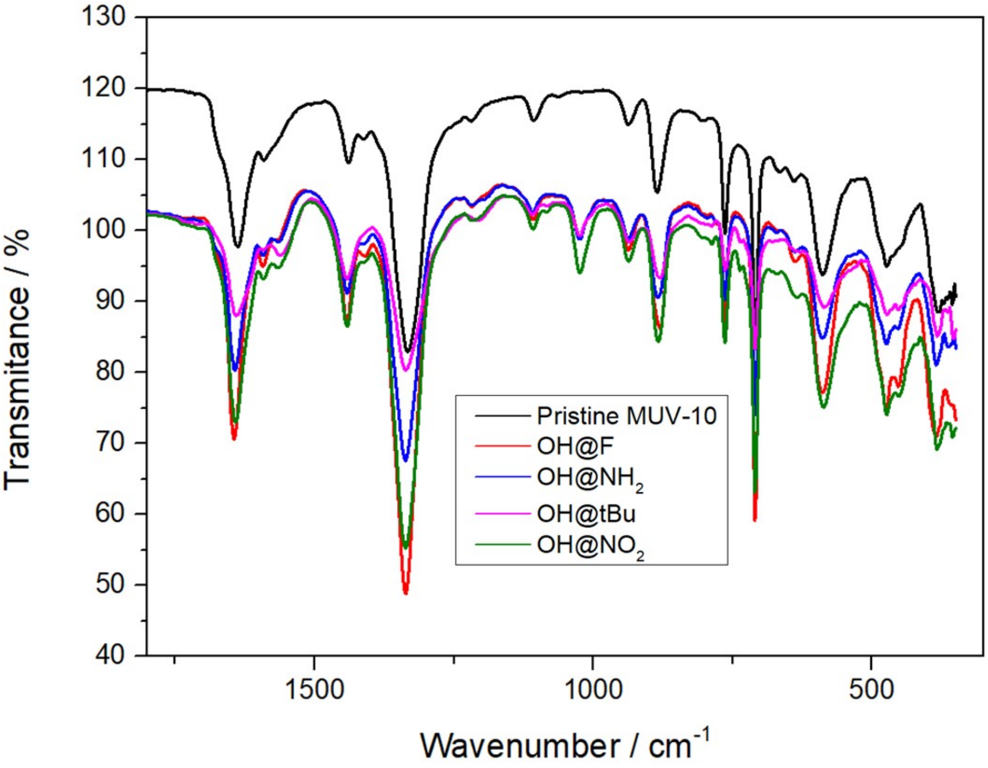

Figure S35: Amplification of the raw FT-IR profiles of OH@MOD MUV-10 compared to pristine MUV-10.

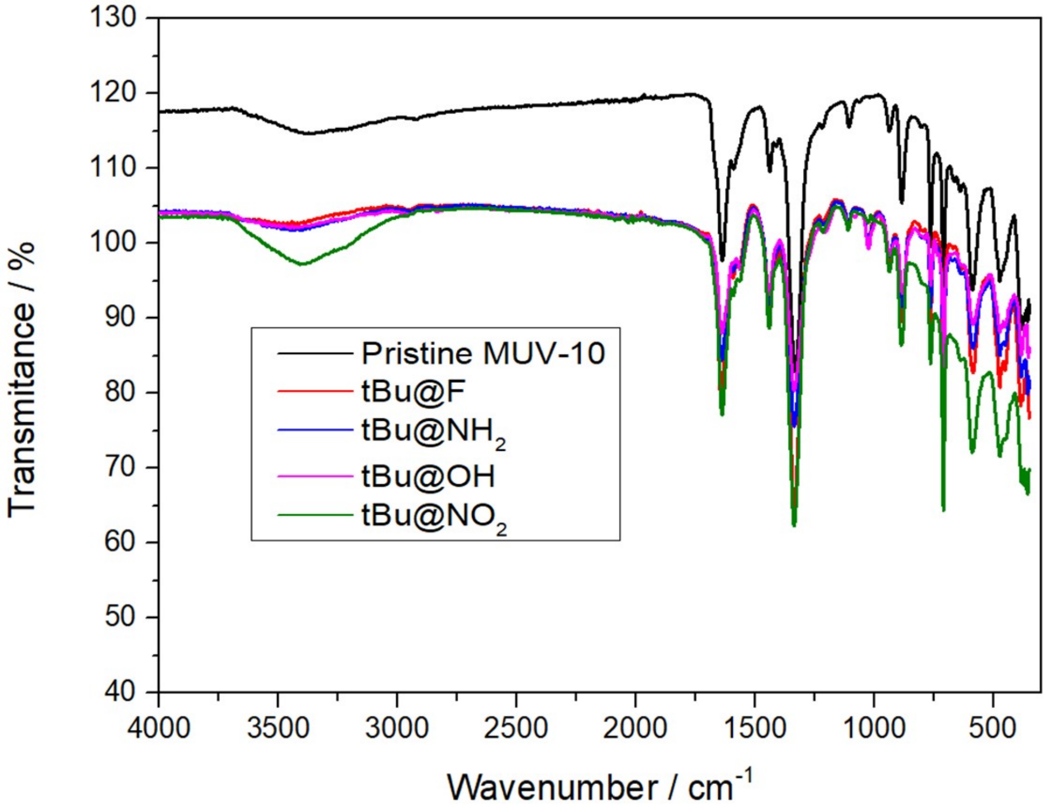

Figure S36: Raw FT-IR profiles of tBu@MOD MUV-10 compared to pristine MUV-10.

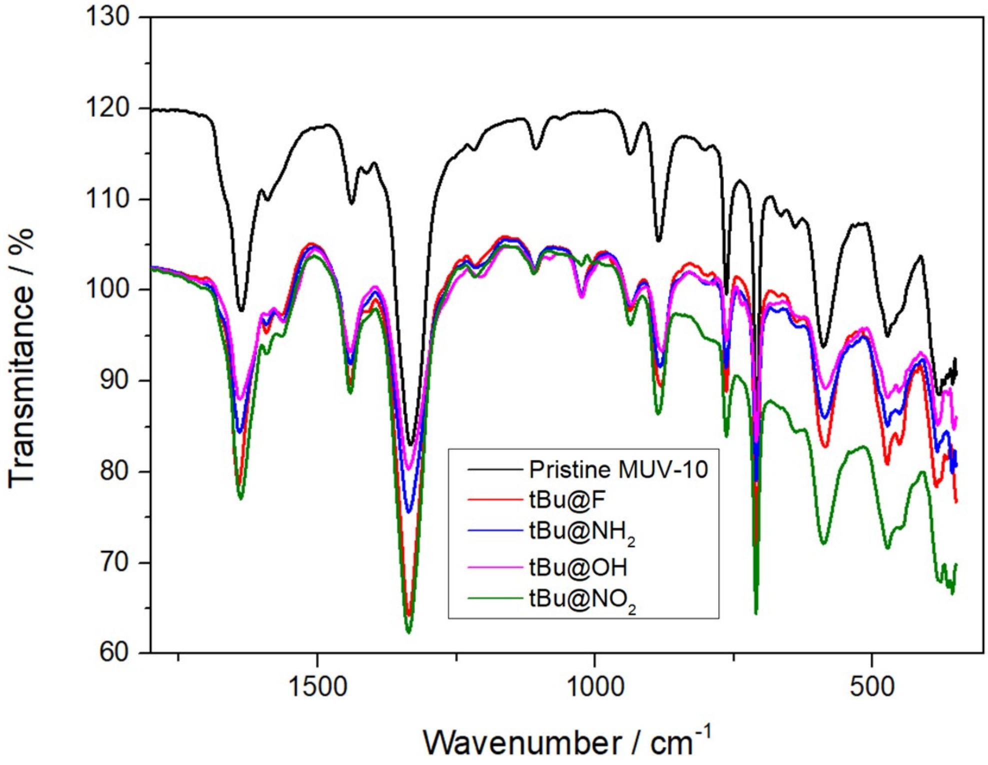

Figure S37: Amplification of the raw FT-IR profiles of tBu@MOD MUV-10 compared to pristine MUV-10.

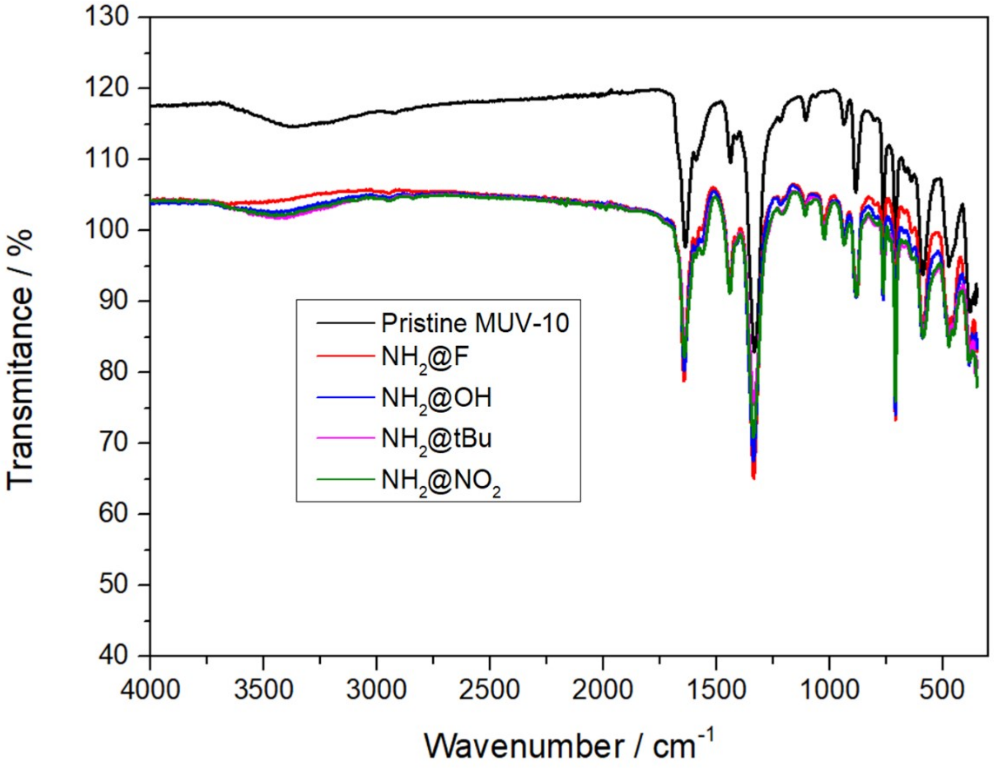

Figure S38: Raw FT-IR profiles of NH$_2$@MOD MUV-10 compared to pristine MUV-10.

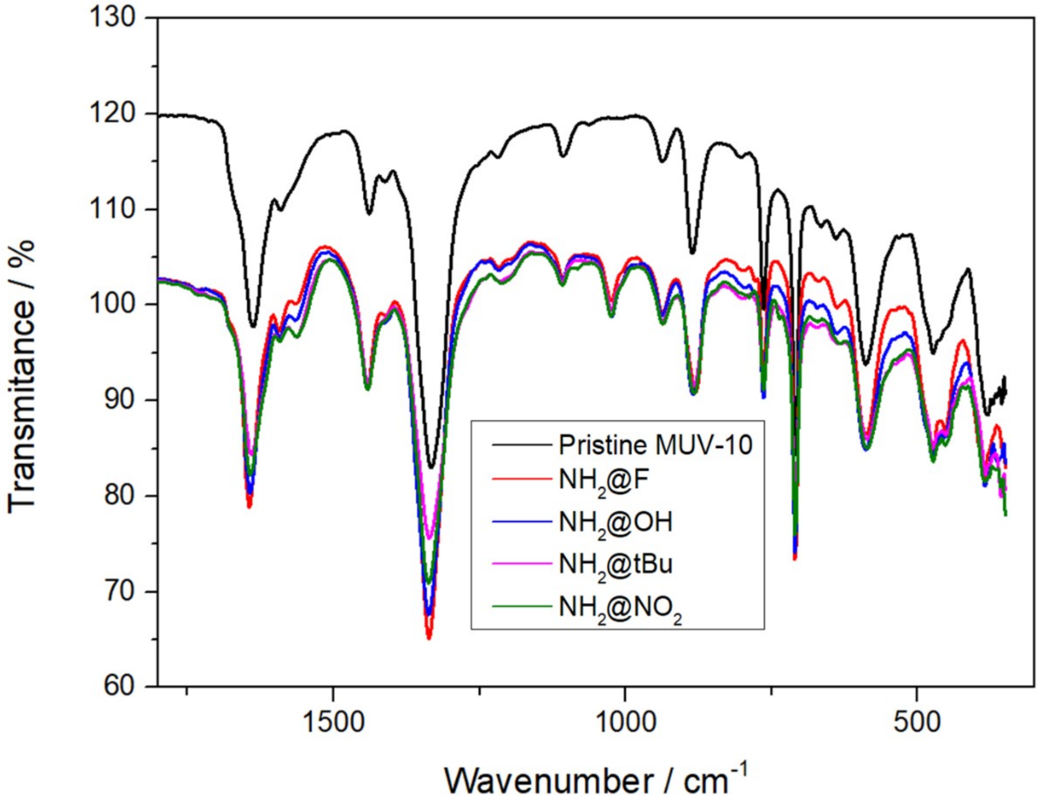

Figure S39: Amplification of the raw FT-IR profiles of NH$_2$@MOD MUV-10 compared to pristine MUV-10.

S.3.4 Scanning Electron Microscopy (SEM)

S.3.4.A Scanning Electron Microscopy Images and single point energy-dispersive X-Ray analysis (EDX)

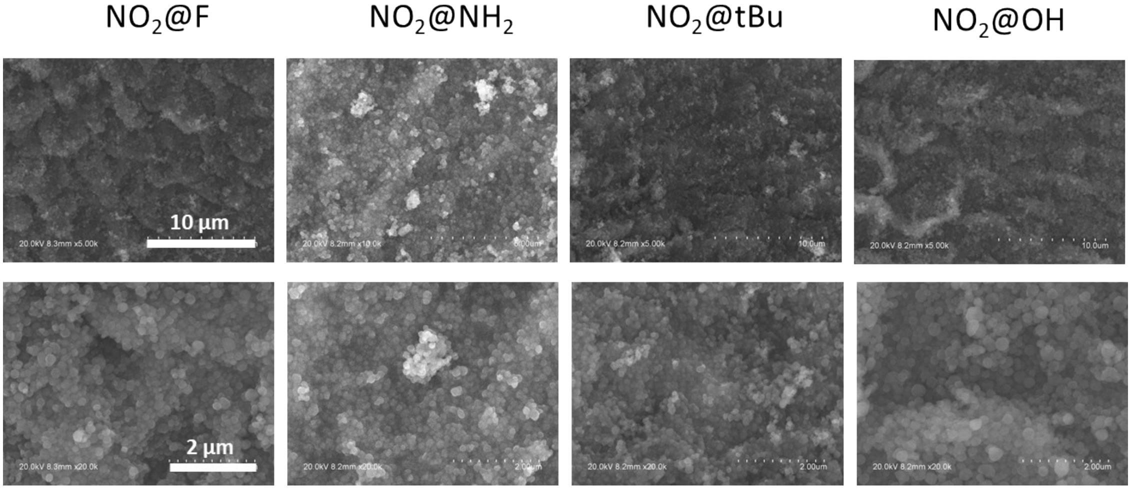

NO_2@F

NO_2@NH_2

NO_2@tBu

NO_2@OH

Figure S40: SEM images of NO_2@MOD MOFs.

Table S14: Tabulated particle sizes, standard deviations and metal content of NO_2@MOD MOFs.

NO_2@MOD	**Size(nm)**	**SD (nm)**	**% Ca *vs* Ti**
F	148.63	35.26	45
OH	259.35	36.85	46
tBu	113.89	25.30	43
NH_2	147.41	33.04	43

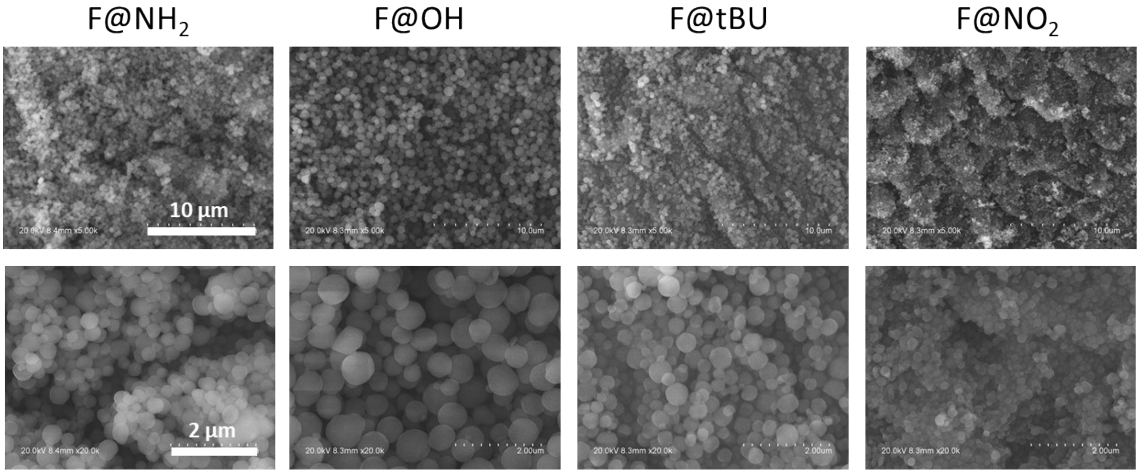

Figure S41: SEM images of F@MOD MOFs.

Table S15: Tabulated particle sizes, standard deviations and metal content of F@MOD MOFs.

F@MOD	Size(nm)	SD (nm)	% Ca *vs* Ti
NO$_2$	148.63	35.26	45
OH	549.82	137.78	42
tBu	315.62	147.09	45
NH$_2$	312.37	81.15	43

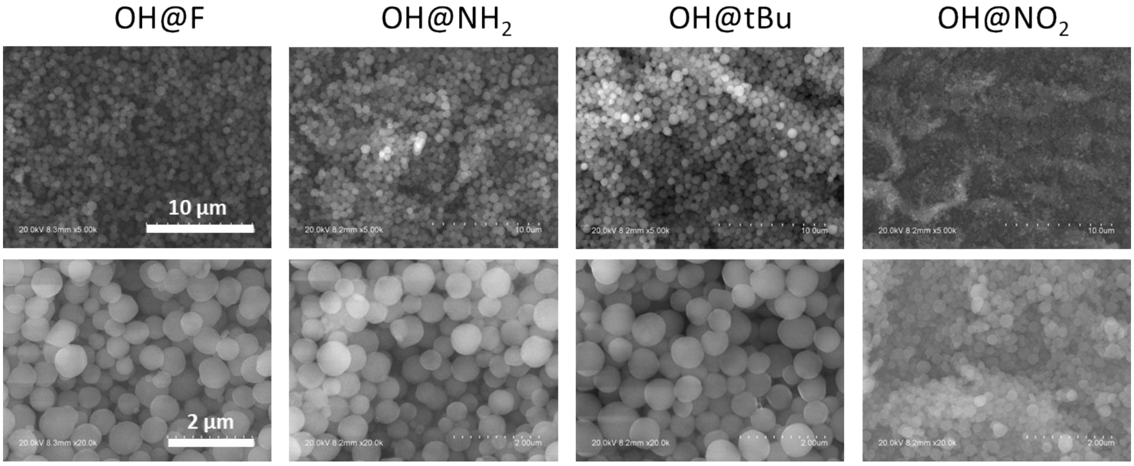

Figure S42: SEM images of OH@MOD MOFs.

Table S16: Tabulated particle sizes, standard deviations and metal content of OH@MOD MOFs.

OH@MOD	**Size(nm)**	**SD (nm)**	**% Ca *vs* Ti**
NO_2	259.35	36.85	46
F	549.82	137.78	42
tBu	624.24	109.41	45
NH_2	523.67	128.69	45

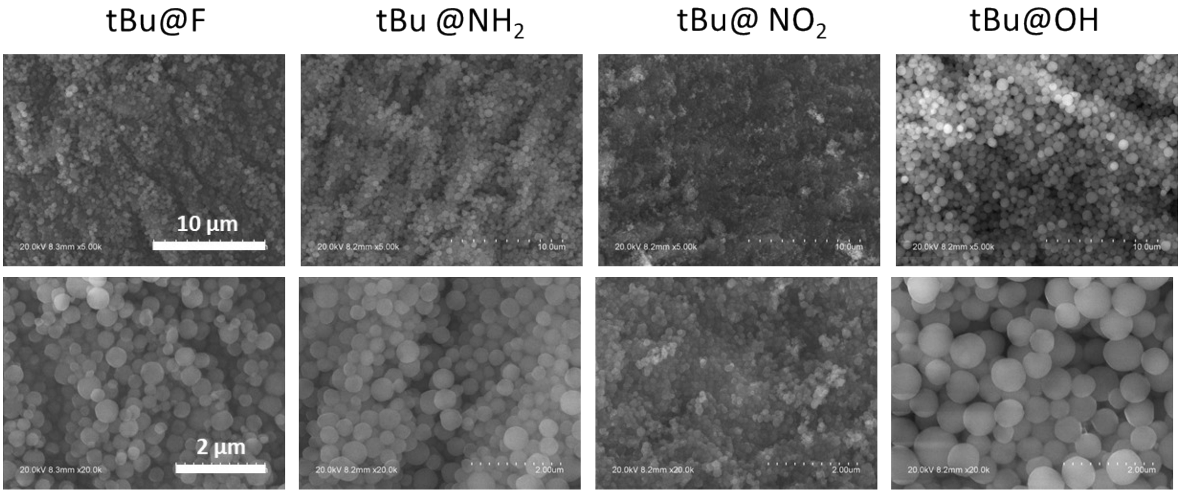

Figure S43: SEM images of tBu@MOD MOFs.

Table S17: Tabulated particle sizes, standard deviations and metal content of tBu@MOD MOFs.

tBu@MOD	**Size(nm)**	**SD (nm)**	**% Ca *vs* Ti**
NO_2	113.89	25.3	43
F	315.62	147.09	45
OH	624.25	109.42	45
NH_2	365.52	91.43	45

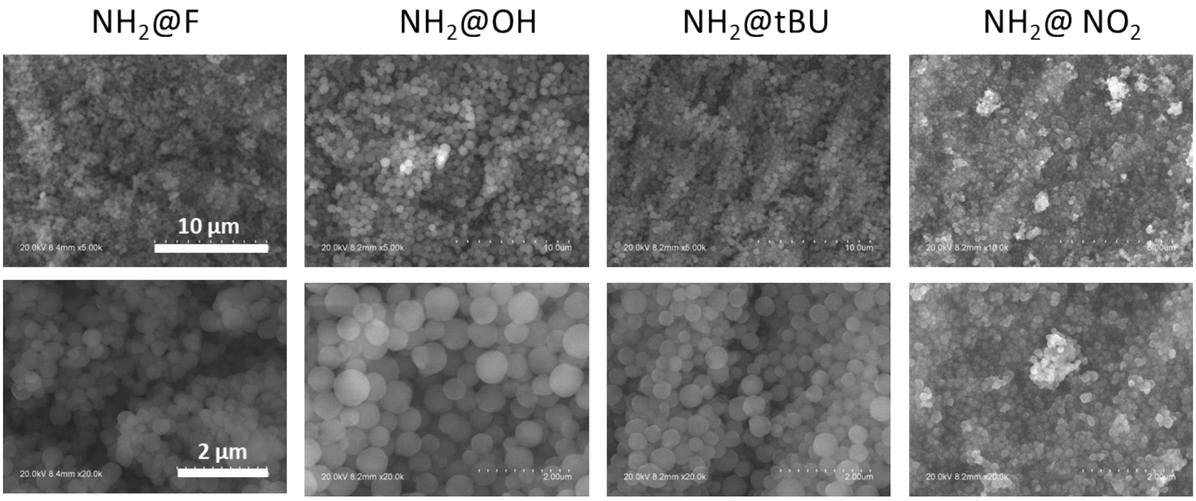

Figure S44: SEM images of NH_2@MOD MOFs.

Table S18: Tabulated particle sizes, standard deviations and metal content of NH_2@MOD MOFs.

NH_2@MOD	**Size(nm)**	**SD (nm)**	**% Ca *vs* Ti**
NO_2	147.41	33.04	43
F	312.37	81.15	43
OH	523.67	128.69	45
tBu	365.52	91.43	47

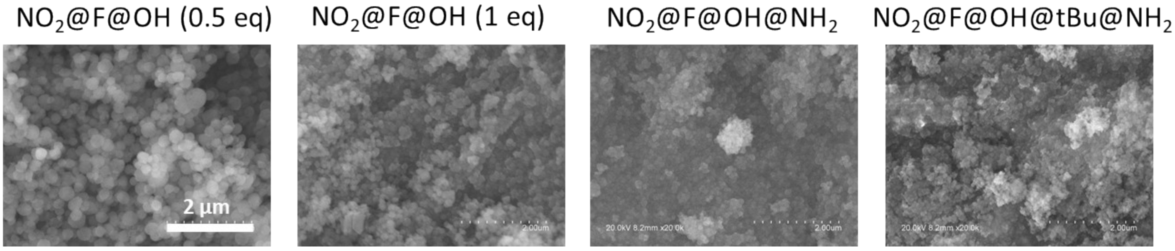

Figure S45: SEM images of multi-modulated MOFs.

Table S19: Tabulated particle sizes, standard deviations and metal content of multi-modulated MOFs.

NH_2@MOD	**Size(nm)**	**SD (nm)**	**% Ca *vs* Ti**
F@NO_2@OH (0.5)	225.0	75.4	
F@NO_2@OH (1)	112.3	33.2	
F@NO_2@OH@NH_2	89.3	19.9	
F@NO_2@OH@NH_2@tBu	47.8	16.9	

S.3.4.B Energy-dispersive X-Ray analysis (EDX) mapping.

Given the signature elements of the 5-Fluor Isophthalic acid modulator, we have performed EDX mapping of the samples containing such modulator (F@mod series and tri, tetra and penta modulated MOFs). Unfortunately, the other functionalised modulators (nitro, hydroxy, tert-butyl and amino) only have carbon, nitrogen or oxygen atoms. While carbon and oxygen are signature elements in the MOF itself, nitrogen might be present in small quantities due to the minor presence of DMF molecules. EDX mapping shows the presence of the signature elements distributed homogeneously. As a proof-of-concept, we have performed EDX on the NH_2@OH sample, showing no presence of fluorine atoms.

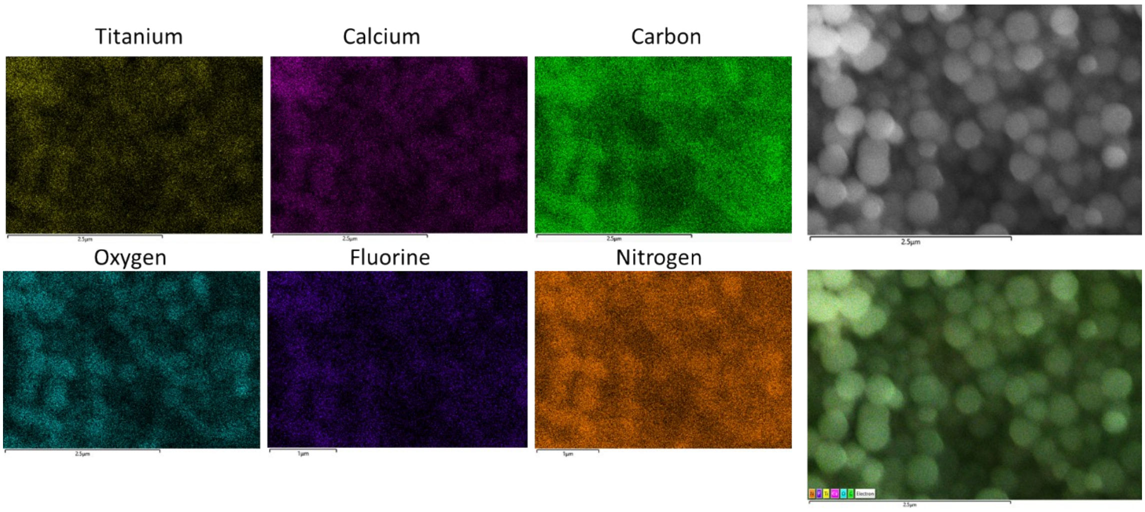

Figure S46: EDX mapping images of F@NH_2.

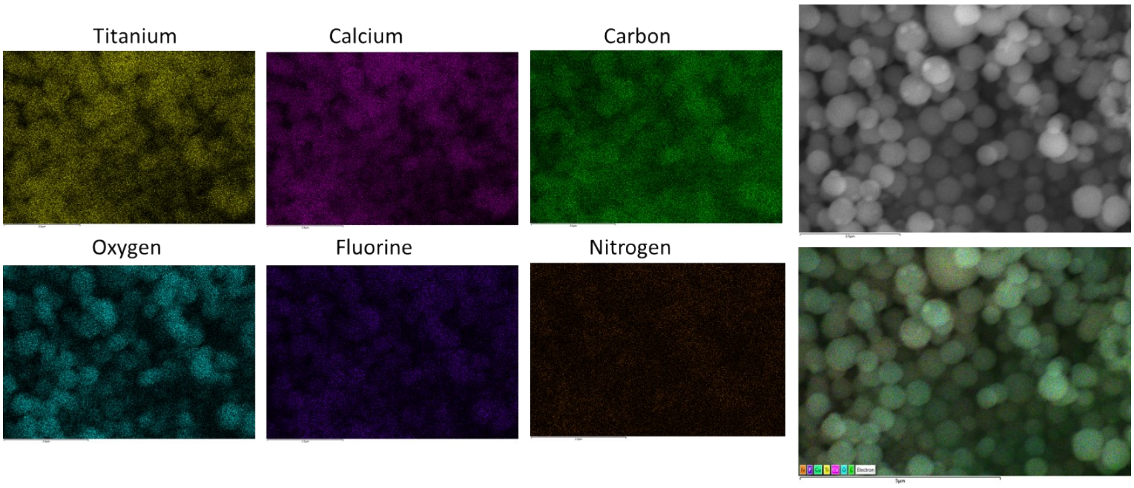

Figure S47: EDX mapping images of F@OH.

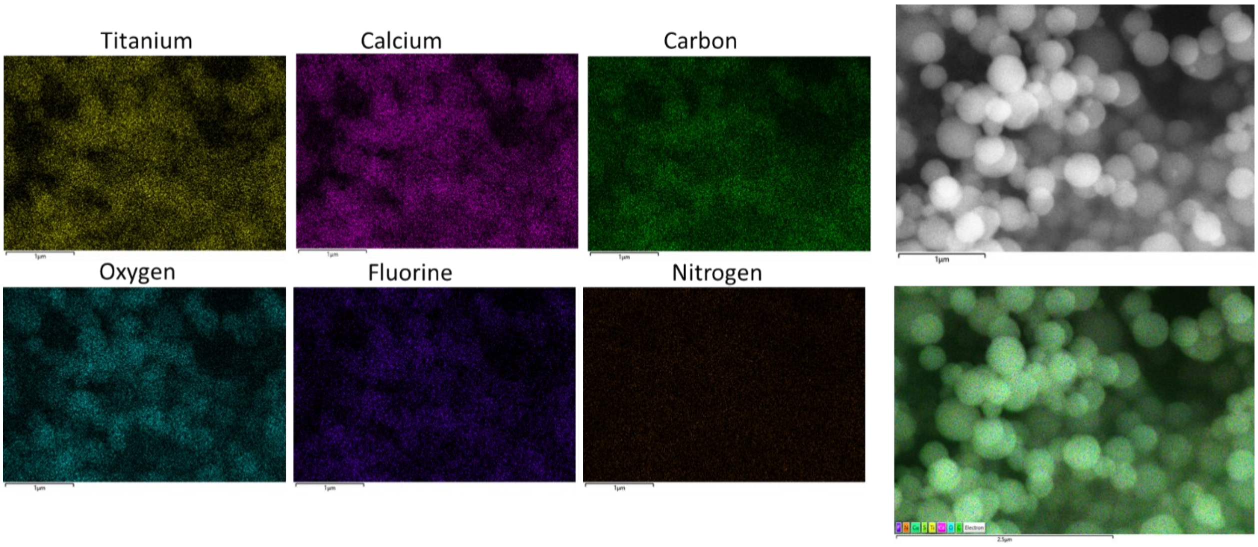

Figure S48: EDX mapping images of F@tBu.

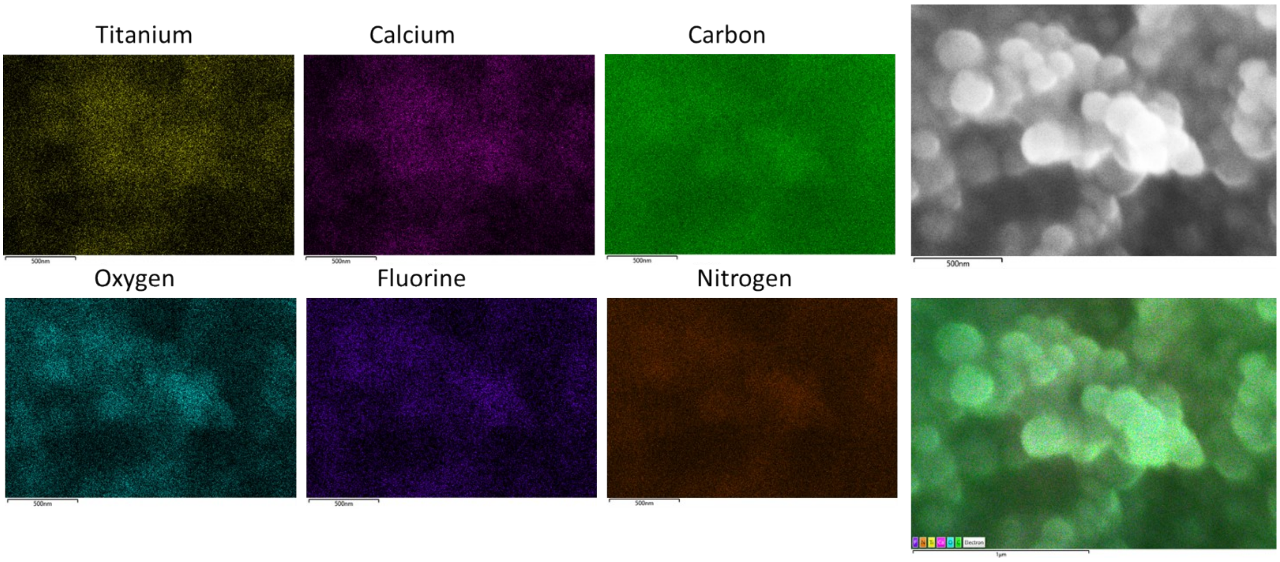

Figure S49: EDX mapping images of F@NO_2.

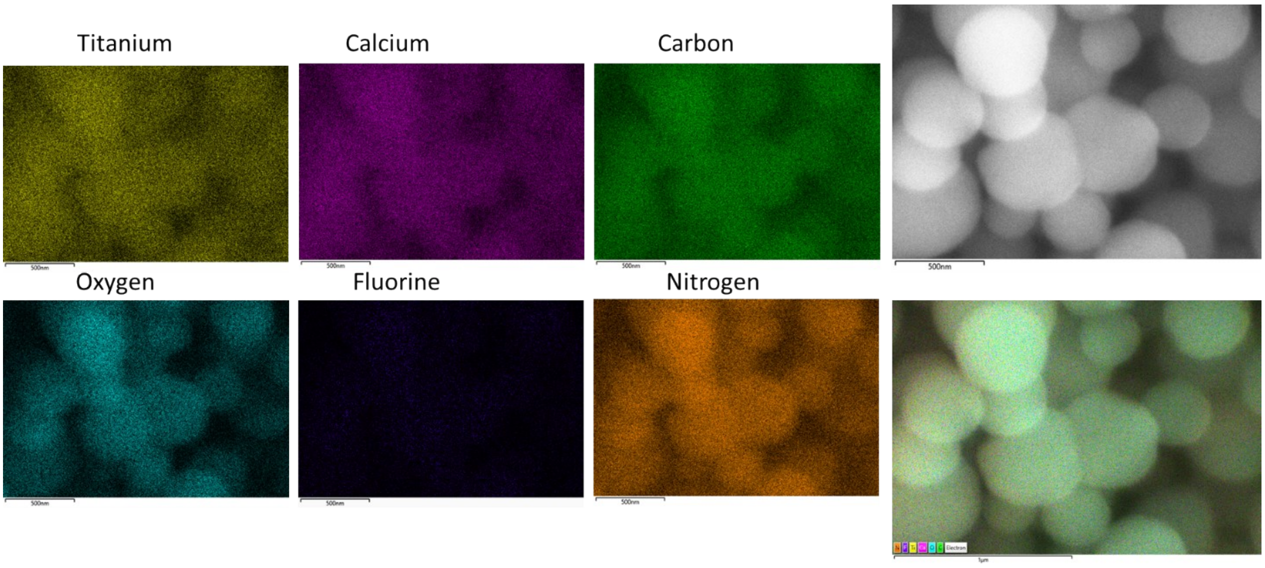

Figure S50: EDX mapping images of NH_2@OH.

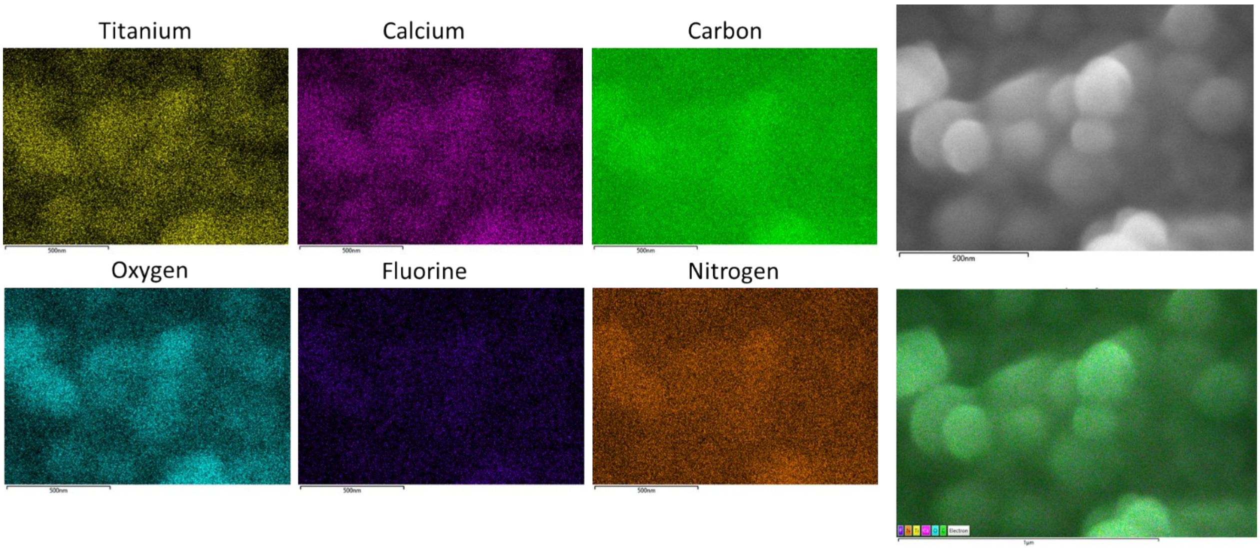

Figure S51: EDX mapping images of F@NO_2@OH (0.5).

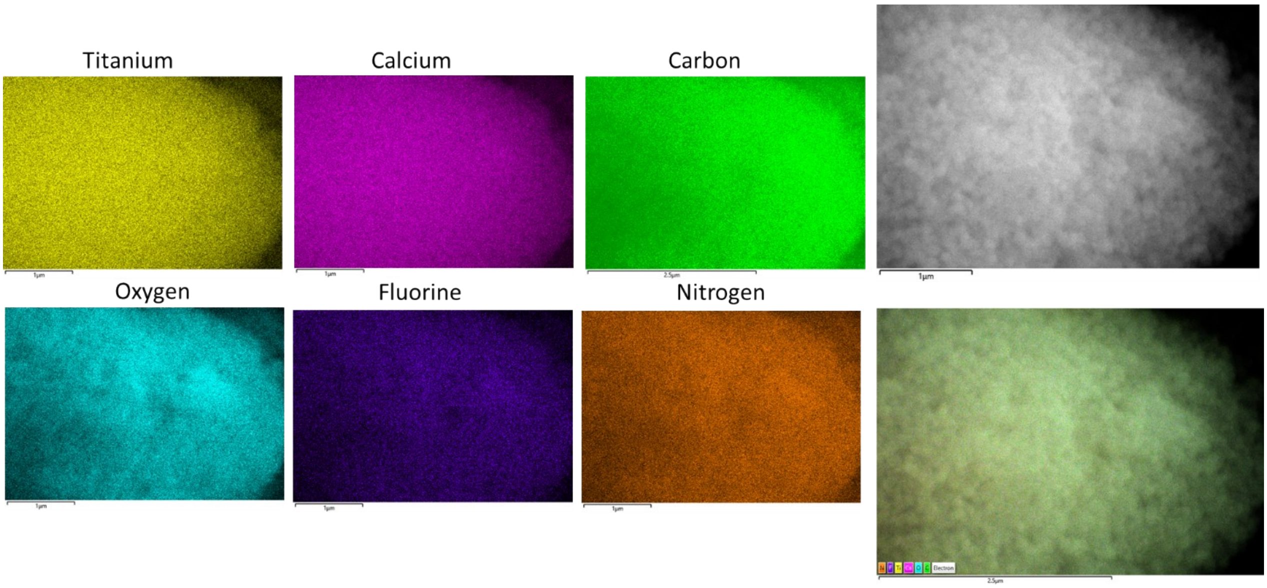

Figure S52: EDX mapping images of F@NO_2@OH (1).

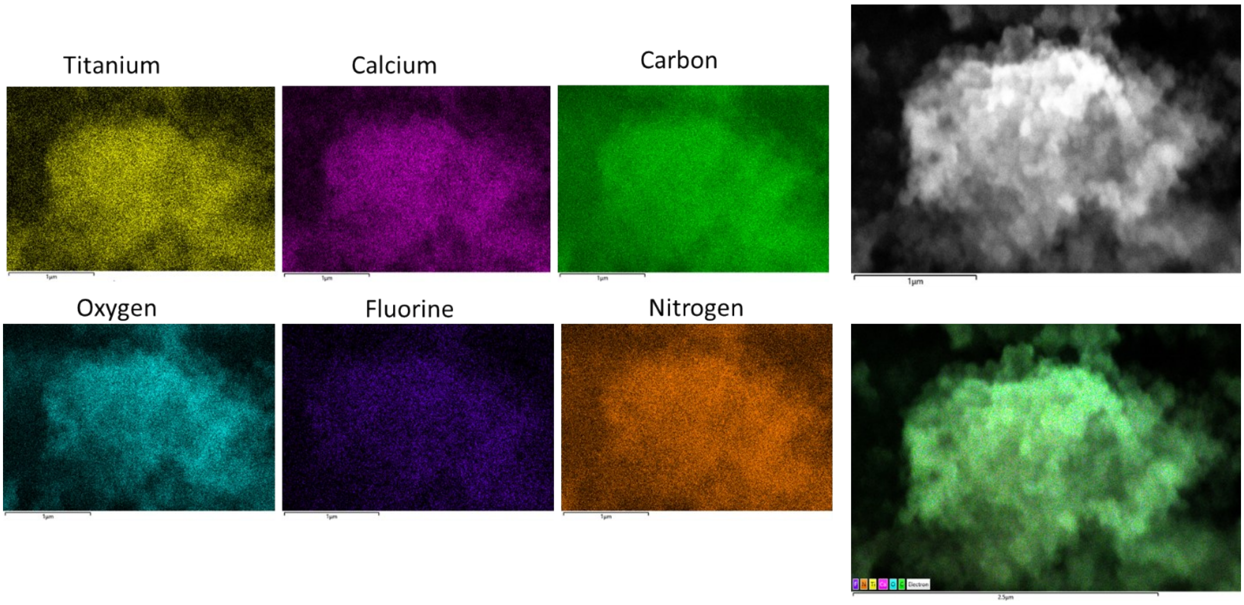

Titanium

Calcium

Carbon

Oxygen

Fluorine

Nitrogen

Figure S53: EDX mapping images F@NO_2@OH@NH_2.

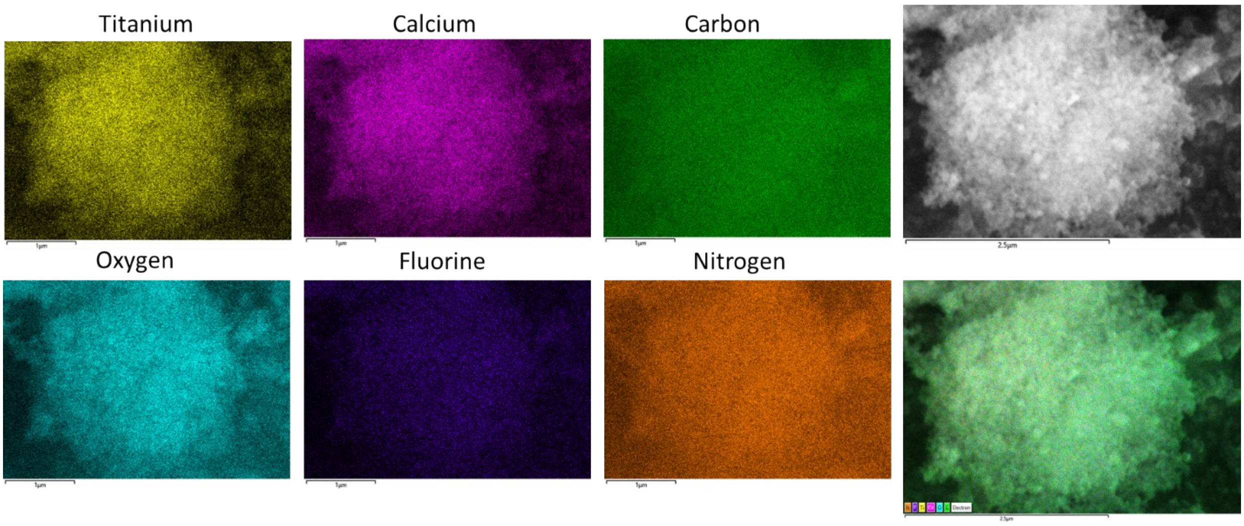

Titanium

Calcium

Carbon

Oxygen

Fluorine

Nitrogen

Figure S54: EDX mapping images F@NO_2@OH@NH_2@tBu.

S.3.5 Thermogravimetric analysis (TGA)

We have analysed the composition of MTVM MUV-10 through the combination of TGA with molar ratios determined by ^{1}HNMR, assuming that the modulators are incorporated into MUV-10 structure **$TiCaO(H_2O)_W(BTC)_X(Mod1)_y(Mod2)_z(FA)_z(OH)_D$** using

previously reported methodology.[3] As Iso-X decomposes during the decomposition range of BTC, the experimental ratio between the molecular weight of the dehydrated MOF (DH MOF) and its residue is expressed as follows for a dimodulated MOF, where Iso1 and Iso2 corresponds to two different functionalised isophthalic acid modulators:

$$\left(R_{expDH}\right) = \frac{M_w\,[DH\,MOF]}{M_w[Residue]} = \frac{M_w\,[TiCaO(BTC)_x(Iso1)_y(Iso2)_z(O)_{\frac{(4-3x-2y-2z)}{2}}]}{M_w\,[TiCaO_3]}$$

Since,

$$y\,Iso-x = x\,BDC * \left(\frac{Iso-x}{BTC}\right) NMR\,ratio$$

Then,

$$R_{expDH} = \frac{M_w\,[TiCaO(BTC)_x(Iso1)_{xnmr1}(Iso2)_{xnmr2}(O)_{\frac{(4-3x-2xnmr1-2xnmr2)}{2}}]}{M_w\,[TiCaO_3]}$$

$$XBTC = \frac{\left(R_{expDH} *\ M_w\,[TiCaO_3]\right) - M_w\,TiCaO - 2 * M_w[O]}{M_w\,[BTC] + nmr1 * M_w[Iso1] + nmr2 * M_w[Iso2] - \Bigg(\frac{(3+2nmr1+2nmr2)}{2}}$$

Once X (ligands, btc) has been obtained,

$$y\,Iso1 = x\,BDC * \left(\frac{Iso1}{BTC}\right) NMR\,ratio1$$

$$z\,Iso2 = x\,BDC * \left(\frac{Iso2}{BTC}\right) NMR\,ratio2$$

$$z\,Formate = number\,of\,BDC * \left(\frac{FA}{BTC}\right) NMR\,ratio$$

The number of OH needed to compensate the charge can be calculated using the following equation:

$$4Ti + 2Ca = 2 + 3XBTC + 2yIso1 + 2zIso2 + XNMRFA + OH$$

Then $OH\ = 4 - 3XBTC - 2yIso1 - 2zIso2 - XNMRFA$

Once the number of linkers, modulators and defect-compensating species has been determined, number of water molecules is calculated as:

$$Experimental\frac{MOF}{Residue}Ratio\,\left(R_{exp}\right) = \frac{M_w\,[Calculated\,MOF] + x * M_w\,[H_2O]}{M_w\,[TiCaO_3]}$$

$$X\,(H_2O) = \frac{\left(R_{exp} * \; M_w\,[TiCaO_3]\right) - M_w\,[Calculated\,MOF]}{M_w\,[H_2O]}$$

Please note that the same mathematical methodology is applied for tri, tetra and penta modulated MOFs. [3]

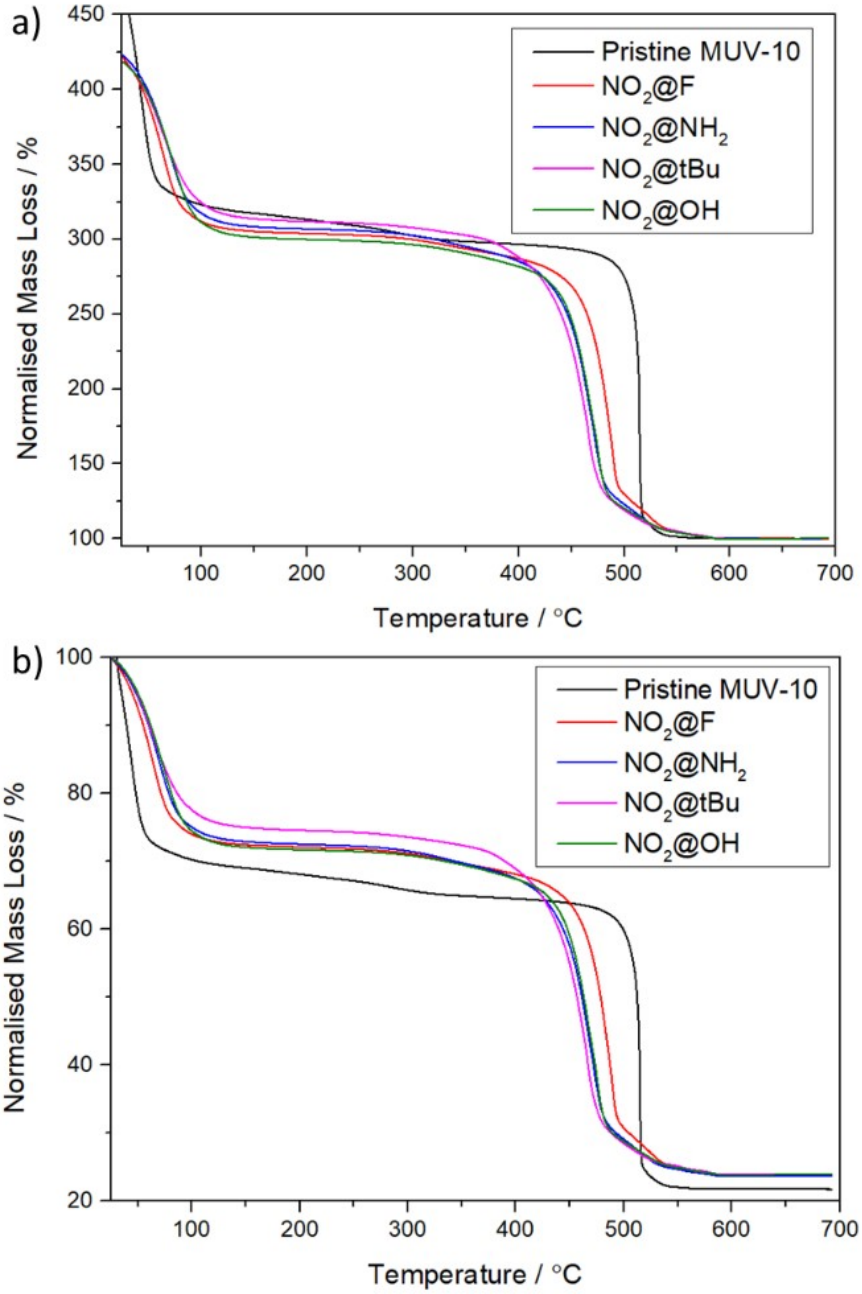

Figure S55: TGA profiles of NO_2@MOD MODs compared to pristine MUV-10, a) with the end of the decomposition profiles (residue) normalised to 100% and b) with the start of the decomposition profile normalised to 100%.

Table S20: Data extracted from TGA analysis for the model framework [$TiCaO(H_2O)_w(btc)_X(Iso\text{-}1)_y(Iso\text{-}2)_z(OH)_d$]. Note that the missing linker is 1.33-x and the missing linker molar percent (ML%) (1.33-btc)/btc*100.[2–4]

Sample	Ratio BTC/TI	Iso-F	Iso-NO_2	Iso-NH_2	Iso-tBu	Iso-OH	OH-	H_2O	ML%	Coordination number
pristine	1.403	0.000	0.000	0.000	0.000	0.000	-0.209	1.840	-5.485	13.05
NO_2@F	0.936	0.140	0.277	0.000	0.000	0.000	0.359	1.443	29.620	11.53
NO_2@OH	1.049	0.000	0.243	0.000	0.000	0.024	0.319	1.440	21.132	11.59
NO_2@tBU	1.041	0.000	0.245	0.000	0.101	0.000	0.186	1.931	21.753	12.053
NO_2@NH_2	1.146	0.000	0.209	0.029	0.000	0.000	0.084	1.395	13.813	11.83

Table S21: Data extracted from TGA analysis.

Sample	Iso per ML	ML out of 8
pristine	0.000	-0.418
NO_2@F	1.057	2.384
NO_2@OH	0.951	1.706
NO_2@tBU	1.196	1.756
NO_2@NH_2	1.298	1.122

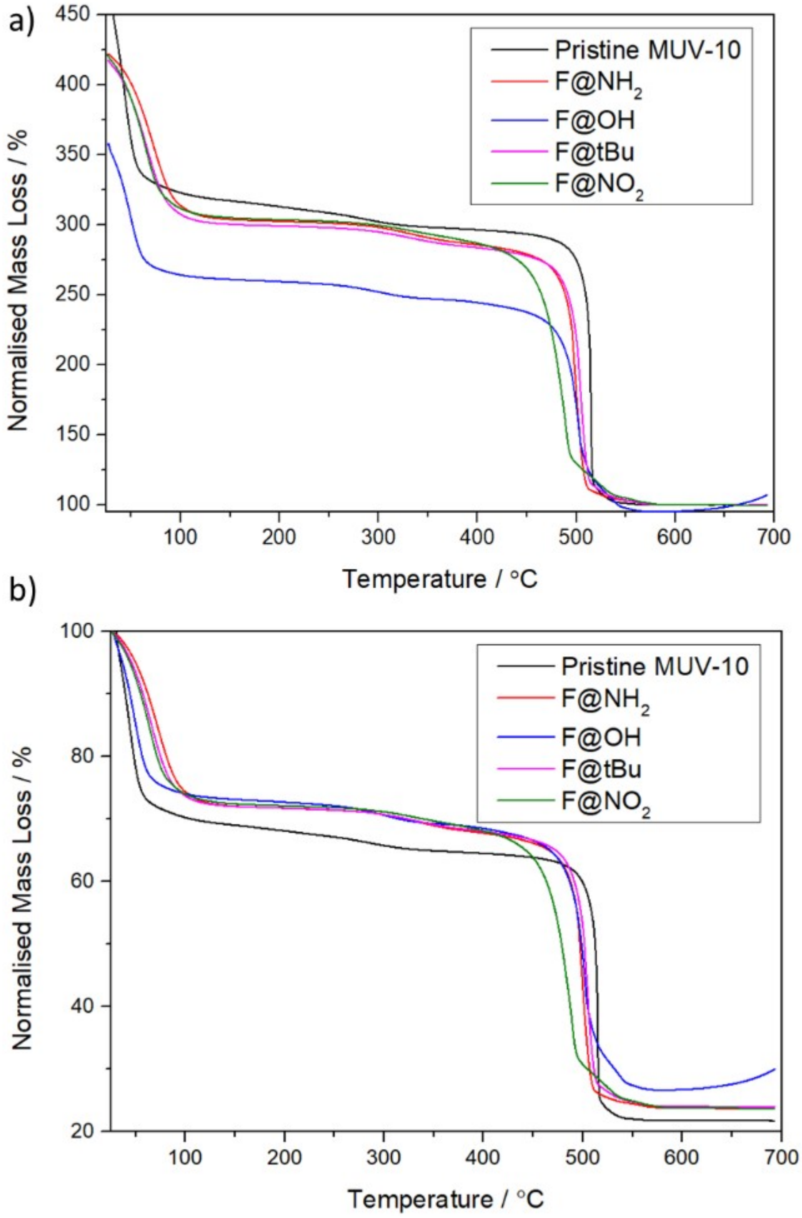

Figure S56: TGA profiles of F@MOD MODs compared to pristine MUV-10, a) with the end of the decomposition profiles (residue) normalised to 100% and b) with the start of the decomposition profile normalised to 100%.

Table S22: Data extracted from TGA analysis for the model framework [$TiCaO(H_2O)_w(btc)_X(Iso\text{-}1)_y(Iso\text{-}2)_z(OH)_d$]. Note that the missing linker is 1.33-x and the missing linker molar percent (ML%) (1.33-btc)/btc*100.[2–4]

Sample	Ratio BTC/TI	Iso-F	Iso-NO_2	Iso-NH_2	Iso-tBu	Iso-OH	OH-	H_2O	Ml%	Coordination number
pristine	1.403	0.000	0.000	0.000	0.000	0.000	-0.209	1.840	-5.485	13.05
F@NO_2	0.936	0.140	0.277	0.000	0.000	0.000	0.359	1.443	29.620	11.53
F@OH	0.876	0.102	0.000	0.000	0.000	0.064	1.038	1.224	34.099	11.06
F@tBu	1.091	0.139	0.000	0.000	0.101	0.000	0.246	1.448	17.935	12.00
F@NH_2	1.138	0.131	0.000	0.066	0.000	0.000	0.192	2.802	14.426	13.48

Table S23: Data extracted from TGA analysis.

Sample	Iso per ML	ML out of 8
pristine	0.000	-0.418
F@NO_2	1.057	2.384
F@OH	0.367	2.741
F@tBu	1.006	1.451
F@NH_2	1.026	1.171

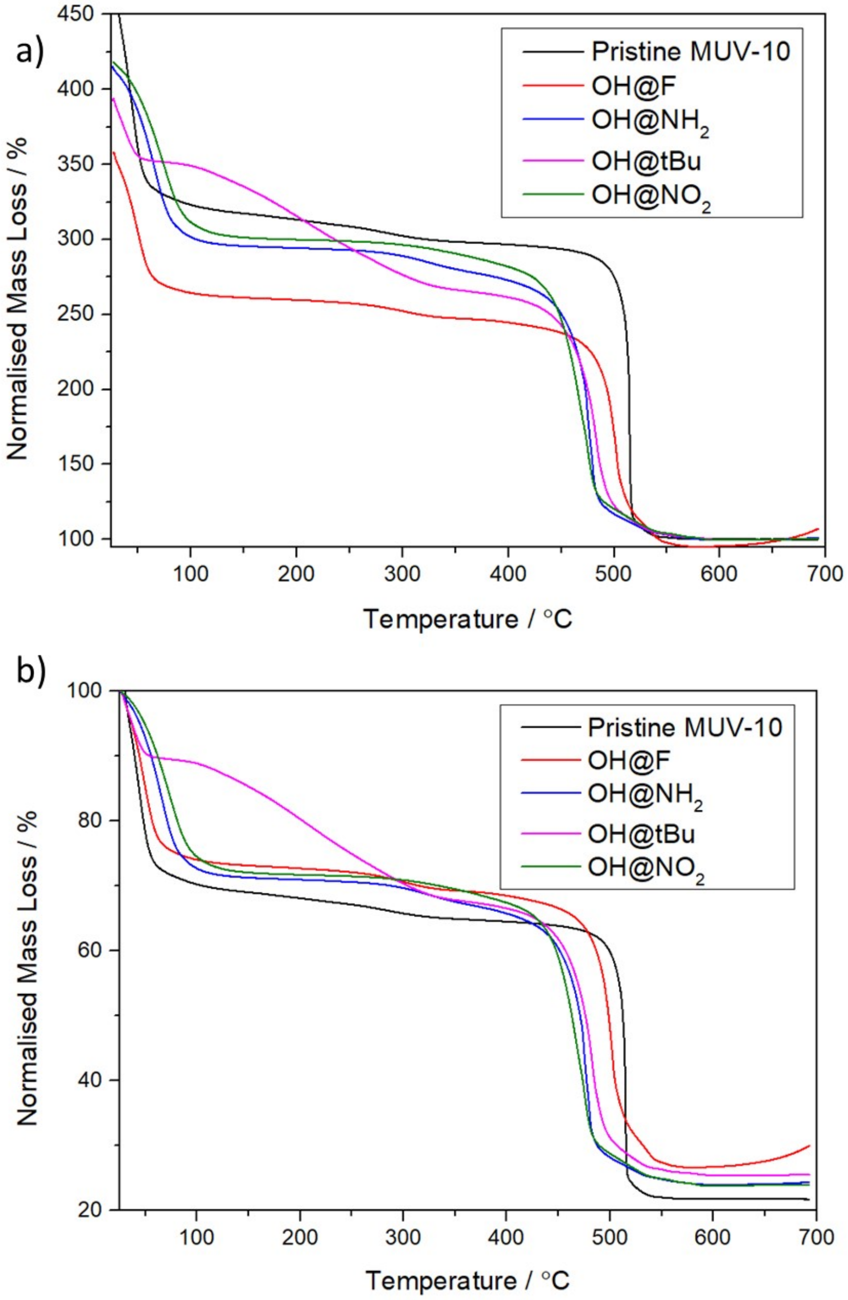

Figure S57: TGA profiles of OH@MOD MODs compared to pristine MUV-10, a) with the end of the decomposition profiles (residue) normalised to 100% and b) with the start of the decomposition profile normalised to 100%.

Table S24: Data extracted from TGA analysis for the model framework [TiCaO(H_2O)$_w$(btc)$_X$(Iso-1)$_y$(Iso-2)$_z$(OH)$_d$]. Note that the missing linker is 1.33-x and the missing linker molar percent (ML%) (1.33-btc)/btc*100.[2–4]

Sample	Ratio BTC/TI	Iso-F	Iso-NO_2	Iso-NH_2	Iso-tBu	Iso-OH	OH-	H_2O	Ml%	Coordination number
pristine	1.403	0.000	0.000	0.000	0.000	0.000	-0.209	1.840	-5.485	13.05
OH@NO_2	1.049	0.000	0.243	0.000	0.000	0.024	0.319	1.440	21.132	11.59
OH@F	0.876	0.102	0.000	0.000	0.000	0.064	1.038	1.224	34.099	11.06
OH@tBU	1.109	0.000	0.000	0.000	0.039	0.050	0.495	6.441	16.628	16.77
OH@NH_2	1.170	0.000	0.000	0.052	0.000	0.095	0.194	1.293	12.017	11.80

Table S25: Data extracted from TGA analysis.

Sample	Iso per ML	ML out of 8
pristine	0.000	-0.418
OH@NO_2	0.951	1.706
OH@F	0.367	2.741
OH@tBU	0.403	1.347
OH@NH_2	0.924	0.979

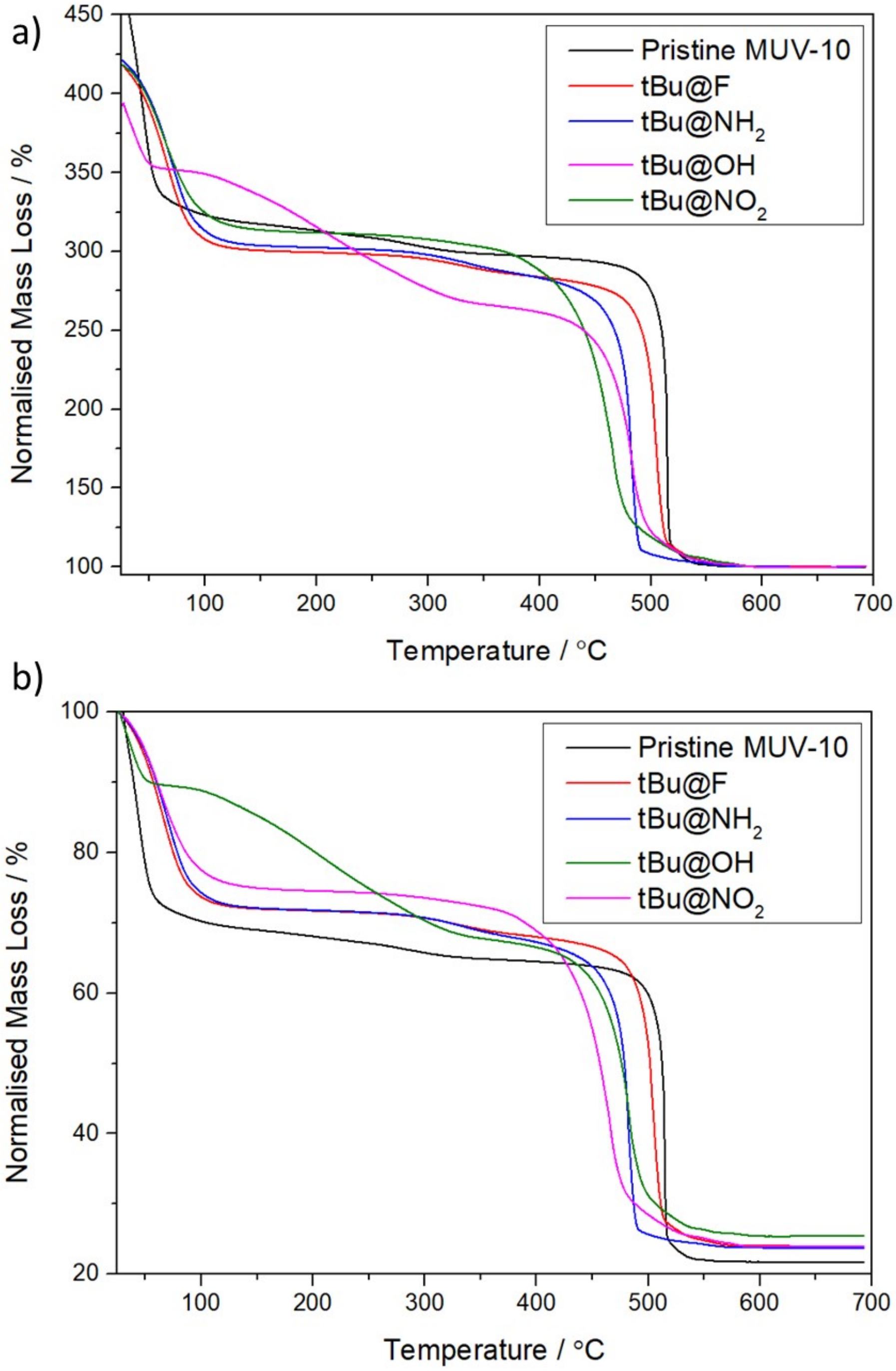

Figure S58: TGA profiles of tBu@MOD MODs compared to pristine MUV-10, a) with the end of the decomposition profiles (residue) normalised to 100% and b) with the start of the decomposition profile normalised to 100%.

Table S26: Data extracted from TGA analysis for the model framework $[TiCaO(H_2O)_w(btc)_X(Iso\text{-}1)_y(Iso\text{-}2)_z(OH)_d]$. Note that the missing linker is 1.33-x and the missing linker molar percent (ML%) (1.33-btc)/btc*100.[2–4]

Sample	Ratio BTC/TI	Iso-F	Iso-NO₂	Iso-NH₂	Iso-tBu	Iso-OH	OH-	H_2O	Ml%	Coordination number
pristine	1.403	0.000	0.000	0.000	0.000	0.000	-0.209	1.840	**-5.485**	13.05
tBU@NO₂	1.041	0.000	0.245	0.000	0.101	0.000	0.186	1.931	**21.753**	12.05
tBU@F	1.091	0.139	0.000	0.000	0.101	0.000	0.246	1.448	**17.935**	12.00
tBU@OH	1.109	0.000	0.000	0.000	0.039	0.050	0.495	6.441	**16.628**	16.77
tBU@NH₂	1.176	0.000	0.000	0.052	0.091	0.000	0.184	1.760	**11.554**	12.29

Table S27: Data extracted from TGA analysis.

Sample	Iso per ML	ML out of 8
pristine	0.000	-0.418
tBU@NO₂	1.196	1.756
tBU@F	1.006	1.451
tBU@OH	0.403	1.347
tBU@NH₂	0.934	0.942

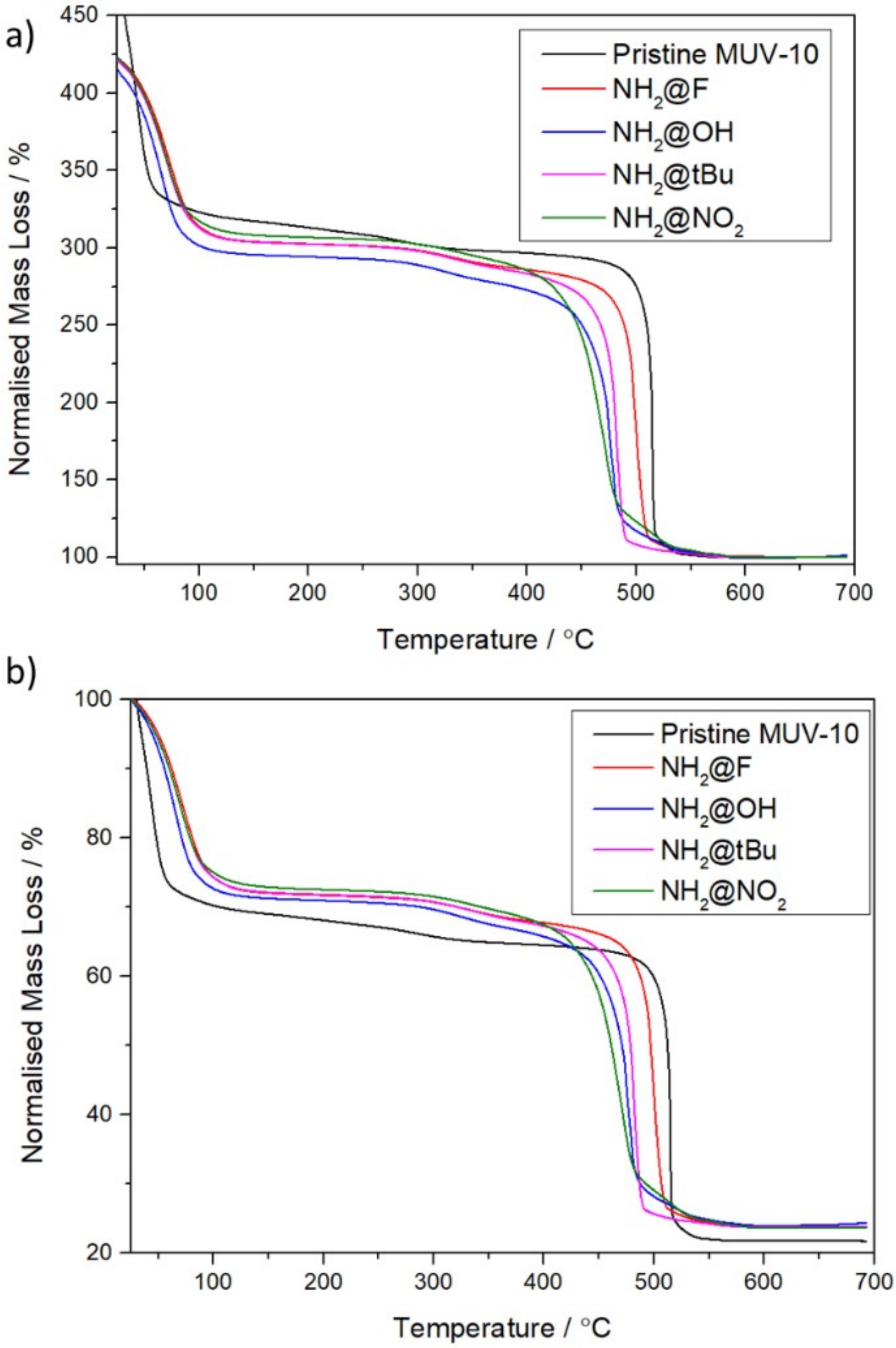

Figure S59: TGA profiles of NH2@MOD MODs compared to pristine MUV-10 a) with the end of the decomposition profiles (residue) normalised to 100% and b) with the start of the decomposition profile normalised to 100%.

Table S28: Data extracted from TGA analysis for the model framework $[TiCaO(H_2O)_w(btc)_X(Iso\text{-}1)_y(Iso\text{-}2)_z(OH)_d]$. Note that the missing linker is 1.33-x and the missing linker molar percent (ML%) (1.33-btc)/btc*100.[2–4]

Sample	Ratio BTC/TI	Iso-F	Iso-NO$_2$	Iso-NH$_2$	Iso-tBu	Iso-OH	OH-	H$_2$O	Ml%	Coordination number
pristine	1.403	0.000	0.000	0.000	0.000	0.000	-0.209	1.840	**-5.485**	13.05
NH$_2$@NO$_2$	1.146	0.000	0.209	0.029	0.000	0.000	0.084	1.395	**13.813**	11.83
NH$_2$@F	1.138	0.131	0.000	0.066	0.000	0.000	0.192	2.802	**14.426**	13.48
NH$_2$@OH	1.170	0.000	0.000	0.052	0.000	0.095	0.194	1.293	**12.017**	11.80
NH$_2$@tBu	1.176	0.000	0.000	0.052	0.091	0.000	0.184	1.760	**11.554**	12.29

Table S29: Data extracted from TGA analysis.

Sample	Iso per ML	ML out of 8
pristine	0.000	-0.418
NH$_2$@NO$_2$	1.298	1.122
NH$_2$@F	1.026	1.171
NH$_2$@OH	0.924	0.979
NH$_2$@tBu	0.934	0.942

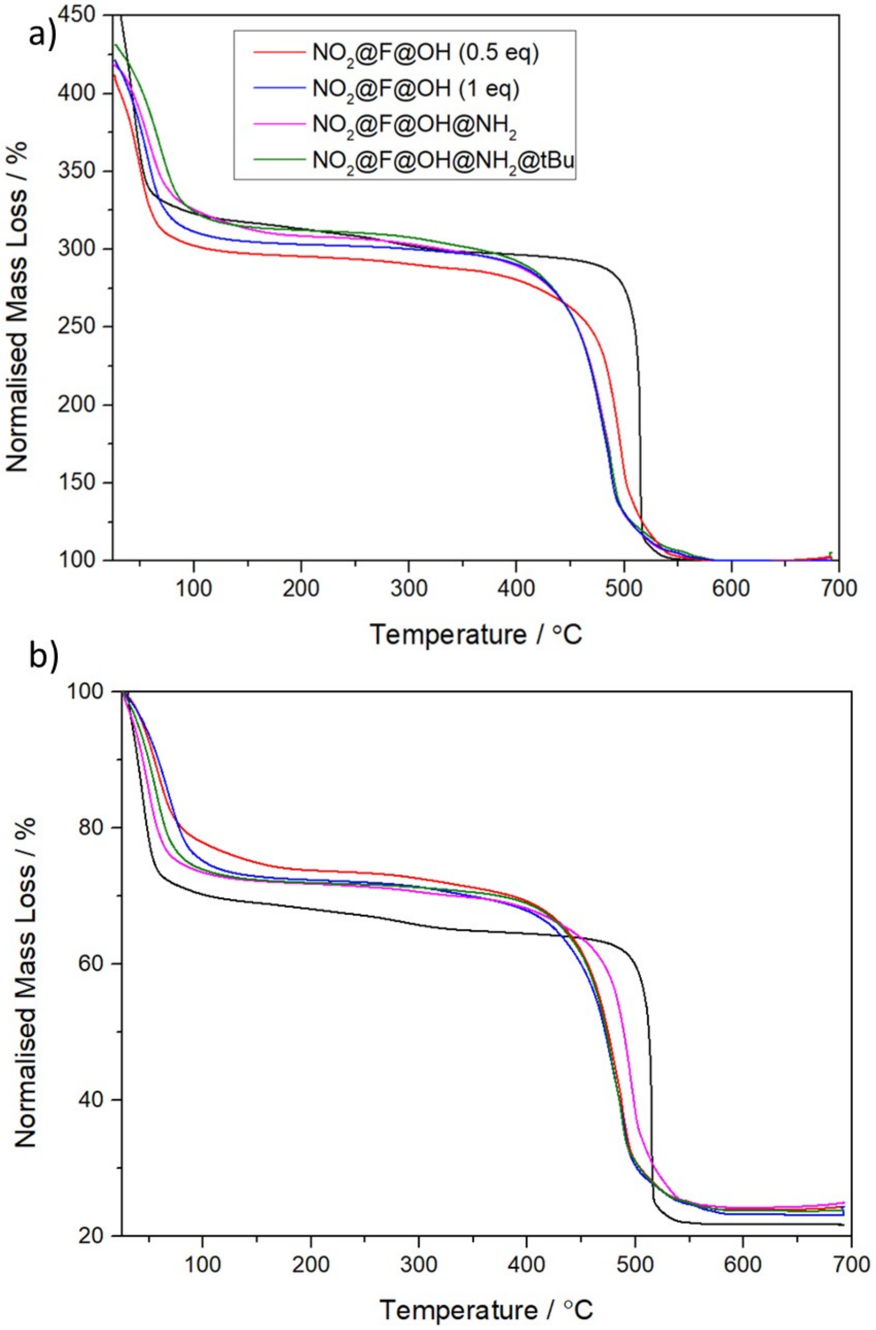

Figure S60: TGA profiles of NO2@MOD MODs compared to pristine MUV-10 a) with the end of the decomposition profiles (residue) normalised to 100% and b) with the start of the decomposition profile normalised to 100%.

Table S30: Data extracted from TGA analysis for the model framework [$TiCaO(H_2O)_w(btc)_X(Iso\text{-}1)_y(Iso\text{-}2)_z(OH)_d$]. [2–4]

Sample	Ratio BTC/TI	Iso-F	Iso-NO_2	Iso-NH_2	Iso-tBu	Iso-OH	OH-	H_2O
pristine	1.403	0.000	0.000	0.000	0.000	0.000	-0.209	1.840
F@NO_2@OH (0.5)	1.045	0.060	0.130	0.000	0.000	0.019	0.445	1.966
F@NO_2@OH (1)	1.018	0.119	0.255	0.000	0.000	0.017	0.165	1.099
F@NO_2@OH@NH_2	1.026	0.086	0.206	0.019	0.000	0.021	0.259	2.453
F@NO_2@OH@NH_2@tBu	0.999	0.089	0.186	0.035	0.052	0.026	0.225	2.033

Table S31: Data extracted from TGA analysis. Note that the missing linker is 1.33-x and the missing linker molar percent(ML%) (1.33-btc)/btc*100. [2–4]

Sample	ML%	Coordination positions	Iso per ML	ML out of 8
pristine	**-5.485**	13.05	0.000	-0.418
F@NO_2@OH (0.5)	**21.420**	12.222	0.736	1.729
F@NO_2@OH (1)	**23.458**	11.390	1.251	1.892
F@NO_2@OH@NH_2	**22.854**	12.704	1.091	1.844
F@NO_2@OH@NH_2@tBu	**24.878**	12.209	1.175	2.005

S.3.6 Nitrogen Adsorption and desorption measurements

Table S32: Tabulated data extracted from N_2 adsorption and desorption measurements of MOD@MOD MOFs showing a general increase in surface area, microporosity and total pore volumes, alongside the theortical molecular weigh of the MOFs calculated by TGA, shiowing that the two MOFs with decreased porosity

Sample	**S_{BET}**	**S_{MICRO}**	**S_{EXT}**	**V_{MICRO}**	**V_{MESO}**	**V_{TOTAL}**
	(m^2 /g)	(m^2 /g)	(m^2 /g)	(cm^3 /g)	(cm^3 /g)	(cm^3 /g)
Pristine	1040	974	66	0.365	0.037	0.402
F@NH_2	1314	1142	172	0.443	0.109	0.552
F@OH	1164	1015	149	0.392	0.096	0.488
F@tBu	736	591	145	0.234	0.094	0.328
F@NO_2	1249	1050	199	0.411	0.166	0.577
NH_2@OH	1116	994	122	0.378	0.076	0.454
NH_2@tBu	1030	834	196	0.324	0.156	0.48
NH_2@NO_2	1124	976	148	0.375	0.088	0.463
tBu@NO_2	1168	893	275	0.35	0.295	0.645
tBu@OH	518	436	82	0.169	0.052	0.221
NO_2@OH	1123	927	196	0.36	0.155	0.515

Note that in all cases S_{BET} corresponds to Brunauer–Emmett–Teller surface area, S_{micro} to micropore surface area, S_{ext} to external surface area, V_{micro} to micropore volume, V_{meso} to mesopore volume and V_{total} to total pore volume.

V_{micro} was calculated using the *t*-plot model with the Harkins and Jura thickness curve based on the BET surface areas. V_{total} was calculated at $P/P_0 = 0.9$, prior to the inter-particle space [5] and $V_{meso} = V_{total} - V_{micro}$.

The pore size distributions of the di-modulated MOFswere calculated using NLDFT oxide surface pore model within the MicroActive software, with no regularisation, whereas the pillared clay model was used for the tri, tetra and penta-modulated MOFs, also with no regularisation, as the oxide surface pore model as providing higher errors due to the loss of the type I isotherm.

The BET surface area was calculated based on the decrease in the Q (1-p/p0) values, which slightly differ between samples given their differences in porosity features. BET plots are given in Figures S61-74

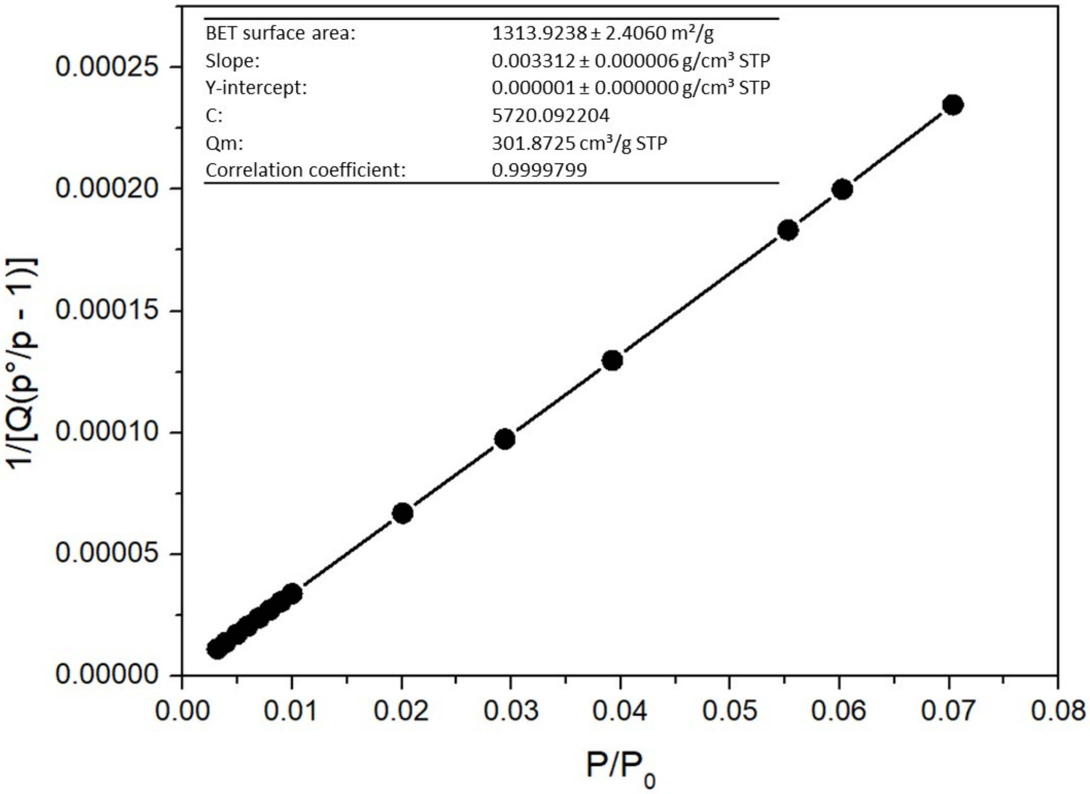

BET surface area:	1313.9238 ± 2.4060 m^2/g
Slope:	0.003312 ± 0.000006 g/cm^3 STP
Y-intercept:	0.000001 ± 0.000000 g/cm^3 STP
C:	5720.092204
Qm:	301.8725 cm^3/g STP
Correlation coefficient:	0.9999799

Figure S61: BET plot of F@NH_2.

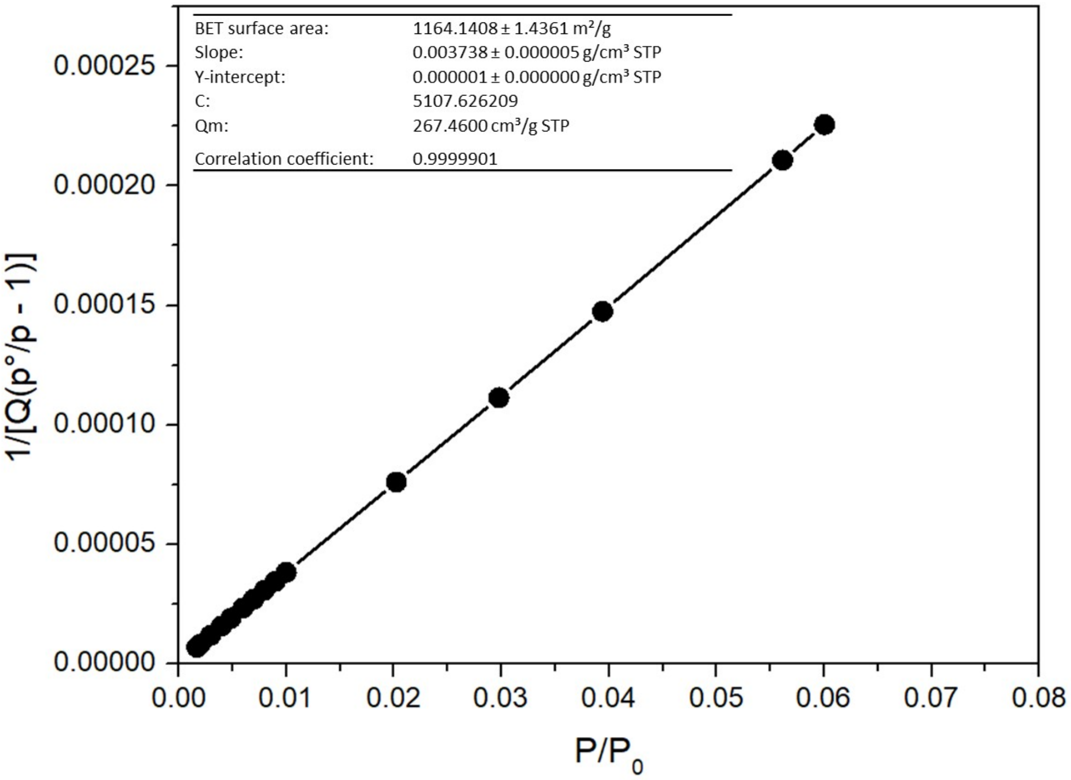

BET surface area:	1164.1408 ± 1.4361 m^2/g
Slope:	0.003738 ± 0.000005 g/cm^3 STP
Y-intercept:	0.000001 ± 0.000000 g/cm^3 STP
C:	5107.626209
Qm:	267.4600 cm^3/g STP
Correlation coefficient:	0.9999901

Figure S62: BET plot of F@OH.

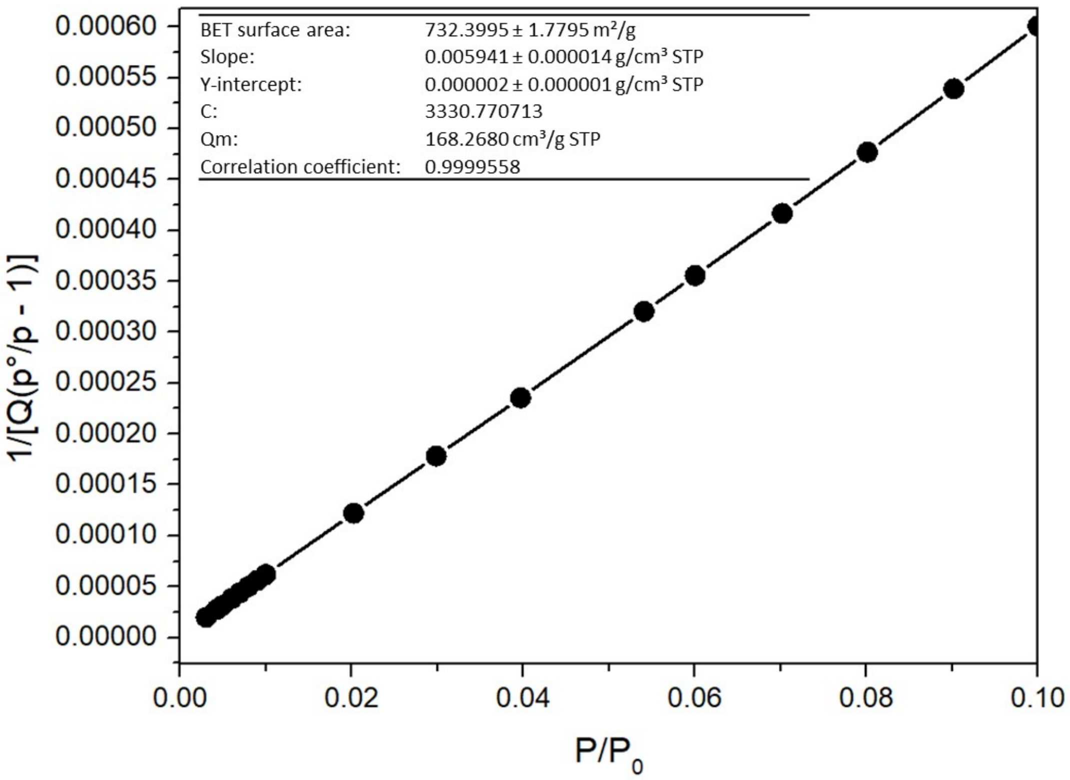

Figure S63: BET plot of F@tBu.

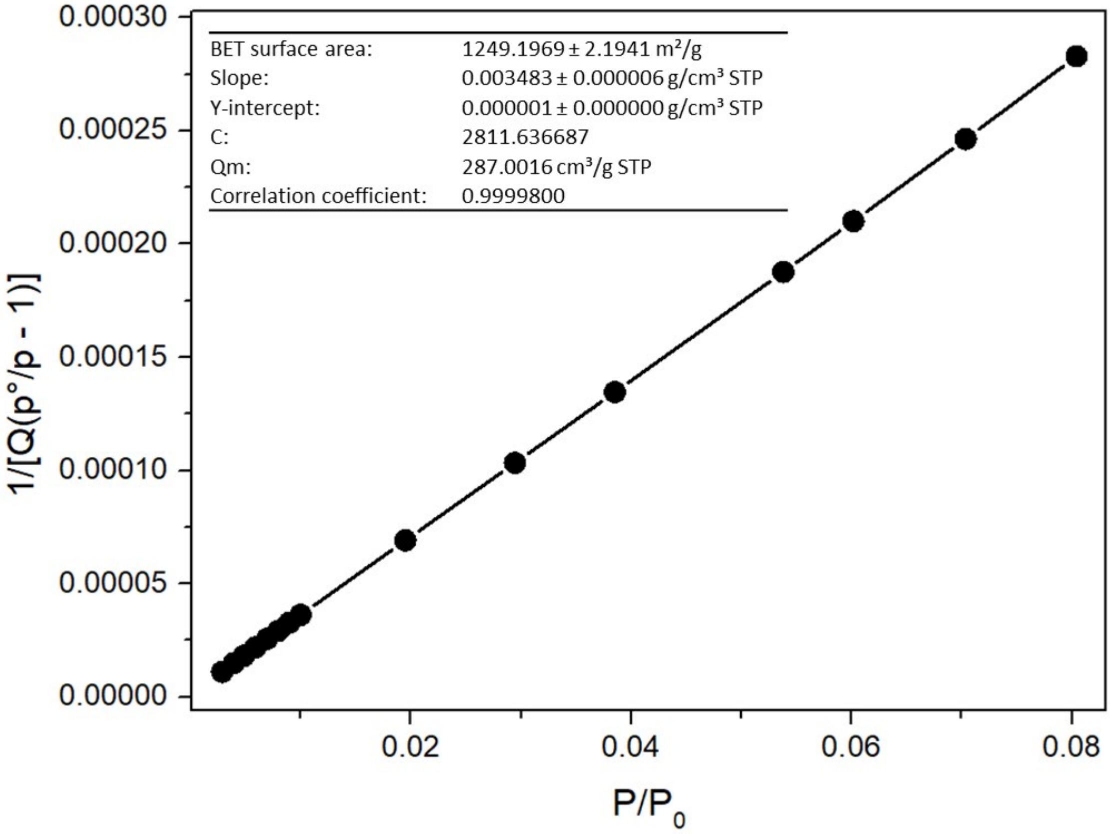

Figure S64: BET plot of F@No$_2$.

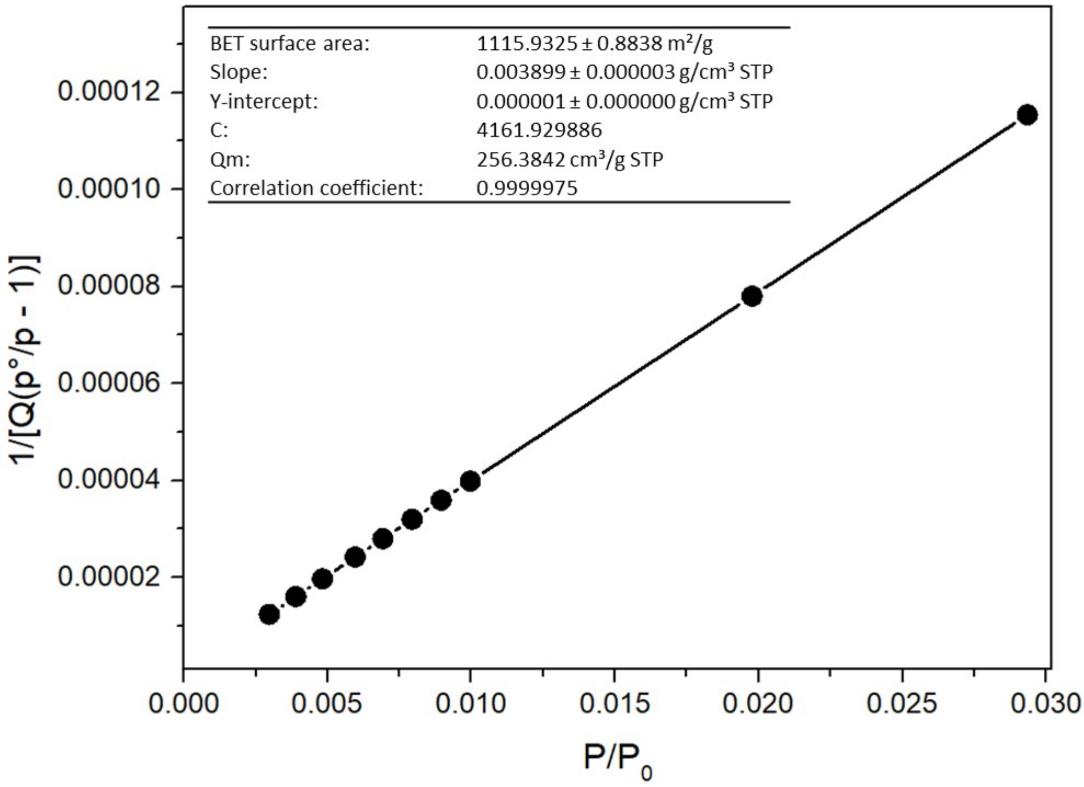

Figure S65: BET plot of NH_2@OH.

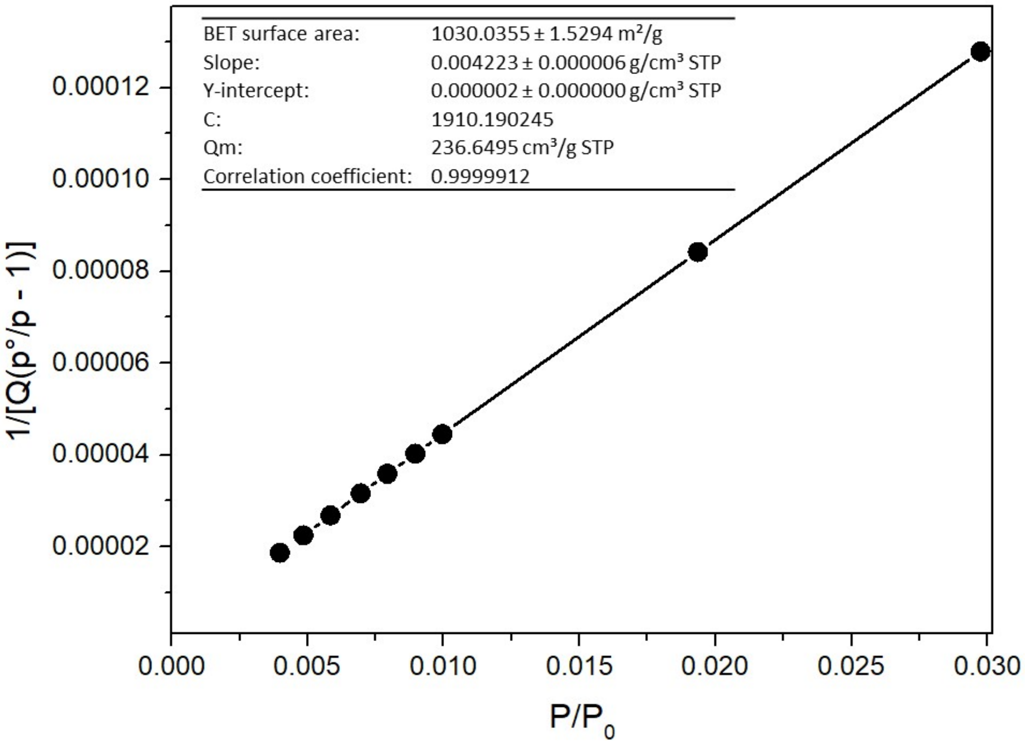

Figure S66: BET plot of NH_2@tBu.

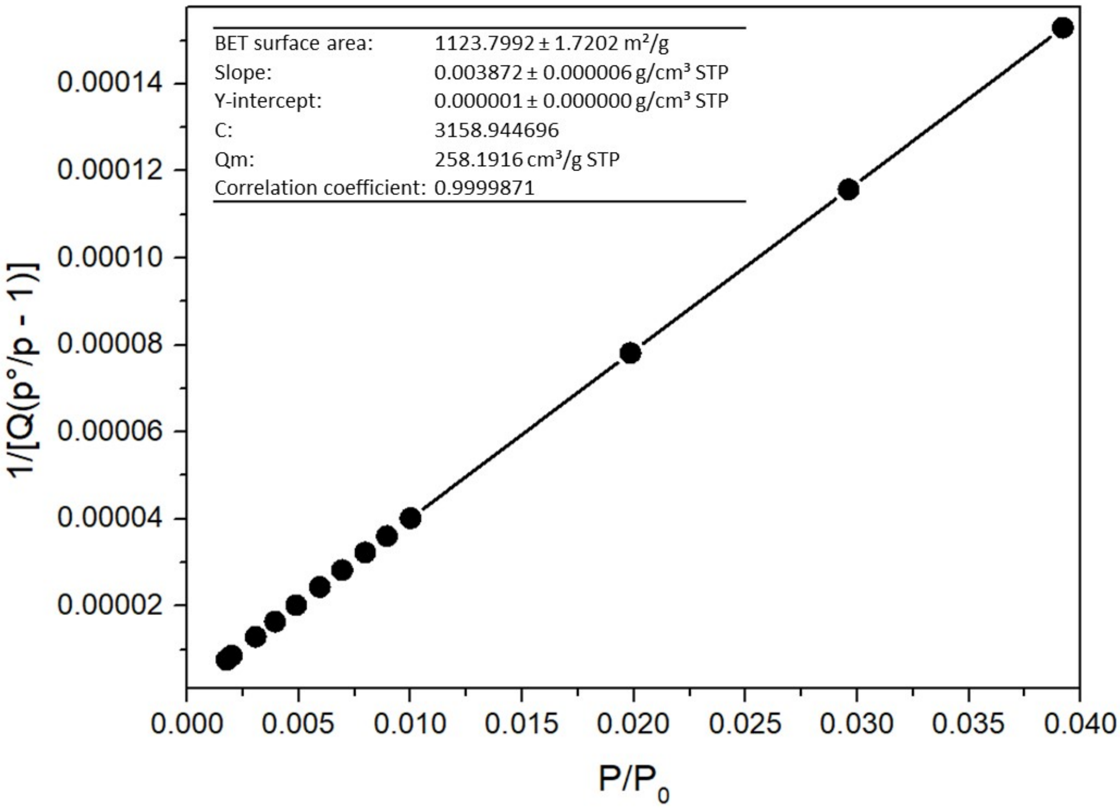

Figure S67: BET plot of NH_2@NO_2.

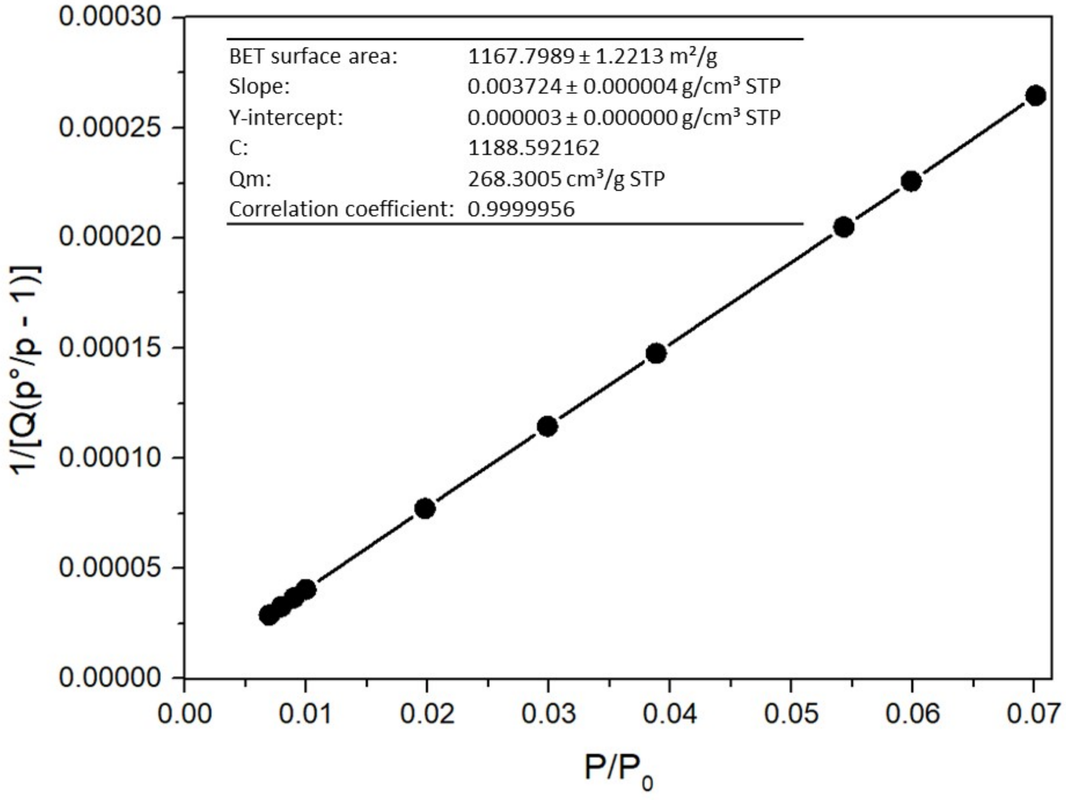

Figure S68: BET plot of NO_2@tBu.

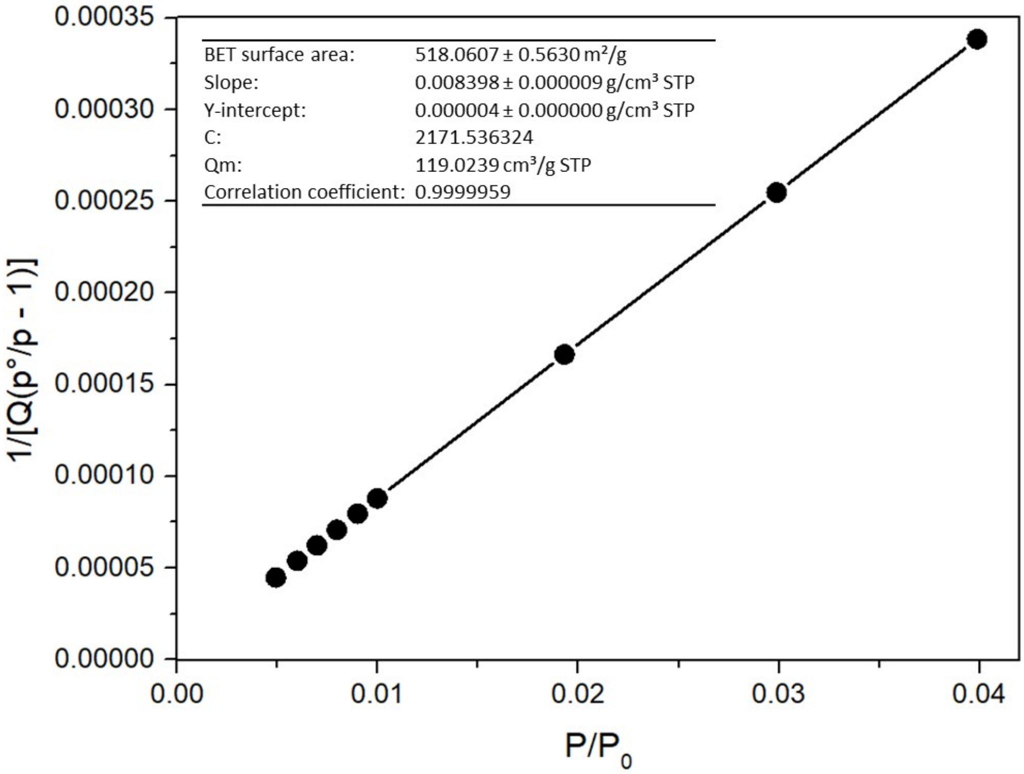

Figure S69: BET plot of tBu@OH.

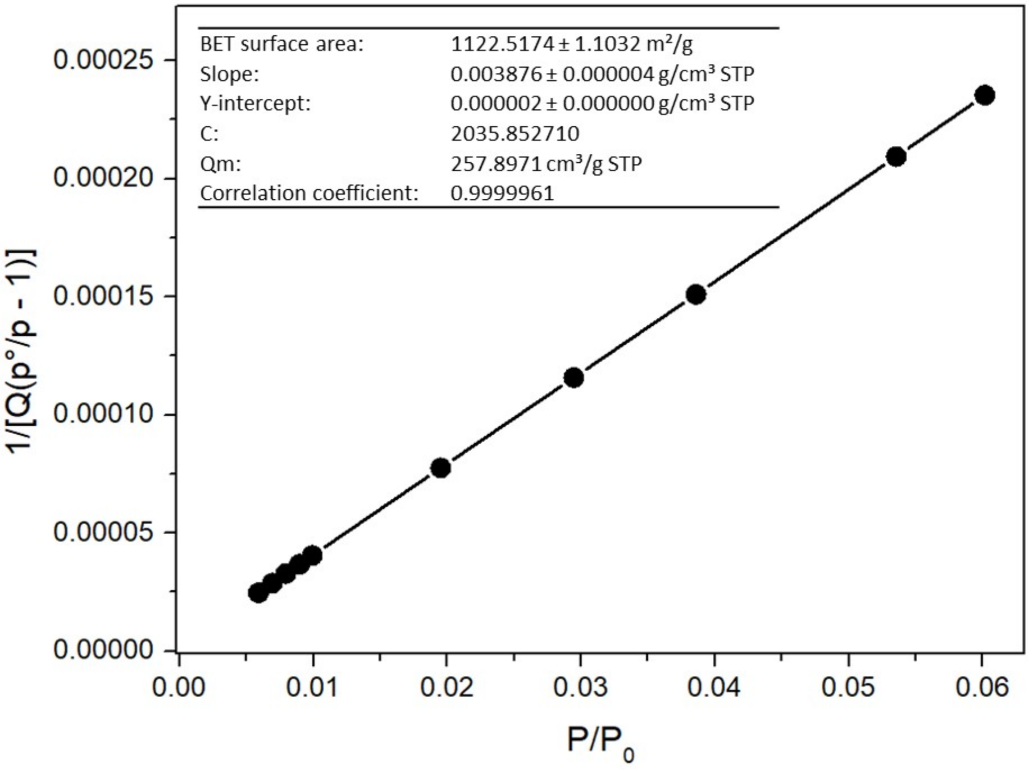

Figure S70: BET plot of NO_2@OH.

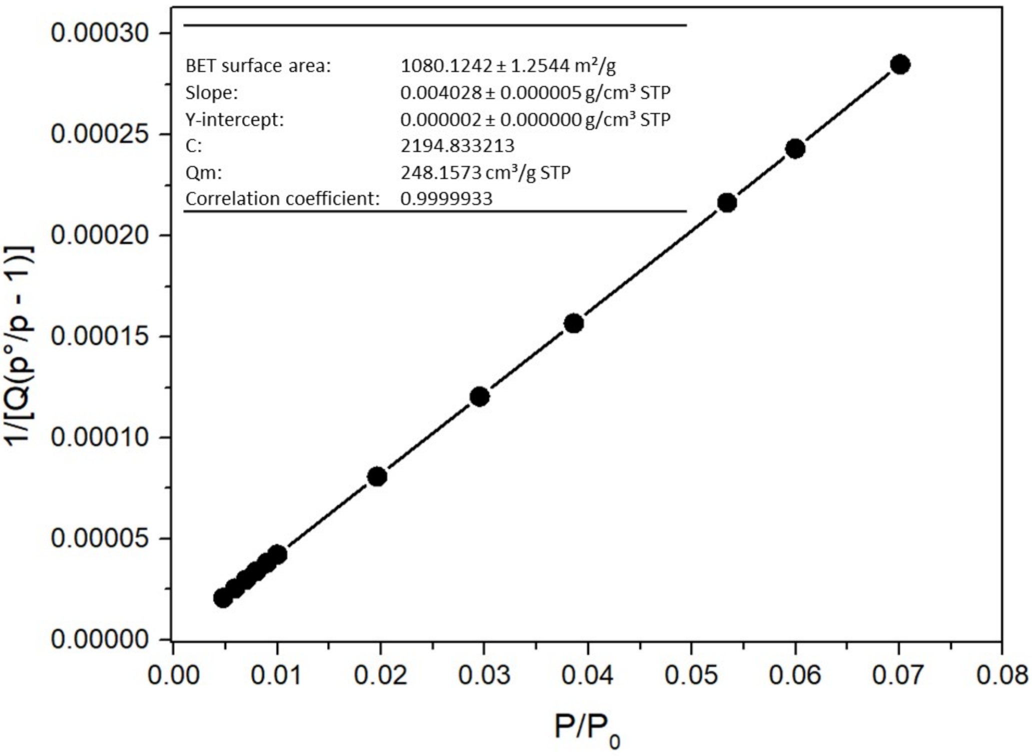

BET surface area: 1080.1242 ± 1.2544 m²/g
Slope: 0.004028 ± 0.000005 g/cm³ STP
Y-intercept: 0.000002 ± 0.000000 g/cm³ STP
C: 2194.833213
Qm: 248.1573 cm³/g STP
Correlation coefficient: 0.9999933

Figure S71: BET plot of F@NO_2@OH (0.5)

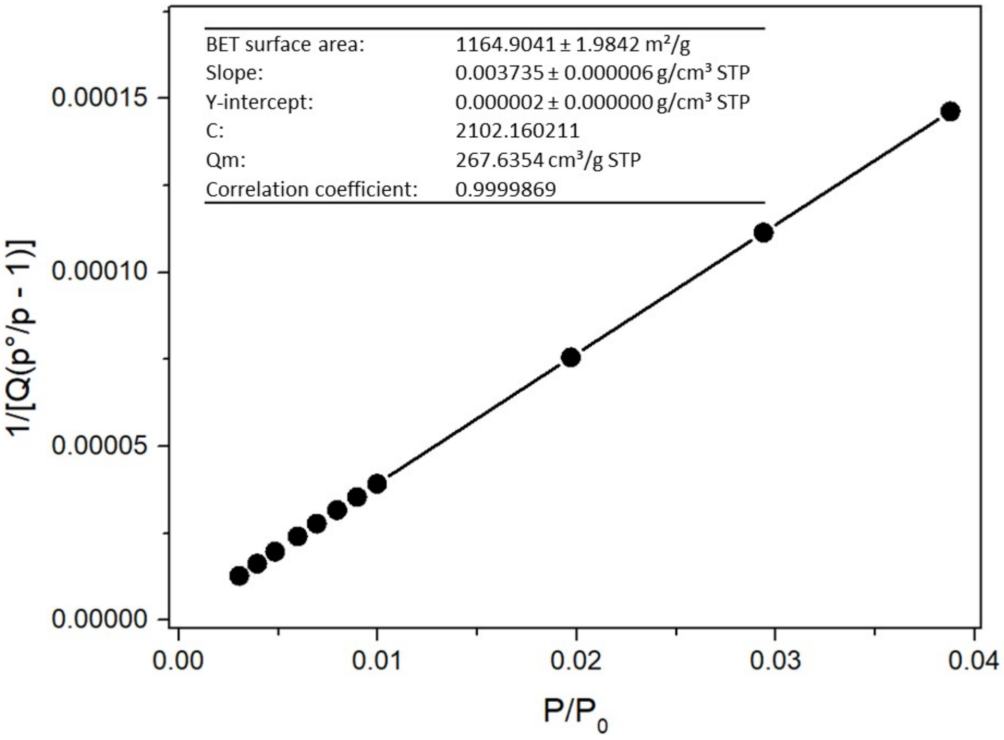

BET surface area: 1164.9041 ± 1.9842 m²/g
Slope: 0.003735 ± 0.000006 g/cm³ STP
Y-intercept: 0.000002 ± 0.000000 g/cm³ STP
C: 2102.160211
Qm: 267.6354 cm³/g STP
Correlation coefficient: 0.9999869

Figure S72: BET plot of F@NO_2@OH (1)

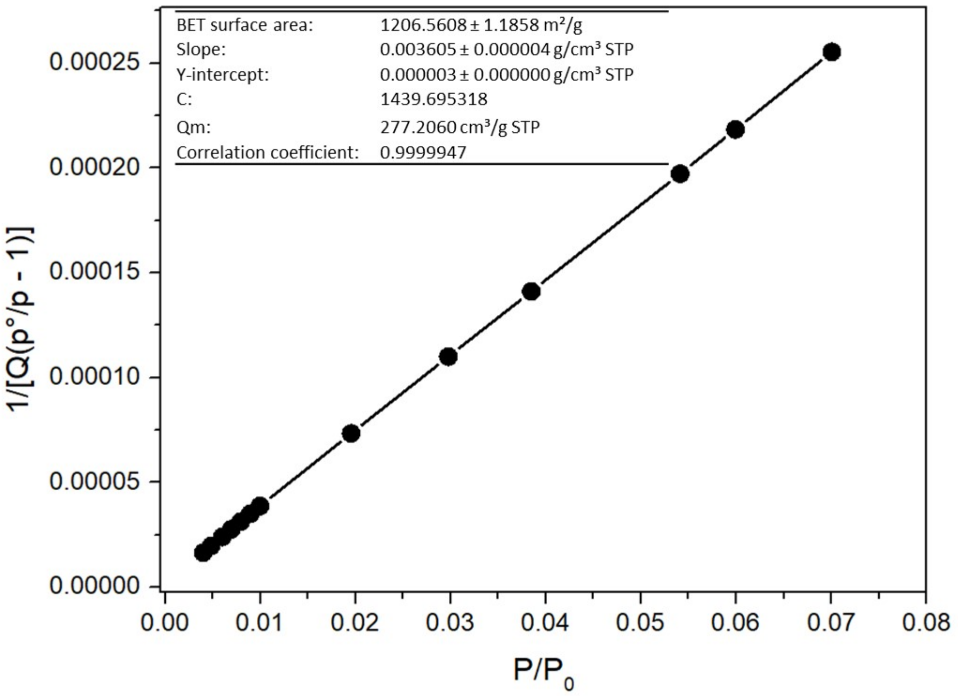

Figure S73: BET plot of $F@NO_2@OH@NH_2$.

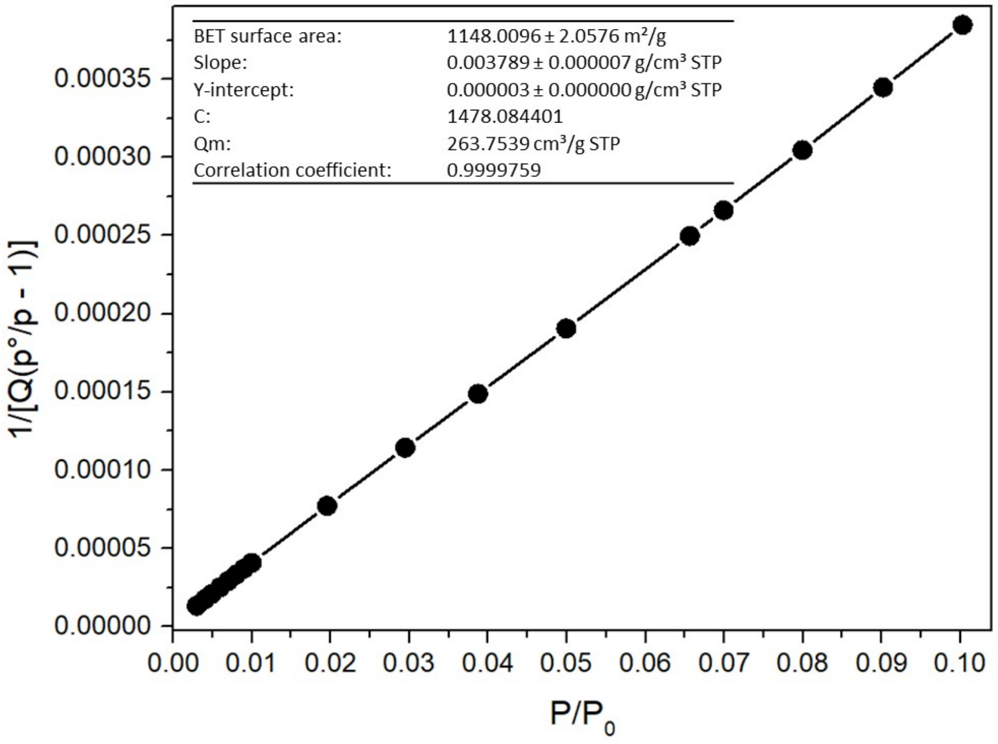

Figure S74: BET plot of $F@NO_2@OH@NH_2@tBu$.

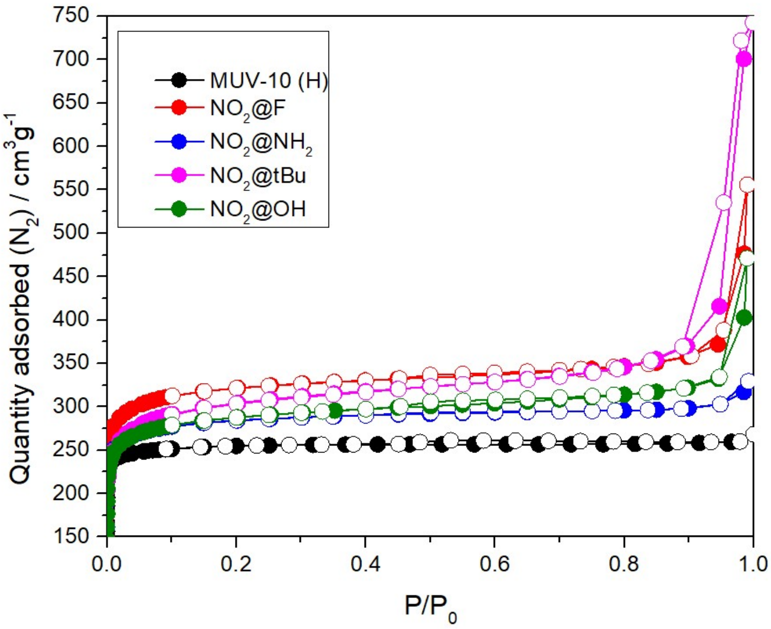

Figure S75: N_2 adsorption and desorption isotherms of NO2@MOD MOFs.

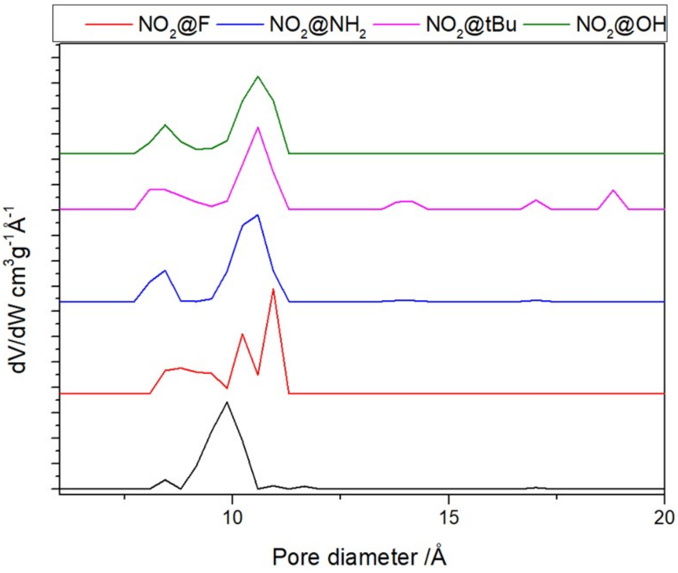

Figure S76: Pore size distributions extracted from the N_2 adsorption isotherms of NO_2@MOD MOFs.

Table S33: Tabulated data extracted from N_2 adsorption and desorption measurements of NO_2@MOD MOFs.

Sample	**S_{BET}**	**S_{MICRO}**	**S_{EXT}**	**V_{MICRO}**	**V_{MESO}**	**V_{TOTAL}**
	(m^2 /g)	(m^2 /g)	(m^2 /g)	(cm^3 /g)	(cm^3 /g)	(cm^3 /g)
Pristine	**1040**	**974**	**66**	**0.365**	**0.037**	**0.402**
NO_2@F	1249	1050	199	0.411	0.166	0.577
NO_2@OH	1123	927	196	0.360	0.155	0.515
NO_2@tBu	1168	893	275	0.350	0.295	0.645
NO_2@NH_2	1124	976	148	0.375	0.088	0.463

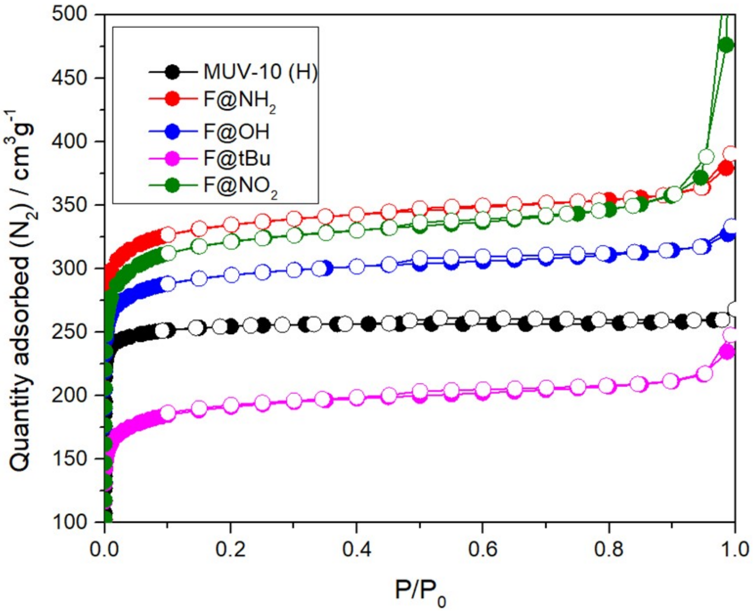

Figure S77: N_2 adsorption and desorption isotherms of F@MOD MOFs.

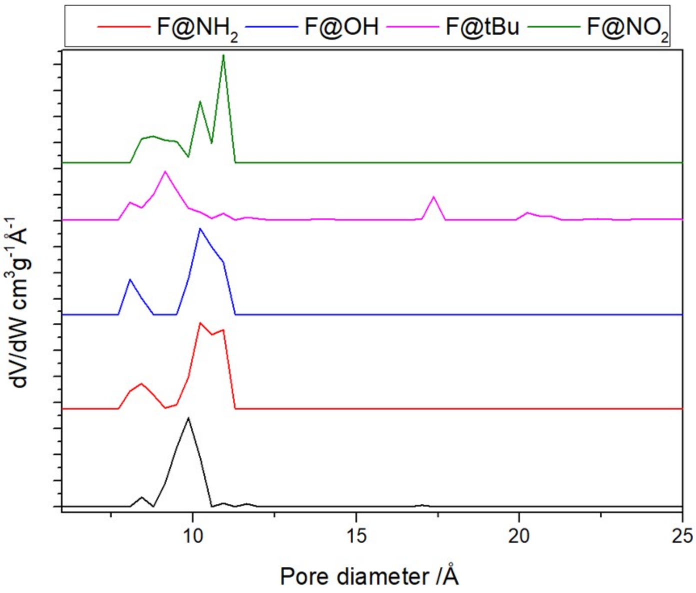

Figure S78: Pore size distributions extracted from the N_2 adsorption isotherms of F@MOD MOFs.

Table S34: Tabulated data extracted from N_2 adsorption and desorption measurements of F@MOD MOFs.

Sample	**S_{BET}**	**S_{MICRO}**	**S_{EXT}**	**V_{MICRO}**	**V_{MESO}**	**V_{TOTAL}**
	(m^2 /g)	(m^2 /g)	(m^2 /g)	(cm^3 /g)	(cm^3 /g)	(cm^3 /g)
Pristine	**1040**	**974**	66	**0.365**	0.037	**0.402**
F@NO$_2$	1249	1050	199	0.411	0.166	0.577
F@OH	1164	1015	149	0.392	0.096	0.488
F@tBu	736	591	145	0.234	0.094	0.328
F@NH$_2$	1314	1142	172	0.443	0.109	0.552

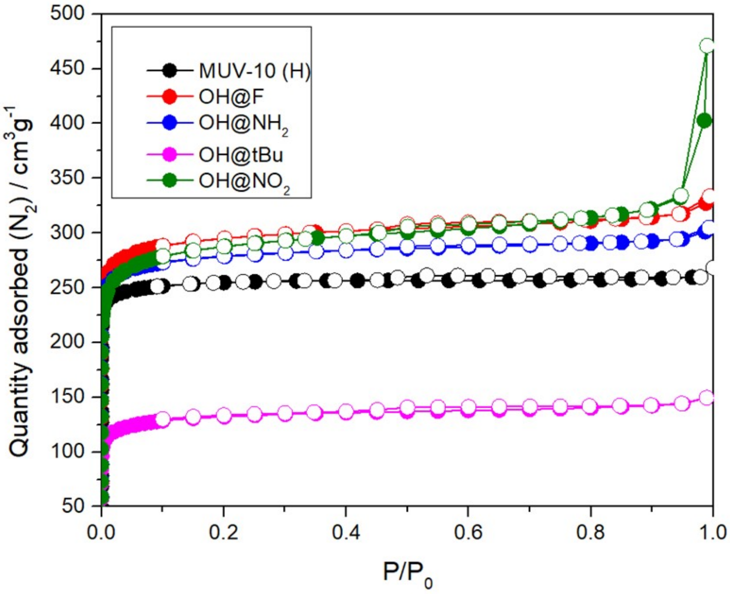

Figure S79: N_2 adsorption and desorption isotherms of OH@MOD MOFs.

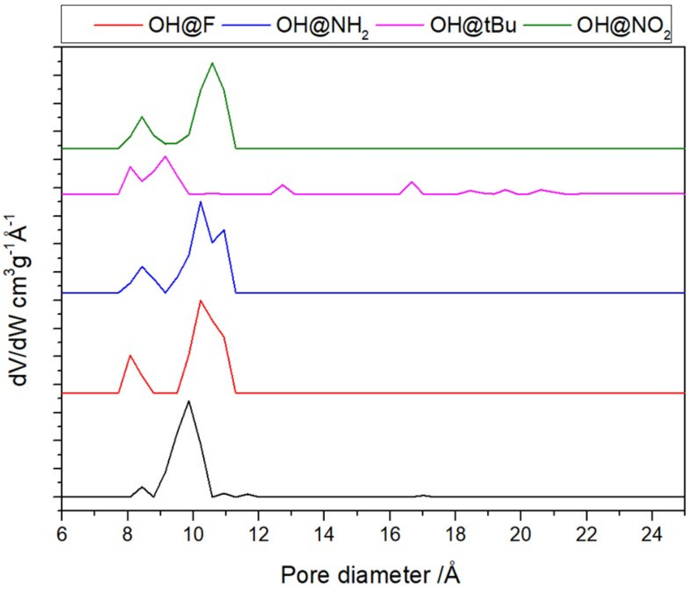

Figure S80: Pore size distributions extracted from the N_2 adsorption isotherms of OH@MOD MOFs.

Table S35: Tabulated data extracted from N_2 adsorption and desorption measurements of OH@MOD MOFs.

Sample	S_{BET}	S_{MICRO}	S_{EXT}	V_{MICRO}	V_{MESO}	V_{TOTAL}
	(m^2 /g)	(m^2 /g)	(m^2 /g)	(cm^3 /g)	(cm^3 /g)	(cm^3 /g)
Pristine	1040	974	66	0.365	0.037	0.402
OH@NO$_2$	1123	927	196	0.36	0.155	0.515
OH@F	1164	1015	149	0.392	0.096	0.488
OH@tBu	518	436	82	0.169	0.052	0.221
OH@NH$_2$	1116	994	122	0.378	0.076	0.454

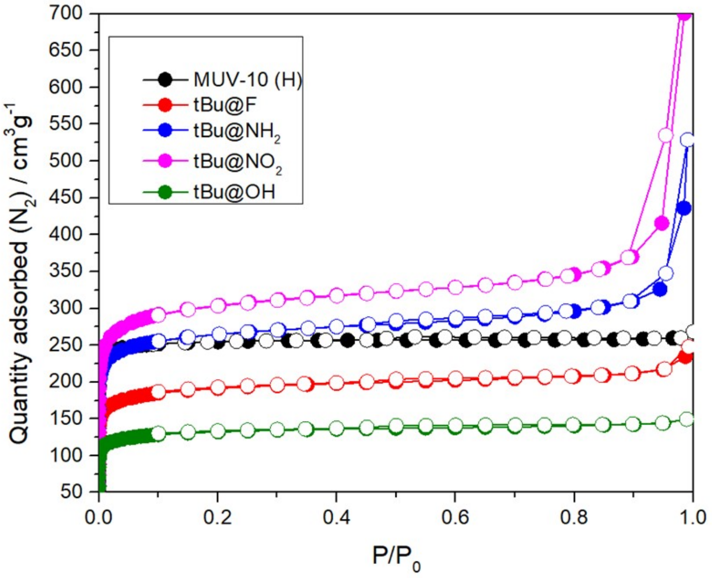

Figure S81: N_2 adsorption and desorption isotherms of tBu@MOD MOFs.

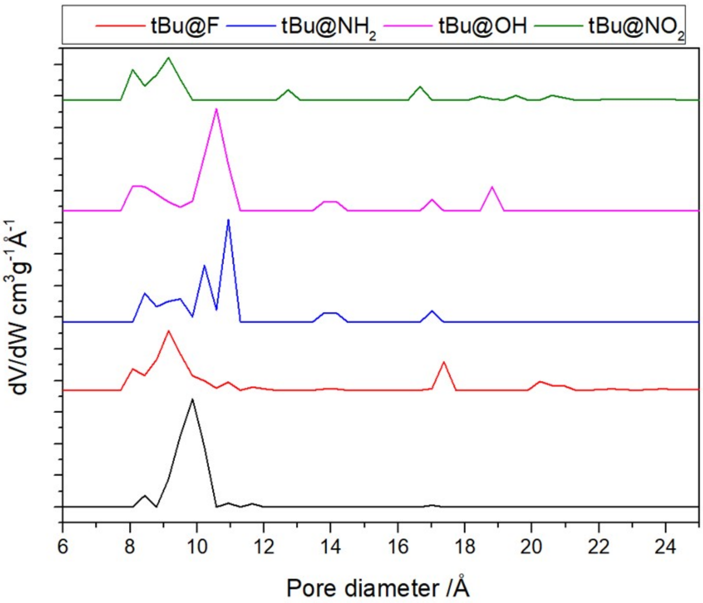

Figure S82: Pore size distributions extracted from the N_2 adsorption isotherms of tBu@MOD MOFs.

Table S36: Tabulated data extracted from N_2 adsorption and desorption measurements of tBu@MOD MOFs.

Sample	**S_{BET}**	**S_{MICRO}**	**S_{EXT}**	**V_{MICRO}**	**V_{MESO}**	**V_{TOTAL}**
	(m^2 /g)	(m^2 /g)	(m^2 /g)	(cm^3 /g)	(cm^3 /g)	(cm^3 /g)
Pristine	1040	974	66	0.365	0.037	0.402
tBu@NO_2	1168	893	275	0.35	0.295	0.645
tBu@F	736	591	145	0.234	0.094	0.328
tBu@OH	518	436	82	0.169	0.052	0.221
tBu@NH_2	1030	834	196	0.324	0.156	0.48

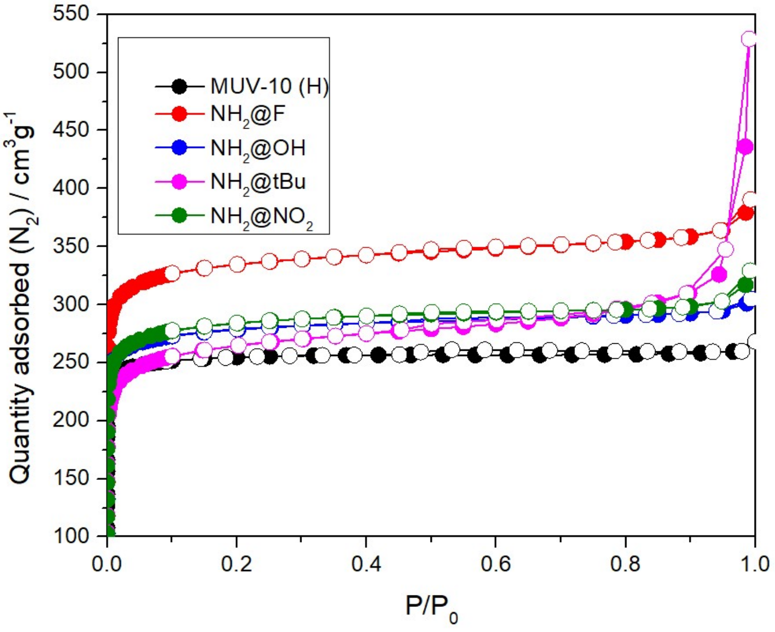

Figure S83: N_2 adsorption and desorption isotherms of NH_2@MOD MOFs.

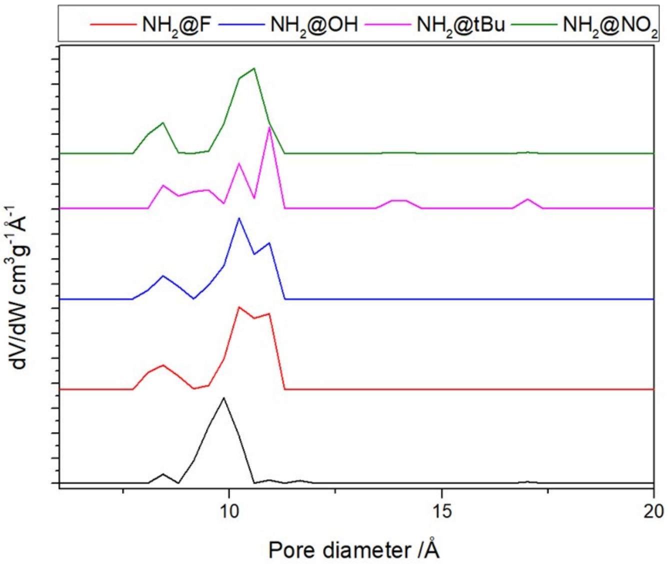

Figure S84: Pore size distributions extracted from the N_2 adsorption isotherms of NH_2@MOD MOFs.

Table S37: Tabulated data extracted from N_2 adsorption and desorption measurements of NH_2@MOD MOFs.

Sample	S_{BET}	S_{MICRO}	S_{EXT}	V_{MICRO}	V_{MESO}	V_{TOTAL}
	(m^2 /g)	(m^2 /g)	(m^2 /g)	(cm^3 /g)	(cm^3 /g)	(cm^3 /g)
Pristine	1040	974	66	0.365	0.037	0.402
NH_2@NO_2	1124	976	148	0.375	0.088	0.463
NH_2@F	1314	1142	172	0.443	0.109	0.552
NH_2@OH	1116	994	122	0.378	0.076	0.454
NH_2@tBu	1030	834	196	0.324	0.156	0.48

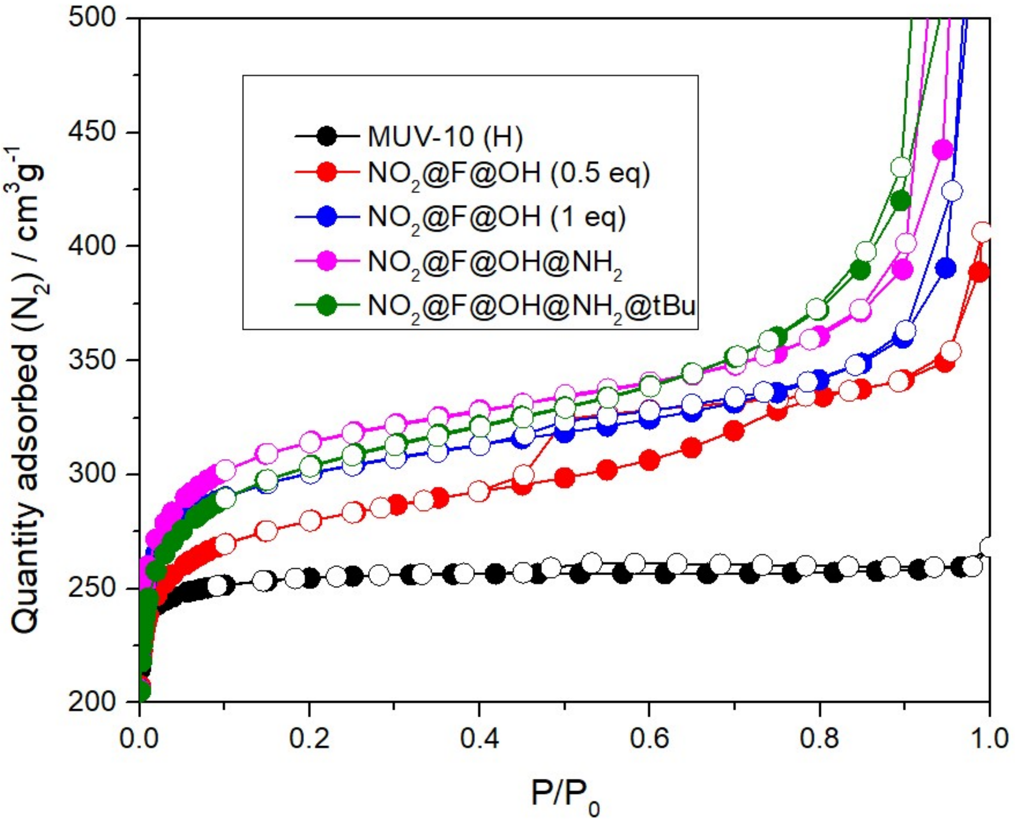

Figure S85: N_2 adsorption and desorption isotherms of multi-modulated MOFs.

Table S38: Tabulated data extracted from N_2 adsorption and desorption measurements of multi-modulated MOFs

Sample	S_{BET}	S_{MICRO}	S_{EXT}	V_{MICRO}	V_{MESO}	V_{TOTAL}
	(m^2 /g)	(m^2 /g)	(m^2 /g)	(cm^3 /g)	(cm^3 /g)	(cm^3 /g)
Pristine	1040	974	66	0.365	0.037	0.402
F@NO$_2$@OH (0.5)	1080	857	223	0.336	0.194	0.53
F@NO$_2$@OH (1)	1164	932	232	0.364	0.194	0.558
F@NO$_2$@OH@NH$_2$	1206	932	274	0.366	0.072	0.438
F@NO$_2$@OH@NH$_2$@tBu	1148	835	313	0.333	0.319	0.652

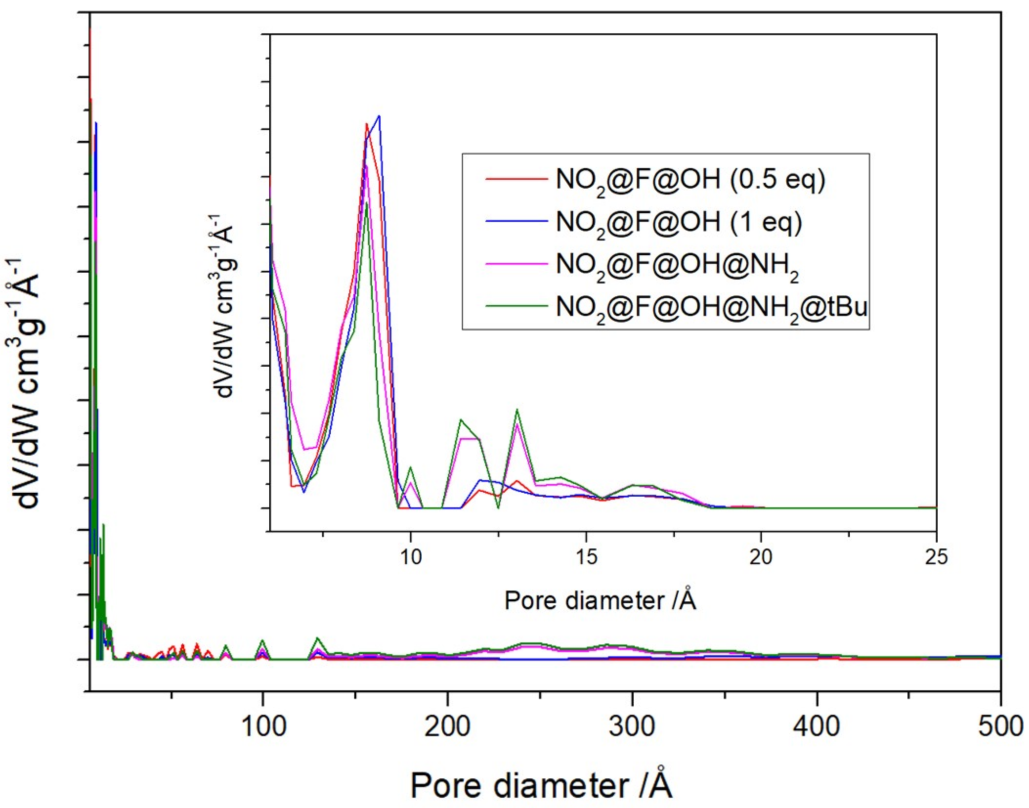

Figure S86: Pore size distributions extracted from the N_2 adsorption isotherms of multi-modulated MOFs.

S.4. Catalytic activity of MTVM MOFs

10 μL of cyclohexane oxide and 10 μL of aniline were dissolved in 0.5 mL of ethanol and let them react at room temperature in the presence of 10 mg of MOF for one day. Sample aliquots were analysed by GC-FID (Gas Chromatography-Flame Ionization Detector.

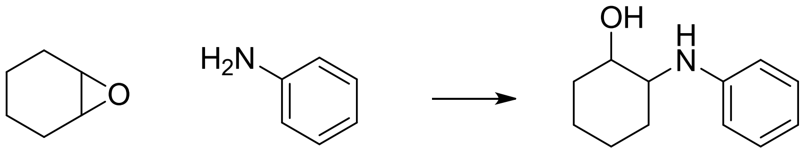

Table S39: Tabulated data of conversion %.

Time	Pristine	F/NO$_2$	F/tBu	NO$_2$/OH	tBu/NH$_2$	NO$_2$/F/OH/NH$_2$/tBu	tBu /NO$_2$
0	0.00	0.00	0.00	0.00	0.00	0.00	0.00
12	5.57	7.36	5.99	13.35	10.78	11.05	11.32
24	13.53	18.57	26.28	23.86	22.30	28.83	38.01
48	11.71	34.28	37.28	38.35	53.13	62.74	62.44
72	44.27	51.80	58.80	62.12	64.81	75.55	78.04

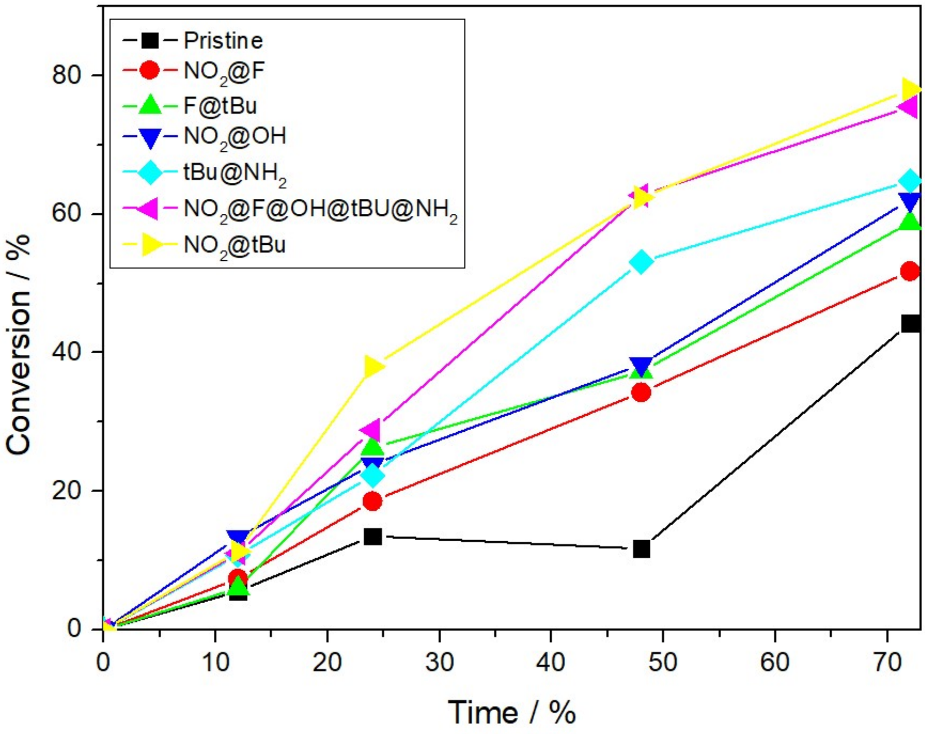

Figure S87: Catalytic activity of the MTVM MOFs.

After 72 hours of reaction, the MOF catalyst were collected by centrifugation and rinsed with MeOH prior to PXRD measurements. Note that compounds different from the reaction substrates and products were not identified in the HPLC analysis of the reaction, suggesting that no linker or modulator were leaching from the samples.

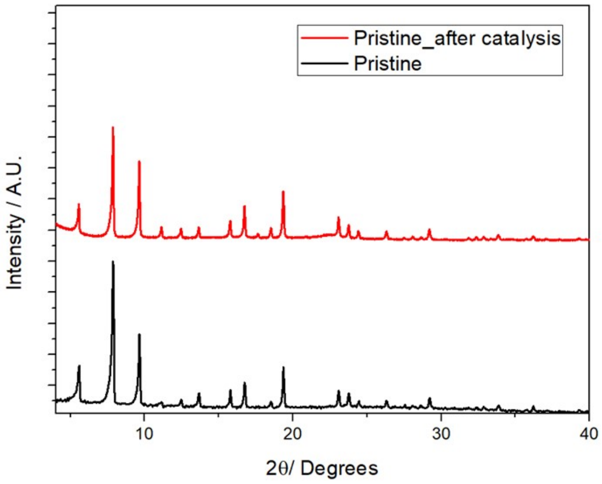

Figure S88: PXRD profile before and after catalysis.

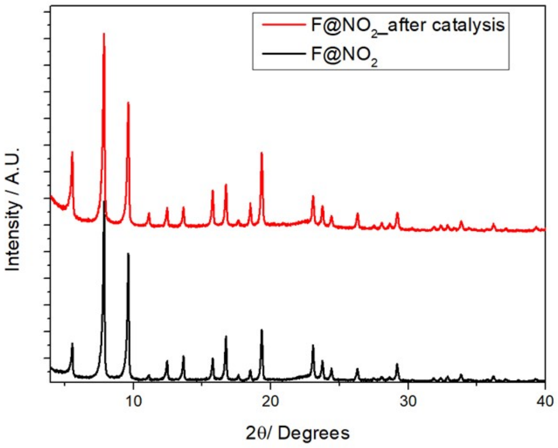

Figure S89: PXRD profile before and after catalysis.

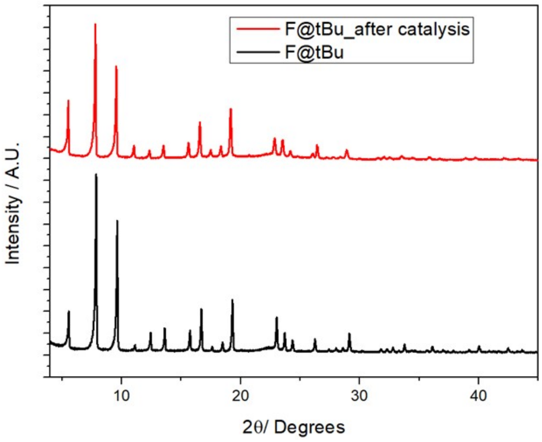

Figure S90: PXRD profile before and after catalysis.

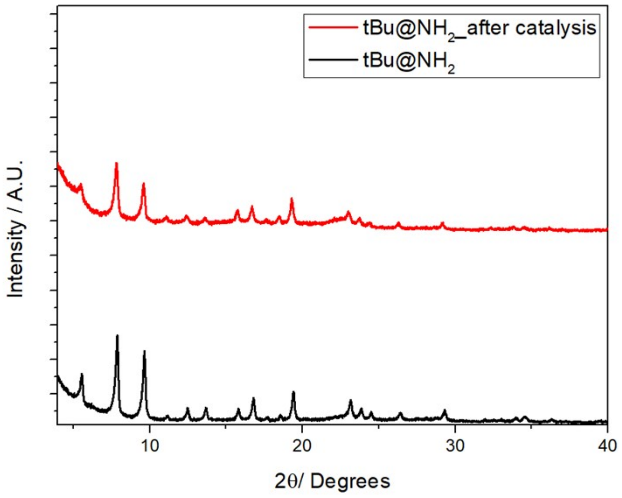

Figure S91: PXRD profile before and after catalysis.

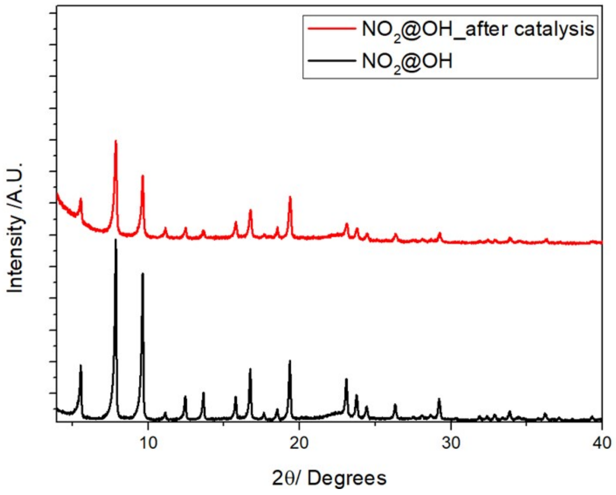

Figure S92: PXRD profile before and after catalysis.

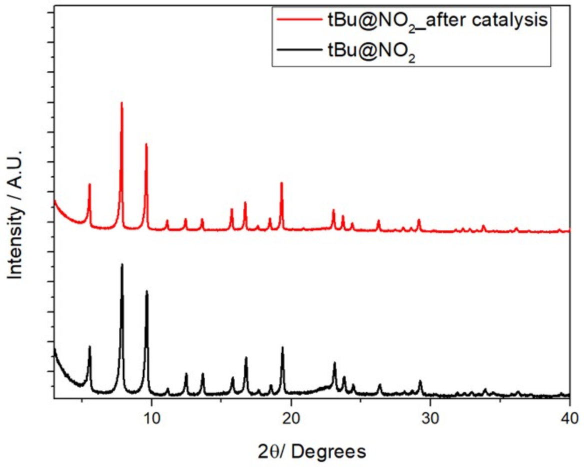

Figure S93: PXRD profile before and after catalysis.

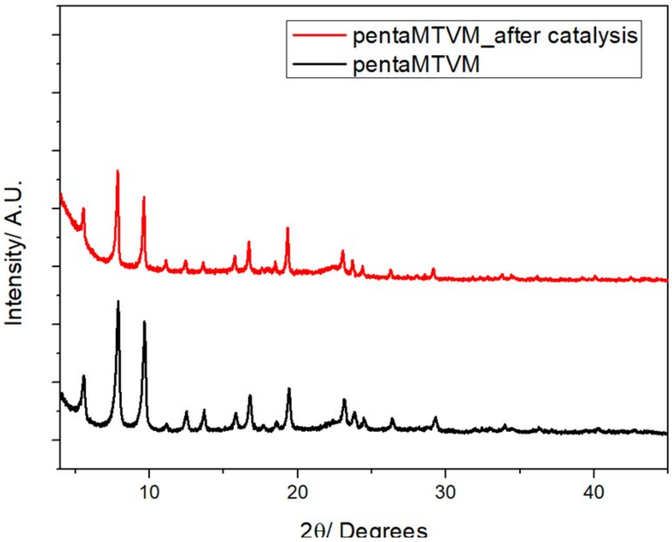

Figure S94: PXRD profile before and after catalysis.

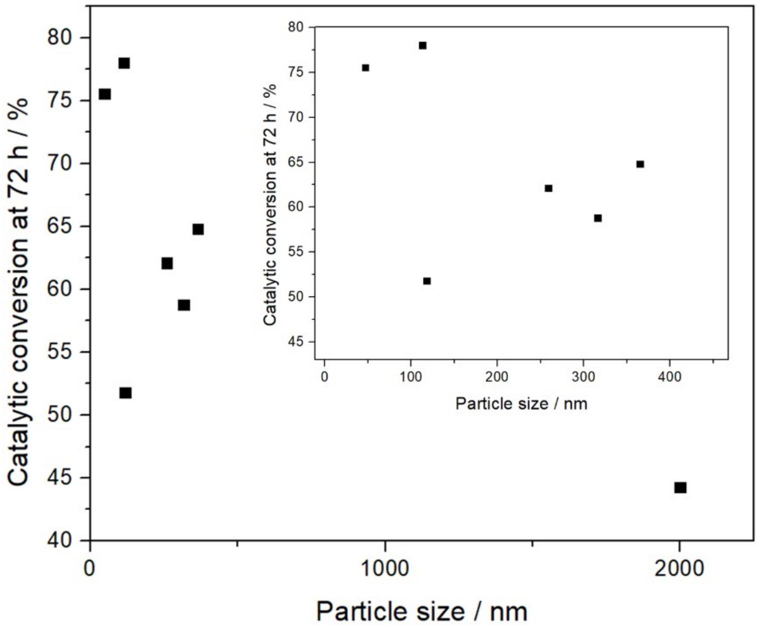

Figure S95: Catalytic conversion after 72 hours as a function of the particle size of the catalysts, showing no relation.

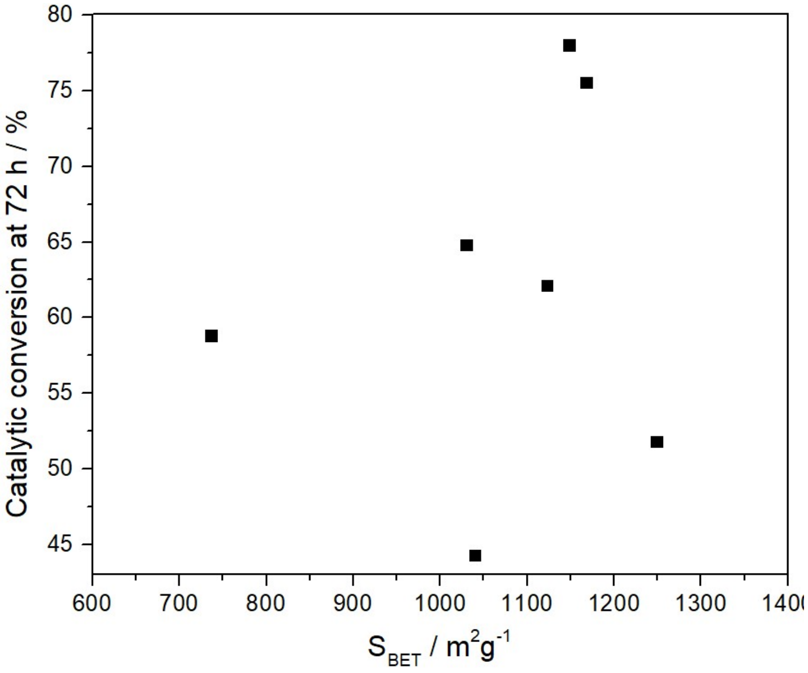

Figure S96: Catalytic conversion after 72 hours as a function of the BET surface area of the catalysts, showing no relation.

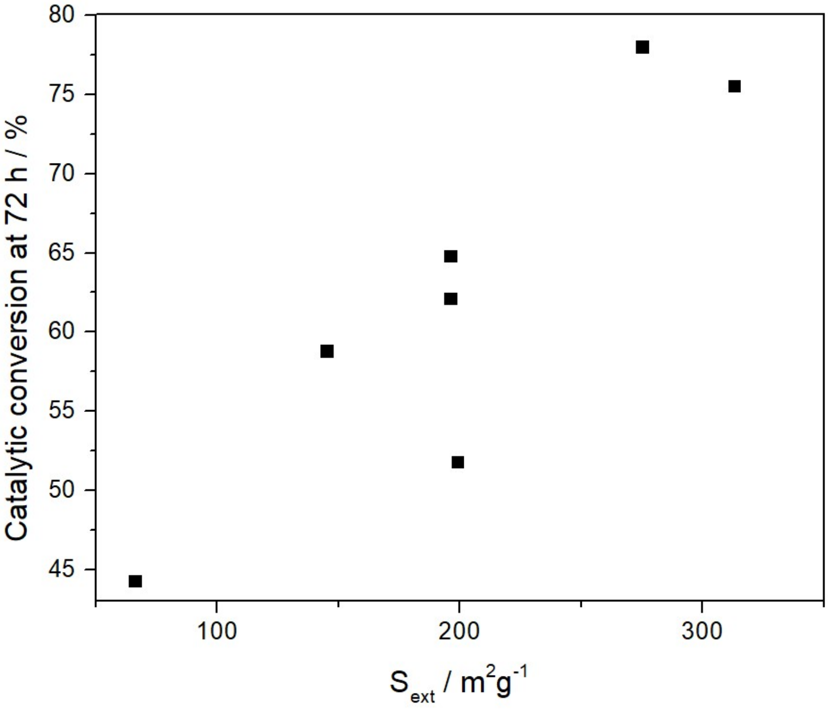

Figure S97: Catalytic conversion after 72 hours as a function of the external surface area of the catalysts, showing no relation.

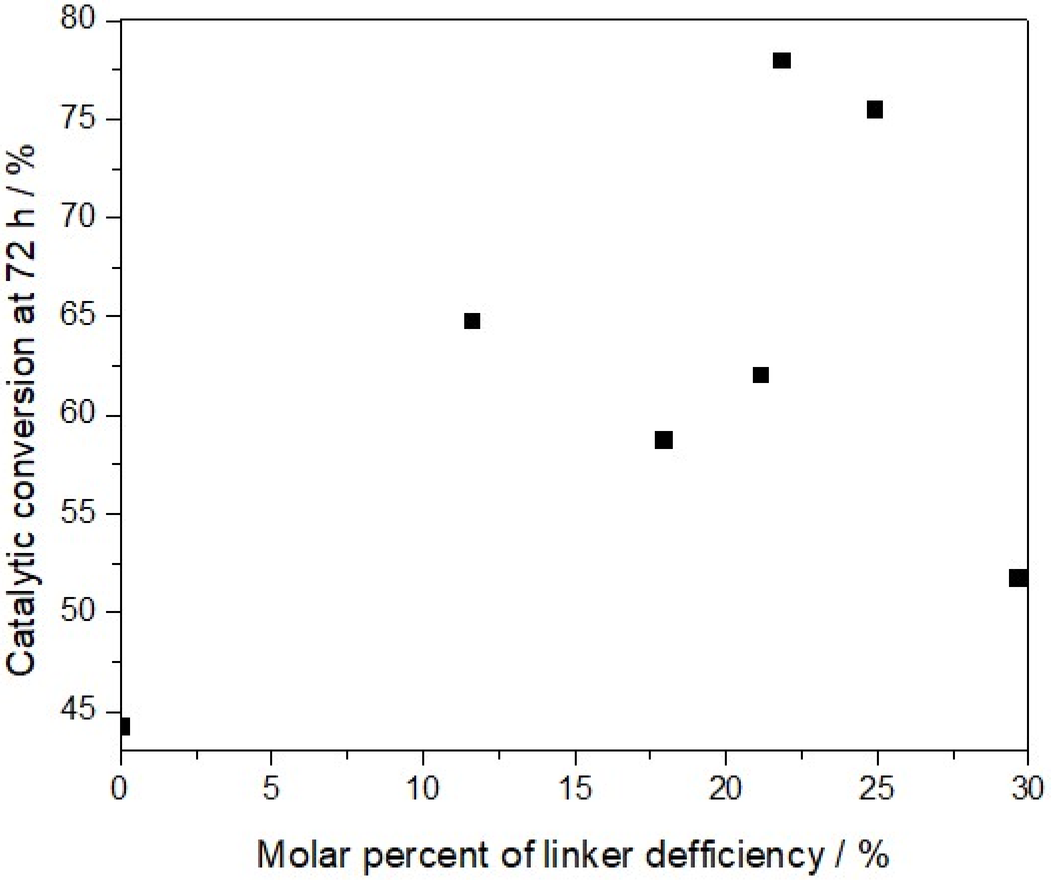

Figure S98: Catalytic conversion after 72 hours as a function of the molar percent of linker deficiency, showing no relation.

S.5. References

[1] G. C. Shearer, S. Chavan, S. Bordiga, S. Svelle, U. Olsbye, K. P. Lillerud, *Chem. Mater.* **2016**, *28*, 3749/3761.

[2] I. A. Lázaro, N. Almora-Barrios, S. Tatay, C. Popescu, C. Martí-Gastaldo, *Chem. Sci.* **2021**, *12*, 11839–11844.

[3] I. A. Lázaro, *Eur. J. Inorg. Chem.* **2020**, *2020*, 4284-4294.

[4] I. A. Lázaro, N. Almora-Barrios, S. Tatay, C. Martí-Gastaldo, *Chem. Sci.* **2020**, *12*, 2586-2593.

[5] F. Rouquerol , J. Rouquerol and K. Sing , *Adsorption by Powders and Porous Solids* , Academic Press, London, 1999, 191–217.